© 2021. Published by The Company of Biologists Ltd | Journal of Cell Science (2021) 134, jcs258602. doi:10.1242/jcs.258602

RESEARCH ARTICLE

# LFA-1 and kindlin-3 enable the collaborative transport of SLP-76 microclusters by myosin and dynein motors

**Keith P. Eidell[1], Alenka Lovy[2], Nicholas R. Sylvain[1], Frank A. Scangarello[1], Hayley I. Muendlein[3], Michael J. Ophir[1], Ken Nguyen[1], Maria-Cristina Seminario[4] and Stephen C. Bunnell[4,*]**

## ABSTRACT

Integrin engagement within the immune synapse enhances T cell activation, but our understanding of this process is incomplete. In response to T cell receptor (TCR) ligation, SLP-76 (*LCP2*), ADAP (*FYB1*) and SKAP55 (*SKAP1*) are recruited into microclusters and activate integrins via the effectors talin-1 and kindlin-3 (*FERMT3*). We postulated that integrins influence the centripetal transport and signaling of SLP-76 microclusters via these linkages. We show that contractile myosin filaments surround and are co-transported with SLP-76 microclusters, and that TCR ligand density governs the centripetal movement of both structures. Centripetal transport requires formin activity, actomyosin contraction, microtubule integrity and dynein motor function. Although immobilized VLA-4 (α4β1 integrin) and LFA-1 (αLβ2 integrin) ligands arrest the centripetal movement of SLP-76 microclusters and myosin filaments, VLA-4 acts distally, while LFA-1 acts in the lamellum. Integrin β2, kindlin-3 and zyxin are required for complete centripetal transport, while integrin β1 and talin-1 are not. CD69 upregulation is similarly dependent on integrin β2, kindlin-3 and zyxin, but not talin-1. These findings highlight the integration of cytoskeletal systems within the immune synapse and reveal extracellular ligand-independent roles for LFA-1 and kindlin-3.

This article has an associated First Person interview with the first author of the paper.

**KEY WORDS: SLP-76, T cell signaling, Immune synapse, Integrin, Microclusters, Myosin**

## INTRODUCTION

T cells are activated via the interaction of T cell receptors (TCR) with antigenic peptides presented by major histocompatibility complex (MHC) proteins. This occurs in the context of a transient (kinapse) or stable (synapse) adhesive junction that links the T cell to an antigen-presenting cell (APC). Persistent immune synapses (ISs) are subdivided into concentric subdomains, or supramolecular activation clusters (SMACs) (Monks et al., 1998). The outermost region, the distal SMAC (dSMAC), is analogous to a circumferential lamellipodium (Freiberg et al., 2002; Varma et al., 2006; Sims et al., 2007; Dustin, 2008). Internal to the dSMAC, a lamellar domain known as the peripheral SMAC (pSMAC) is enriched in the active form of the integrin LFA-1 (αLβ2) (Monks et al., 1997, 1998; Dustin, 2008). The innermost region, the central SMAC (cSMAC), can be subdivided into regions engaged in co-stimulatory signaling, signal termination and secretion (Varma et al., 2006; Stinchcombe and Griffiths, 2007; Yokosuka et al., 2008; Saito et al., 2010; Vardhana et al., 2010). The kinapses formed by migratory T cells contain similar domains, oriented asymmetrically, with the leading edge corresponding to the dSMAC.

In response to ligand recognition, TCRs are assembled into microclusters and phosphorylated by Src kinases, leading to the recruitment of the tyrosine kinase ZAP-70 (Bunnell et al., 2002; Choudhuri et al., 2005; Varma et al., 2006; Dushek et al., 2012). TCR microclusters form in the dSMAC, at contact sites generated via the dynamic polymerization of actin (Valitutti et al., 1995; Varma et al., 2006). When the TCR ligands are laterally mobile, these microclusters traverse the immune synapse and accumulate in a central region. Movement through the dSMAC is driven by Arp2/3-dependent actin flows, while movement through the pSMAC is governed by the contraction of formin-dependent actomyosin arcs (Ilani et al., 2009; Babich et al., 2012; Beemiller et al., 2012; Yi et al., 2012; Murugesan et al., 2016). Although a sparse network of actin filaments is present in the cSMAC, the last step in the centralization of TCR microclusters requires dynein motors, which concentrate TCR microclusters near the microtubule-organizing center (MTOC) (Hashimoto-Tane et al., 2011; Murugesan et al., 2016; Fritzsche et al., 2017). Signaling microclusters are terminated by endocytosis or exocytosis from the central region (Lee et al., 2003; Vardhana et al., 2010; Choudhuri et al., 2014). Nevertheless, the myosin-dependent forces that drive the peripheral movements of TCR microclusters favor the phosphorylation of Src kinases, ZAP-70, LAT and CasL (*NEDD9*) and have been linked to the quality of the stimulatory ligand, implying that contractile forces contribute to T cell activation (Yu et al., 2012; Murugesan et al., 2016; Hong et al., 2017).

The triggering of the TCR also leads to the assembly of microclusters containing the adaptor SLP-76 (*LCP2*), which is crucial for T cell development and activation. These structures form at distal sites adjacent to TCR microclusters and are normally co-transported with TCR microclusters. However, when the triggering ligands are immobile, SLP-76 microclusters separate from TCR microclusters and are independently transported towards the center of the synapse (Bunnell et al., 2002; Yokosuka et al., 2005; Nguyen et al., 2008; Yi et al., 2019). The persistence and movement of SLP-76 microclusters require cooperative interactions among their constituents and with surrounding actin filaments (Barda-Saad et al., 2005; Braiman et al., 2006; Bunnell et al., 2006; Houtman et al., 2006; Balagopalan et al., 2007; Barda-Saad et al., 2010; Pauker et al., 2011; Sylvain et al., 2011; Pauker et al., 2012; Coussens et al., 2013; Ophir et al., 2013; Lewis et al., 2018). Within these small

[1]Graduate Program in Immunology, Tufts Graduate School of Biomedical Sciences, Boston, MA 02111, USA. [2]Department of Neuroscience, Tufts University School of Medicine, Boston, MA 02111, USA. [3]Graduate Program in Genetics, Tufts Graduate School of Biomedical Sciences, Boston, MA 02111, USA. [4]Department of Immunology, Tufts University School of Medicine, Boston, MA 02111, USA.

*Author for correspondence (stephen.bunnell@tufts.edu)

K.P.E., 0000-0002-5971-218X; A.L., 0000-0002-8167-3199; N.R.S., 0000-0003-4325-1953; F.A.S., 0000-0002-3993-608X; H.I.M., 0000-0003-3006-5780; M.J.O., 0000-0002-5516-1237; K.N., 0000-0002-3644-3490; M.-C.S., 0000-0003-0762-8661; S.C.B., 0000-0001-6887-0828

**Handling Editor: Daniel Billadeau**
**Received 2 March 2021; Accepted 13 July 2021**

Journal of Cell Science (2021) 134, jcs258602. doi:10.1242/jcs.258602

'signalosomes', SLP-76 enters signaling complexes nucleated by another critical adaptor, LAT, and partitions, in an actin-dependent manner, into a ring that surrounds the LAT-containing core (Sherman et al., 2011; Barr et al., 2016; Sherman et al., 2016). In primary cells, similar SLP-76 microclusters are surrounded and stabilized by 'micro-adhesion rings' containing actomyosin filaments, LFA-1 (αLβ2 integrin), and several integrin-associated proteins (Hashimoto-Tane et al., 2016). The elimination of the SLP-76- and actin-binding adaptor ADAP (*FYB1*) destabilizes SLP-76 microclusters, suggesting that microcluster cohesion requires the coupling of SLP-76 to these enclosures (Lewis et al., 2018).

The interactions among the cytoskeletal systems in the immune synapse and the mechanisms by which these systems influence SLP-76 microcluster centralization and TCR signaling remain incompletely understood. SLP-76-associated proteins, such as ADAP, Nck (*NCK1* and *NCK2*) and WASP (*WAS*), interact with various cytoskeletal systems and may provide the motive force for the transport of SLP-76 microclusters (Barda-Saad et al., 2005; Nguyen et al., 2008; Pauker et al., 2011; Lewis et al., 2018; Ditlev et al., 2019). In contrast, in the presence of immobile ligands, the integrin VLA-4 (α4β1) slows actin flows and immobilizes SLP-76 microclusters in the dSMAC (Nguyen et al., 2008; Jankowska et al., 2018). Immobile LFA-1 ligands also slow actin flows, and may inhibit the movement of SLP-76 microclusters in this manner (Murugesan et al., 2016). Conversely, integrins might promote the centripetal movement of SLP-76 microclusters by tethering these structures to cytoskeletal systems via the adaptors ADAP and SKAP55 (*SKAP1*), which regulate integrin activation and integrin signaling via SLP-76 (Hunter et al., 2000; Griffiths et al., 2001; Peterson et al., 2001; Kliche et al., 2006; Baker et al., 2009; Ophir et al., 2013; Lewis et al., 2018). In support of this model, SKAP55 promotes the translocation of the integrin-activating protein talin-1 from the margin of the immune synapse to the center of the contact, where it accumulates in proximity to SLP-76 (Ophir et al., 2013).

We now show that contractile actomyosin filaments, microtubule-dependent dynein motors and SLP-76 microclusters reciprocally regulate one another, and that the centralization of SLP-76 microclusters and contractile filaments are co-regulated by myosin II and dynein motors. These processes are coordinated by SKAP55, kindlin-3, β2 integrins and several integrin-associated cytoskeletal proteins, but do not involve β1 integrins or the integrin-activating protein talin-1. The factors that regulate centripetal transport processes govern the TCR-induced upregulation of CD69, which is unaffected by the loss of talin-1. These findings emphasize the importance of cytoskeletal function in T cell activation, clarify the distinct and specialized roles played by integrins and their associated proteins, and demonstrate that LFA-1 supports critical signaling functions, even in the absence of an extracellular ligand.

## RESULTS

### SLP-76 drives the centripetal accumulation of contractile myosin filaments

SLP-76 microclusters display position-dependent transitions in cluster velocity similar to those occurring with TCR microclusters (Nguyen et al., 2008). To address the involvement of contractile actomyosin systems in the transport of SLP-76 microclusters, we visualized SLP-76, myosin IIA (heavy chain *MYH9*) and the activated form of the regulatory myosin light chain (pMLC) in J14.SY cells stimulated on anti-CD3ε coated glass substrates. The pMLC antibody targets an S19-phosphorylated epitope thet is perfectly conserved between MRLC1/MLC-9 (*MYL9*) and MRLC2/MLC-12B (*MYL12B*). The J14.SY cell line, previously derived from SLP-76-deficient J14 Jurkat T cells, stably expresses a SLP-76.YFP chimera. In a serum-independent manner, TCR-induced SLP-76 microclusters move from the periphery into a compact domain at the center of the contact (Fig. 1A; Fig. S1A). Immunofluorescence staining reveals that a subset of endogenous myosin IIA accumulated in a dense structure at the center of the contact, overlapping with SLP-76, while thinner filaments of myosin extended from this structure to the periphery of the contact and terminated near to SLP-76 microclusters (Fig. 1A, white arrows emphasize radial filaments). These structures were even more prominent in the pMLC channel, indicating that they are contracting (Fig. 1A). Because this distribution differs from previous reports, we also evaluated the patterning of myosin IIA in wild-type Jurkat E6.1 cells and in Jurkat E6.1 cells expressing SLP-76.YFP (E6.SY cells). Whereas Jurkat E6.1 cells generate circumferential arcs of myosin IIA, exogenous SLP-76 at about three times endogenous levels reproduced the centripetal accumulation of myosin IIA and pMLC observed in the J14.SY cells, without affecting TCR expression (Fig. 1B; Fig. S1B, C). In all three lines, and in primary human T cells stimulated on analogous substrates, most myosin IIA accumulated in a ring 7–9 µm from the center of the contact (Fig. S1D). Increased SLP-76 expression shifted the average radial positions of myosin IIA and pMLC towards the center of the contact and created a small, but distinct, central pool that was enriched in pMLC (Fig. S1D).

### TCR signal strength determines the extent of SLP-76 microcluster centralization and the position of contractile myosin filaments

We derived from J14.SY cells a cytoskeletal reporter line (J14.SY-CRL) that expresses fluorescent chimeras of the filamentous actin-binding protein F-Tractin and the human regulatory myosin light chain encoded by *MYL9* (MLC-9). These chimeras did not alter the centralization of SLP-76 microclusters and the distribution of MLC-9 mirrored that of pMLC (Fig. 1C). In this line, the SLP-76 microclusters formed in response to weak stimuli do not centralize and MLC-9 is not recruited into distinctive structures (Fig. 1D). Intermediate ligand densities drive the appearance of filamentous MLC-9 structures in the cell periphery but do not elicit microcluster centralization. Further increases in ligand density shift MLC-9 filaments from the cell periphery first to a pSMAC-like ring, and then to a compact central cluster linked via radial spokes to the cell periphery (Fig. 1E). Concurrently, SLP-76 microclusters display partial, and then full centralization, suggesting that the subcellular distribution of contractile myosin is linked to that of SLP-76, and that both processes are influenced by TCR signal strength.

### SLP-76 microclusters associate with contractile myosin filaments and rings

Background-corrected versions of the images in Fig. 1B revealed that myosin IIA and pMLC form a network of closed cells, or rings, of ∼1–2 µm in diameter (Fig. 1F,G). These units are most prominent in the periphery of the contact, while more loosely interconnected myosin IIA structures are present in the center of the contact. SLP-76 microclusters are frequently found within these closed cells (yellow brackets) or alongside myosin filaments (white arrows). In primary human $CD4^+$ and $CD8^+$ T cell blasts stimulated on analogous substrates, myosin IIA forms circumferential arcs similar to those observed here and in earlier TIRF-SIM studies (Fig. S2A) (Murugesan et al., 2016; Hong et al., 2017). Most of these cells also develop a 'purse-string'-like structure (red arrowheads) at the inner boundary of the myosin IIA arcs. This contractile structure often separates from distal myosin structures (gaps denoted by red

Journal of Cell Science (2021) 134, jcs258602. doi:10.1242/jcs.258602

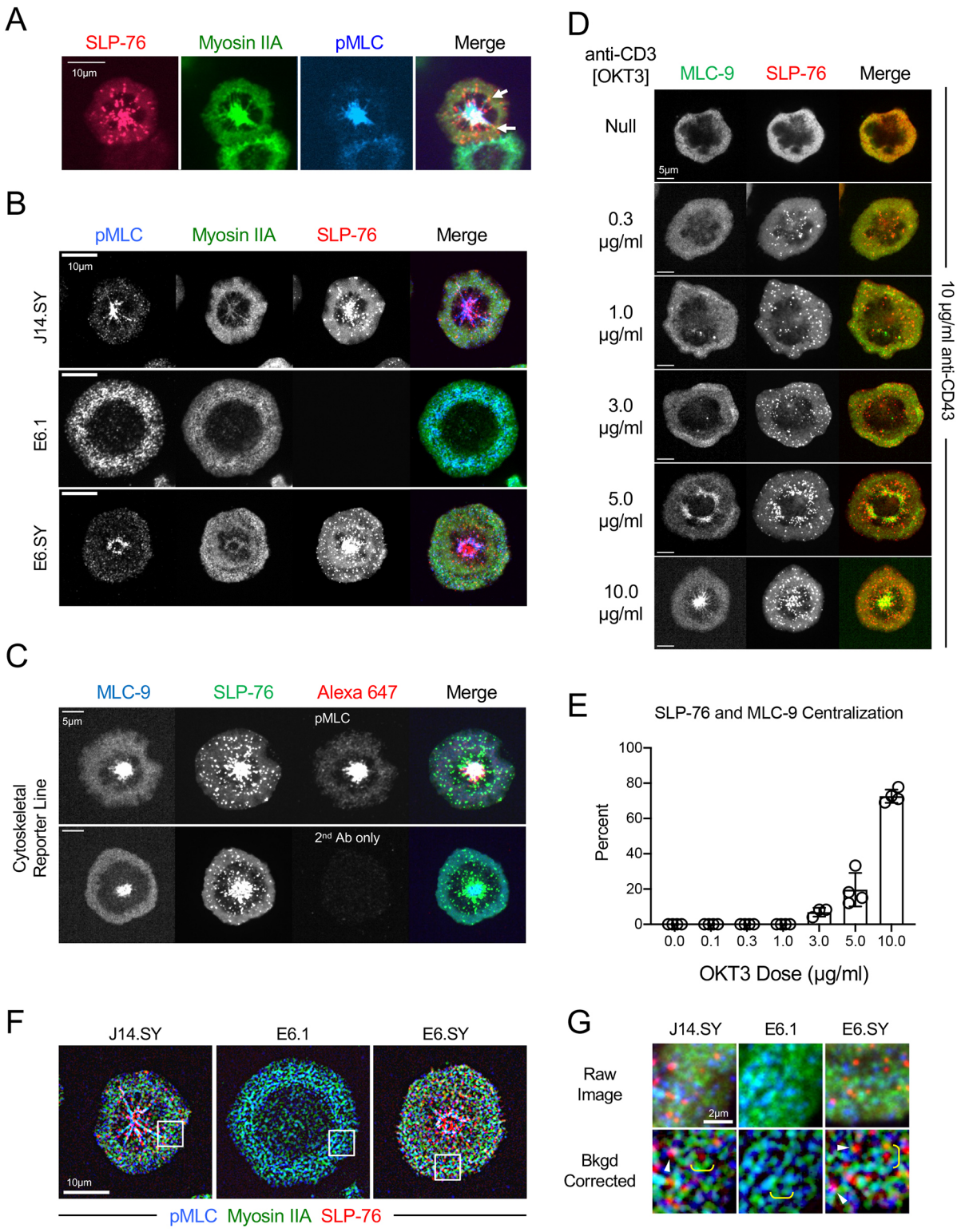


**Fig. 1. Ligand dose and SLP-76 expression coordinately regulate myosin organization and SLP-76 microcluster centralization.** (A) J14.SY cells were stimulated on anti-CD3 (OKT3, 10.0 μg $ml^{-1}$)-coated glass wells, fixed after 7 min, and stained for myosin IIA and the phosphorylated form of the myosin light chain (pMLC). White arrows indicate radially oriented myosin spokes. (B) J14.SY cells, E6.1 cells and E6.1 cells stably transduced with SLP-76.YFP were prepared as in A. Images in A and B are representative of ∼250–500 cells in five experiments. (C) J14.SY-CRL cells were prepared as in A. Representative of three experiments. (D,E) J14.SY-CRL cells were plated on substrates coated with anti-CD43 (10.0 μg $ml^{-1}$) and the indicated doses of anti-CD3 (OKT3). (D) Representative images from three (3.0 μg $ml^{-1}$ OKT3) or four (all other doses) replicates, each including >10 cells. (E) Mean±s.e.m. is depicted at each dose. (F) Images in B were background corrected using a ∼350 nm rolling ball filter on all channels. Identical non-linear normalizations (γ=0.43) were applied to emphasize features in the centers of the contacts. (G) Enlarged versions of the boxed regions in F. Yellow brackets (1.5 μm) highlight ring-like myosin IIA structures. White arrowheads identify SLP-76 microclusters adjoining myosin filaments.

Journal of Cell Science (2021) 134, jcs258602. doi:10.1242/jcs.258602

brackets). Links between the myosin IIA arcs give rise to cells resembling those observed in Jurkat T cells (Fig. S2B). By algorithmically identifying the centers of voids within the myosin IIA meshwork (Fig. S2C, top row), we were able to determine that the peaks of myosin IIA intensity, as function of radial distance, did not differ in Jurkat E6.1 cells, E6.SY cells, J14.SY cells, primary human $CD4^+$ T cells, primary human $CD8^+$ T cells, or E6.1 cells expressing a tagged form of myosin IIA (Fig. S2D). The diameters of the ring-like structures defined in this manner averaged 1.74±0.06 µm (mean ±s.d.), which is comparable to the size of the previously reported micro-adhesion rings (Hashimoto-Tane et al., 2016). SLP-76 and pMLC are also reduced in the centers of these voids and are enriched at a similar distance to that of myosin IIA. However, SLP-76 does not colocalize extensively with either myosin IIA or pMLC, and SLP-76 microclusters are typically associated with the inner or outer margins of the myosin rings (Fig. S2C, bottom row; Fig. S2E). This is consistent with the intensities of myosin IIA and pMLC respectively peaking ∼0.26 µm and ∼0.45 µm from the centers of SLP-76 microclusters (Fig. S2D, right).

### SLP-76 microcluster centralization requires myosin ATPase activity, myosin light chain kinases and myosin heavy chain expression

To examine the role of myosin IIA in the transport of SLP-76 microclusters, we pretreated J14.SY cells for 30 min with the myosin ATPase inhibitor blebbistatin or with H1152 or Y27632, which are inhibitors of the Rho kinase (ROCK) subfamily of myosin light chain kinases. Kymographs are used to illustrate the rates of microcluster movement within the indicated regions (Fig. 2A,B). All three compounds inhibit the centripetal movement of SLP-76 microclusters, demonstrating that Rho kinase-dependent contractility is a driver of SLP-76 centralization. To verify the impacts of blebbistatin and H1152 on myosin filament organization, we treated Jurkat E6.1 cells expressing an EGFP-tagged myosin IIA chimera with blebbistatin or H1152 (Fig. 2C). Blebbistatin retards the continuous transport of myosin IIA filaments from the cell periphery without disrupting these filaments or perturbing the ‘cells’ defined by myosin IIA. In contrast, H1152 prevents the appearance of myosin filaments, consistent with its mode of action. However, we were unable to suppress the centripetal movement of SLP-76 microclusters by knocking down myosin IIA (data not shown). A parallel effort to characterize the SLP-76 microcluster proteome provided new insight into this longstanding problem (Hammer and Burkhardt, 2013; Le Floc’h and Huse, 2015). These studies involved the stimulation of J14.SY cells using beads coated with anti-CD3ε antibody and recombinant human VCAM-1, the fixation and sonication of the cells, and the magnetic recovery of bead-bound signaling complexes (Fig. S3A). This approach activates cells and enriches TCR-associated signaling molecules (Fig. S3B,C). Mass spectrometry of individual bands yields proteins with molecular masses appropriate to their positions within the original gel (Fig. S3D,E). The resulting hits include proteins involved in cytoskeletal function, membrane transport and signal transduction (Fig. S3F, see Table S2 for full dataset). Myosin IIA (MYH9) is captured by stimulatory beads, but not by beads coated with a pro-adhesive and non-stimulatory antibody (Fig. S3G,H). Peptides unique to myosin IIB (MYH10) are found in these complexes, even though primary murine T cells only express myosin IIA (Fig. S3F) (Jacobelli et al., 2004). When transfected into J14.ST cells (analogous to the J14.SY cell line but expressing SLP-76.TRT), EGFP-tagged variants of myosin IIA and IIB assemble into filaments that associate with SLP-76 microclusters (Fig. 2D). Transitive western blots employing specific antibodies confirm that myosin IIB is expressed in Jurkat T cells, although at lower levels than myosin IIA (Fig. S3I). Endogenous myosin IIB is also assembled into filaments after TCR ligation, and these myosin IIB filaments display a sensitivity to SLP-76 expression that is identical to myosin IIA (Fig. S3J). Finally, we were able to show that the suppression of myosin IIA and IIB impairs the centripetal transport and central accumulation of SLP-76 microclusters (Fig. 2E–H).

### Formins, microtubules and dynein motors drive the centripetal accumulation of both SLP-76 microclusters and contractile myosin

To determine whether Arp2/3-dependent actin flows, formin-dependent actomyosin filaments and microtubule-dependent dynein motors contribute to the movement of SLP-76 and myosin, we visualized the dynamic redistribution of SLP-76 and MLC-9 (*MYL9*) in the presence or absence of inhibitors of these systems (Bunnell et al., 2002; Hashimoto-Tane et al., 2011). Maximum-over-time (MOT) projections (Fig. 2I) and kymographs (Fig. S4A) show the direction, extent and speed of movement. The Arp2/3 inhibitor CK666 abolishes T cell spreading and precludes the formation of SLP-76 microclusters (data not shown). A photostable inhibitor of myosin ATPase function, para-amino-blebbistatin (paBB), suppresses microcluster centralization (Kolega, 2004; Varkuti et al., 2016). The formin inhibitor SMIFH2 prevents SLP-76 microcluster centralization and disrupts MLC-9-labeled filaments, leaving small specks of MLC-9 (Fig. 2I, white arrows versus red arrowhead). The microtubule-disrupting agent colchicine impairs the movement of SLP-76 microclusters, but also prevents the central accumulation of MLC-9 (Fig. S4B). Finally, the dynein ATPase inhibitor EHNA also prevents the accumulation of SLP-76 and MLC-9 at the center of the contact (Fig. S4B). Collectively, these findings suggest that the centralized myosin filaments observed here are analogous to the actomyosin arcs that drive the transport of TCR microclusters and extend this model by demonstrating that dynein-dependent interactions between microtubules and peripheral actomyosin fibers dictate the final arrangement of actomyosin and the ultimate position of SLP-76 microclusters. We also note that paBB impairs the extension of microtubules into the periphery of the contact and impedes the polarization of the MTOC towards the contact interface (Fig. S4C). Thus, dynein motors embedded in the actomyosin system may reciprocally regulate MTOC polarization and centripetal transport processes (Nath et al., 2016; Maskalenko et al., 2020).

### VLA-4 and LFA-1 block the centralization of actomyosin filaments and SLP-76 microclusters, but act in distinct domains of the synapse

Immobilized VLA-4 ligands prevent the centripetal movement of TCR-induced SLP-76 microclusters and slow actin flows (Nguyen et al., 2008). In response, myosin IIA and pMLC shift from radial arrays into peripheral, circumferential structures (Fig. 3A, left-hand panels, see enlarged views for greater detail). However, myosin filaments continue to incorporate SLP-76 microclusters and to terminate at or near to peripheral SLP-76 microclusters. Using an objective with a higher numerical aperture, these myosin IIA filaments can be resolved as regularly spaced, sarcomere-like puncta (Fig. 3A, right-hand main panels and magnified views). SLP-76 microclusters interdigitate between these puncta in the same manner as TCR microclusters (Murugesan et al., 2016). Immobilized VCAM-1 also shifts MLC-9 into a distal ring and retains SLP-76 microclusters outside of this ring (Fig. 3B,C). LFA-1 ligation by immobilized ICAM-1 also shifts MLC-9 into a circumferential ring, but this ring is

Journal of Cell Science (2021) 134, jcs258602. doi:10.1242/jcs.258602

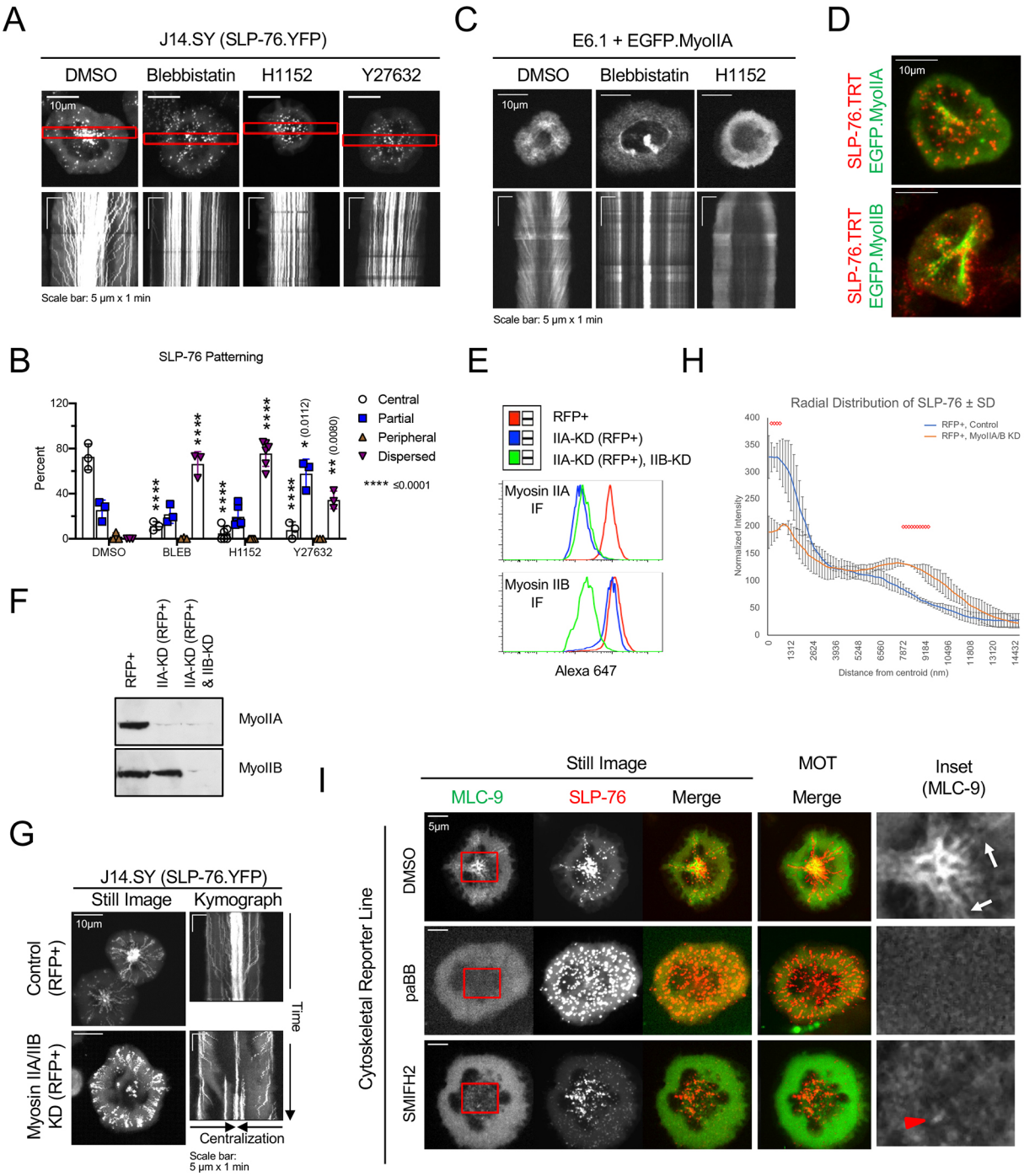


**Fig. 2.** See next page for legend.

displaced inward, and SLP-76 microclusters are arrested inside the pSMAC (Fig. 3B,C). Plots of SLP-76 and MLC-9 intensity as a function of distance from the outer edge of the cell confirm these effects (Fig. S5A). Thus, integrin ligation inhibits the centripetal flow of myosin filaments and hinders the centripetal movement of SLP-76 microclusters, but VLA-4 and LFA-1 act at distinct sites.

### SLP-76 microclusters exclude integrins but are surrounded by and interact with integrin-containing structures

Centralized SLP-76 microclusters interact with β1 integrin and talin, indicating that integrins could engage SLP-76 microclusters and direct their centripetal transport (Ophir et al., 2013). In TCR-stimulated J14.SY cells, SLP-76 microclusters either align with radial structures containing α4 integrin and talin or are found within α4 ‘rings’ that are similar in size to actomyosin rings (Fig. 3D, see yellow brackets in magnified views). VLA-4 ligation does not alter the segregation of SLP-76 from α4 integrin and talin but favors more uniform distributions of α4 integrin and talin. When cells are sheared from substrates lacking VCAM-1, SLP-76 microclusters remain attached, but very little α4 is retained (Fig. 3E). In contrast, VCAM-1 promotes the retention of a reticular network of α4 integrin and traps SLP-76 microclusters in

**Fig. 2. Myosin assembly, myosin ATPase activity and formin function are required for SLP-76 centralization.** (A) J14.SY cells were pretreated for 30 min with DMSO, blebbistatin (50 µM), H1152 (20 µM) or Y27632 (20 µM) and stimulated in the presence of these compounds as in Fig. 1A. One frame was collected every 2.1 s for at least 86 frames (3 min). Kymographs were derived from the indicated regions. (B) SLP-76.YFP microcluster localization in images acquired in A. Scores are the mean±s.e.m. ($n$=3; ≥10 cells per replicate). *$P$<0.05, **$P$<0.01, ****$P$<0.0001 from the DMSO control (post-hoc Bonferroni corrected tests versus DMSO controls are shown where one-way ANOVA tests confirm significant differences between groups). (C) Jurkat E6.1 cells transfected with EGFP.MyosinIIA were pretreated with DMSO, blebbistatin or H1152 and stimulated as in A. Images were collected every 2.1 s for at least 95 frames (3.3 min). Representative of 5–14 drug treatments imaged in 2–7 experiments. (D) J14.ST cells transfected with EGFP-tagged myosin IIA (MyoIIA) or IIB (MyoIIB), were stimulated as in A and fixed after 7 min. Representative images are shown ($n$=3). (E–H) J14.SY cells were transfected with an RFP-marked control vector, an RFP-marked myosin IIA shRNA vector, and/or an unmarked myosin IIB shRNA vector, as indicated. (E) On day 2 cells were fixed, stained for myosin IIA or IIB, and analyzed by flow cytometry. Histograms were prepared from RFP+ gated cells. (F–H) On day 3 RFP+ cells enriched by fluorescence activated cell sorting were lysed and western blotted (F) or imaged as in A (G). In G, one image was collected every 3.15 s for 96 frames (5 min). Representative blots and images are shown ($n$=4). (H) Mock and double-knockdown cells imaged in G were used to prepare MOTs. Average-over-time images prepared from independent experiments conducted under identical conditions were used to determine the radial distributions of SLP-76 intensity. The mean±s.d. is shown ($n$=3, 11–28 cells per condition per experiment, totaling 50-52 cells per condition). Red diamonds indicate $P$<0.05 (two-tailed Student's $t$-test for unpaired samples). (I) J14.SY-CRL cells were pretreated as above with DMSO or para-amino-blebbistatin (paBB, 50 µM), or for 10 min with SMIFH2 (25 µM). Cells were stimulated on substrates coated with anti-CD3 (10.0 µg ml$^{-1}$) and anti-CD43 (10.0 µg ml$^{-1}$). Each channel was imaged every 5.6 s for 150 frames (14 min). Still images are shown for MLC and SLP-76 and a merged MOT is shown for SLP-76. Kymographs are in Fig. S1. Insets are expanded at right. White arrows indicate radial myosin spokes, red arrowhead marks a myosin speck.

the cavities of this network, implying that SLP-76 is tightly coupled to VLA-4. Finally, in J14.ST cells expressing tagged β1 and β2 integrins, the ligation of either VLA-4 or LFA-1 immobilizes SLP-76 microclusters, even though these tagged integrins are excluded from SLP-76 microclusters (Fig. 3F). In sharpened images, β1 and β2 appear to surround and overlap minimally with SLP-76 microclusters, as observed for α4 integrin (Fig. 3G). The radial positions α4 and β2 integrins relative to SLP-76 microclusters, derived using raw images, confirm this effect and indicate that integrins and SLP-76 microclusters are enriched in distinct but adjacent subdomains (Fig. S5B).

### The integrin LFA-1 plays a unique role in the centralization of SLP-76 microclusters

Because our model system does not require integrin co-ligation for T cell attachment, it is ideally suited to the analysis of how integrins contribute to microcluster transport. In J14.SY control cells, TCR-induced SLP-76 microclusters accumulate in the center of the synapse (Fig. 4A; Movie 1). In A1 cells expressing SLP-76.TRT (A1.ST), SLP-76 microclusters centralize normally (Fig. 4A; Movie 2) (Romzek et al., 1998). By contrast, cells lacking β2 (see Fig. 4B) cannot accumulate SLP-76 microclusters in the center of the synapse, even though the suppression of β2 does not eliminate microcluster movement in the distal, lamellipodial region of the cell (Fig. 4A; Movie 3). These cells were also scored for microcluster localization using four categories: central (SLP-76 microclusters are absent from the center of the contact); partial (SLP-76 microclusters adopt a multifocal and/or asymmetric pattern); peripheral (SLP-76 microclusters are absent from the center of the contact); and dispersed (SLP-76 microclusters are uniformly distributed). As noted, the loss of β1 integrin does not alter the behavior of SLP-76 microclusters (Fig. 4C). In contrast, the suppression of β2 integrin decreases the proportion of cells scored as 'central' and increases the fractions of cells scored as 'peripheral' or 'dispersed'. This effect is eliminated by reconstitution with αL.mCFP and β2.mYFP (Fig. 4D, E). The depletion of integrins or integrin associated proteins does not alter the expression of SLP-76.YFP or the TCR, β1 or β2 (Fig. S1C, D). Using a similar scoring system to assess a β2-deficient version of our cytoskeletal reporter cell line (Fig. 4F), we confirmed that the suppression of β2 decreases the central accumulation of MLC-9 and SLP-76 microclusters (Fig. 4G,H). Finally, we examined the distribution of LFA-1 in the contacts formed by Jurkat T cells. High-affinity mAb24-reactive LFA-1 forms a prominent ring ∼7 µm from the center of the contact (Fig. S5C, upper). Radial analyses reveal that a subset of high-affinity LFA-1 is recruited to the center of the synapse, with SLP-76. When superimposed on earlier data, the distribution of open LFA-1 follows that of myosin IIA (Fig. S5C, lower). Thus, active β2, but not β1, integrins mediate the centralization of SLP-76 microclusters and the transport of contractile myosin filaments to the center of the synapse.

### The integrin-activating protein SKAP55 supports the central accumulation of SLP-76 and contractile myosin filaments, even when deprived of its talin-binding motif

The integrin-activating adapters SKAP55 and ADAP enhance the persistence and movement of SLP-76 microclusters (Ophir et al., 2013; Lewis et al., 2018). The N-terminal dimerization motif in SKAP55 recruits several LFA-1-activating proteins, including RAPL (*RASSF5*), MST1 (*STK4*), RIAM (*APBB1IP*) and talin-1, suggesting that SKAP55 could link SLP-76 to LFA-1 (Kliche et al., 2006; Menasche et al., 2007; Lee et al., 2009; Raab et al., 2010; Kliche et al., 2012). J14.SY cells lacking SKAP55 (i.e. JSKAP.SY cells) are unable to form TCR-induced central clusters of myosin IIA and pMLC, and are less able to centralize SLP-76 microclusters, whereas reconstituted JSKAP.SY cells behave like the parental J14.SY line (Fig. S6A,B). Previously, we showed that a SKAP55-derived tandem dimer (TD) of SH3 domains that lacks a critical talin-1-binding and integrin-activating domain supports the persistence and centralization of SLP-76 microclusters (Ophir et al., 2013). This chimera also restores the centralization of MLC-9, implying that talin-1 is dispensable for both forms of movement (Fig. S6B).

### Kindlin-3 is required for the centralization of SLP-76 microclusters and myosin

The acquisition of an extended, high-affinity conformation by integrins requires the integrin-activating proteins, talin-1 and kindlin-3, which bind, respectively, to the proximal and distal NPxF/Y motifs in the tails of β-integrins (Morse et al., 2014). The near elimination of talin-1 has virtually no effect on the centralization of SLP-76 microclusters (Fig. 5A–C; Movie 4). By contrast, the partial suppression of kindlin-3 impairs microcluster centralization, yielding effects comparable to the suppression of β2 (Fig. 5A–C; Movie 5). Similarly, the suppression of kindlin-3, but not of talin-1, prevents the co-accumulation of active myosin with SLP-76 microclusters (Fig. 5D,E).

### The kindlin-3-binding NPKF motif in the β2 subunit drives the centralization of SLP-76 microclusters and myosin filaments

To verify that these centripetal movements depend on kindlin-3 but not talin-1, we transfected a J14.ST β2 knockdown (β2-KD) line

Journal of Cell Science (2021) 134, jcs258602. doi:10.1242/jcs.258602

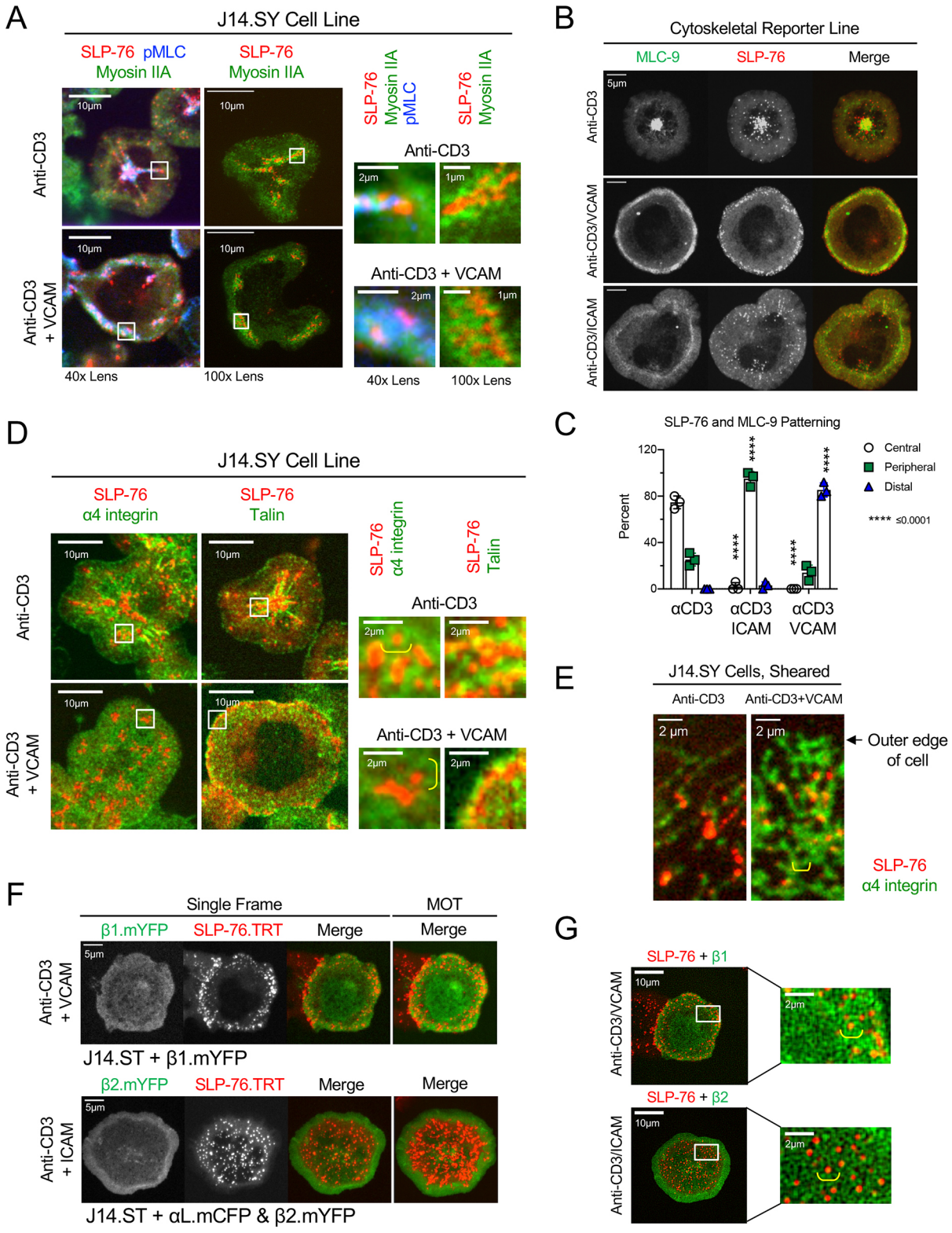


**Fig. 3.** See next page for legend.

with wild-type (WT) αL.mCFP and with alanine-replacement NPxF motif-mutant versions of β2.mYFP (Fig. 6A). As expected, the suppression of β2 alters the patterning of SLP-76 and pMLC in J14.ST cells (Fig. 6B,C). Reconstitution with wild-type αL.mCFP and β2.mYFP reproduces the behavior of the parental line. A β2 chimera that lacks the proximal talin-binding NPLF motif also restores the parental patterns of myosin and SLP-76. In contrast, β2 chimeras that lack the distal kindlin-3-binding NPKF motif are impaired in their ability to centralize myosin and SLP-76, but are not as impaired as the β2-KD line. Finally, cells reconstituted with the dual NPxF mutant are more defective than cells expressing the NPKF mutant, implying that the proximal NPLF motif weakly

**Fig. 3. VLA-4 and LFA-1 ligands immobilize SLP-76 microclusters and myosin structures in distinct regions.** (A) J14.SY cells were stimulated on substrates coated with anti-CD3 (10 µg ml$^{-1}$) with or without VCAM-1 (1 µg ml$^{-1}$), and fixed, stained and imaged as in Fig. 1A. Representative of ∼250–500 cells in five experiments. Boxed regions are enlarged at right. Enlarged images in the right column were collected using a 100× NA 1.45 objective. (B,C) J14.SY-CRL cells were stimulated and prepared as above, with the addition of stimulation via anti-CD3 with ICAM (20 µg ml$^{-1}$). The mean ±s.e.m. is shown ($n$=3, ≥10 cells per replicate). ****$P$<0.0001 from stimulation on anti-CD3 (post-hoc Bonferroni corrected tests versus the anti-CD3 stimulated controls are shown where one-way ANOVA tests confirm significant differences between groups). (D) J14.SY cells were prepared as in A and stained for α4 integrin or talin. Boxed regions are enlarged at right. Representative of three or four experiments. (E) J14.SY cells were stimulated and fixed as in A. The stimulatory substrates were subjected to shear forces and the retained material was stained for α4 integrin. Images were captured under identical conditions and normalized identically ($n$=2). (F) J14.ST cells were transfected with β1.mYFP and stimulated on anti-CD3 with or without VCAM, or transfected with β2.mYFP and αL.mCFP and stimulated on anti-CD3 with ICAM, as in B. Images were collected every 2 s for 150 frames (5 min). Representative frames and MOT projections are shown. (G) Images from E were subjected to a sharpening filter and the indicated regions are enlarged at right. In D,E and G, yellow brackets (1.5 µm) highlight ring-like integrin structures.

impacts centripetal movements in cells lacking the distal NPKF motif. Thus, kindlin-3, rather than talin-1, plays a decisive role in the LFA-1-mediated central accumulation of myosin filaments and SLP-76 microclusters.

### Additional stress fiber components, including the actin-associated protein zyxin, are required for the centralization of SLP-76 microclusters and active myosin

The contractile filaments observed here resemble stress fibers, implying that other stress-fiber constituents contribute to the centralization of SLP-76 microclusters (Tojkander et al., 2012). We observed that the shRNA-mediated suppression of zyxin, filamin-A (*FLNA*), or vinculin (*VCL*) either abolishes or impairs the centralization of SLP-76 microclusters (Fig. 7A; Fig. S1B,C). A later screen revealed that α-actinin-1 (*ACTN1*) and α-actinin-4 (*ACTN4*) also participate in SLP-76 microcluster centralization, although α-actinin-1 appears to play a more decisive role (Fig. S7). Consistent with these findings, filamin-A and α-actinin-4 also appear in our analysis of the shear-resistant signaling complexes retained on stimulatory beads after sonication (Fig. S3F). To characterize the distribution of zyxin in the immune synapse, we stained for zyxin in our cytoskeletal reporter line. Zyxin puncta appear throughout the immune synapse, but do not consistently colocalize with SLP-76 microclusters and do not accumulate in the center of the contact (Fig. 7B). Nevertheless, the suppression of zyxin reduces the central accumulation of MLC-9 and the centralization of SLP-76 microclusters (Fig. 7C,D).

### The β2 subunit of LFA-1, kindlin-3 and zyxin contribute to talin-1-independent TCR-proximal signaling events

To determine how proteins that impact microcluster and myosin transport influence T cell activation, we examined the upregulation of the activation marker CD69 and the secretion of interleukin (IL)-2 by J14.SY cells stimulated on substrates identical to those used in our imaging assays. Integrin β2, kindlin-3 and zyxin are all required for the maximal upregulation of CD69 by J14.SY cells; however, talin-1 is not required (Fig. 8A,B). In contrast, all four proteins are required for optimal IL-2 secretion (Fig. 8C). All four knockdown cell lines adhere to anti-CD3ε-coated plates over a broad range of shear forces, indicating that the signaling defects observed in these lines are not secondary to defects in contact formation (Fig. 8D) (Nguyen et al., 2008; Ophir et al., 2013).

## DISCUSSION

Actomyosin arcs clearly contribute to the centripetal movement of TCR microclusters within the immune synapse (Yi et al., 2012; Yu et al., 2012; Hammer and Burkhardt, 2013; Murugesan et al., 2016; Hong et al., 2017; Hammer et al., 2019). However, the participation of these arcs in the centripetal transport of SLP-76 microclusters, which play distinct and critical roles in T cell activation, has received less study (Babich et al., 2012). Here, we visualized the interactions of SLP-76 microclusters with actively contracting myosin filaments using antibodies against phosphorylated myosin light chain (pMLC) and a fluorescent chimera of human MLC-9. This allowed us to demonstrate that, in Jurkat T cells, TCR ligand density and SLP-76 expression favor the co-accumulation of myosin with SLP-76 microclusters in compact central structures. The centripetal movement of SLP-76 microclusters is blocked by the same factors that prevent the centralization of TCR microclusters: Rho-family kinase inhibitors, myosin II ATPase inhibitors, and the formin inhibitor SMIFH2. As previously reported, the partial suppression of myosin IIA does not suppresses microcluster transport (Babich et al., 2012). However, we show that myosin IIB is expressed in Jurkat T cells, and that the simultaneous suppression of myosin IIA and myosin IIB inhibits the sustained centripetal movement of SLP-76 microclusters in these cells. Jointly, these findings indicate that TCR and SLP-76 microclusters are identically dependent on the contraction of formin-nucleated actomyosin filaments, even though the overall topology of myosin in T cells expressing exogenous SLP-76 deviates from the largely circumferential pattern observed in unmanipulated Jurkat T cells and primary T cells.

Our data confirm that SLP-76 microclusters are enclosed by, but remain distinct from, actomyosin-containing rings (Hashimoto-Tane et al., 2016). The separation of SLP-76 microclusters from their surrounding actin-containing structures is consistent with previous nanoscale analyses of LAT and SLP-76 microclusters (Sherman et al., 2011, 2016). Remarkably, these rings are unaffected by the expression of exogenous SLP-76. VLA-4 and LFA-1 are both excluded from SLP-76 microclusters but are enriched in the surrounding region, at a distance compatible with their participation in actomyosin rings. The recruitment of integrins into these rings is less pronounced than in the transient structures observed by Hashimoto-Tane et al. This may reflect the later timepoints used in our study, or other differences between our model systems. Importantly, these weak integrin rings form in the absence of exogenous integrin ligands. Thus, ADAP could stabilize SLP-76 microclusters in cells stimulated via the TCR alone by tethering nascent microclusters to surrounding actomyosin rings, even when the salient exogenous integrin ligands are absent (Lewis et al., 2018).

Our observations also provide insights into processes occurring in primary T cells and cells stimulated via physiological ligands. SLP-76 microclusters accumulate in the center of the stimulatory contacts formed by human peripheral blood T cell (PBT) blasts (Nguyen et al., 2008). In addition, SLP-76 microclusters arise in the distal regions of the T cell–B cell conjugates induced by antigenic peptides or superantigens, and these microclusters accumulate in the centers of the associated synapses, even when exogenous SLP-76 is absent (Yokosuka et al., 2005; Bunnell et al., 2006; Purbhoo et al.,

Journal of Cell Science (2021) 134, jcs258602. doi:10.1242/jcs.258602

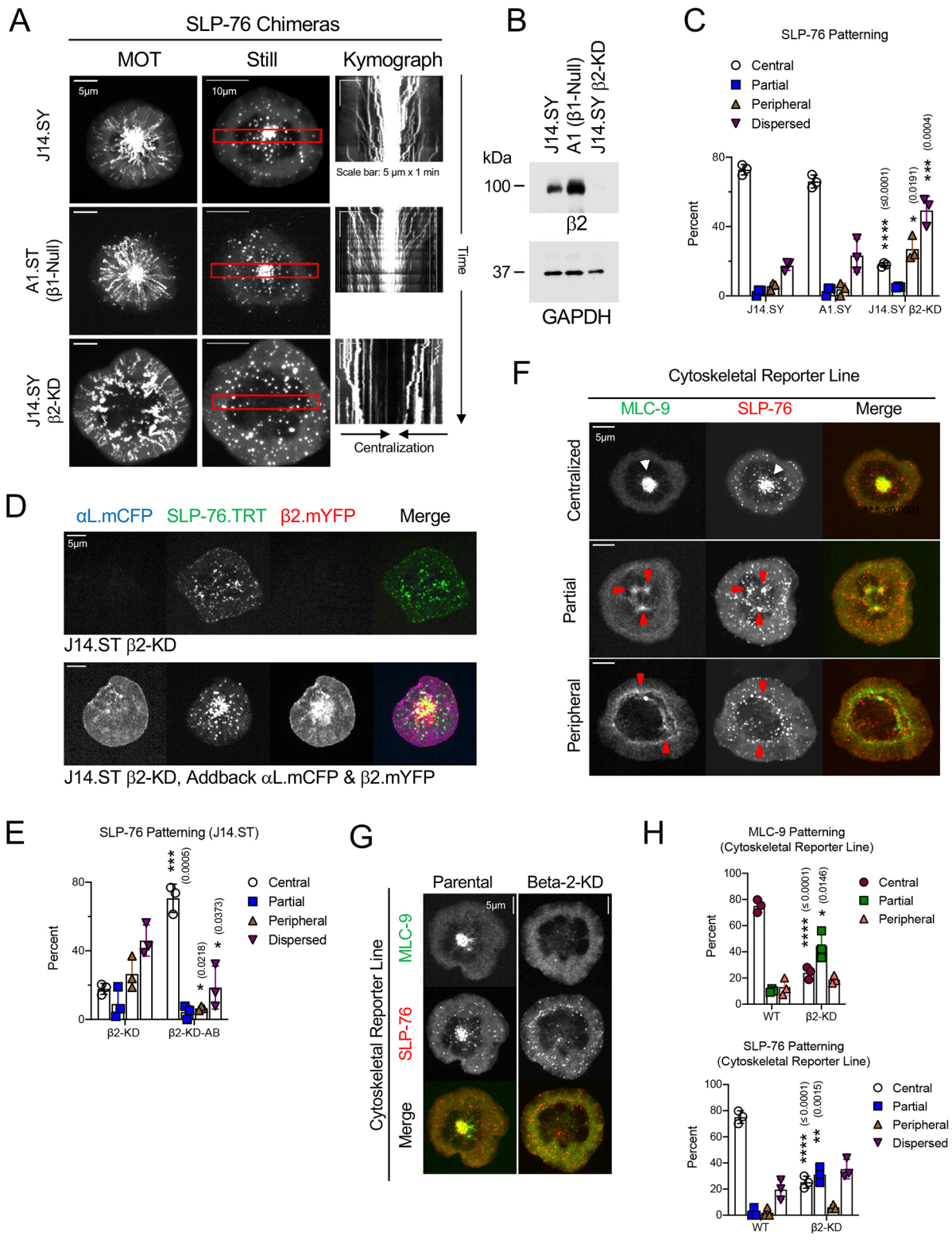


**Fig. 4. LFA-1 governs the centralization of TCR-induced SLP-76 microclusters and myosin filaments.** (A) J14.SY cells, A1.ST cells and J14.SY β2-KD J14.SY cells were stimulated as in Fig. 1A and images were collected every 2 s for 150 frames (5 min). Representative still images and MOT projections are shown; kymographs derive from the indicated regions. (B,C) The indicated cell lines were blotted for β2 and GAPDH (B) or were prepared as in Fig. 1A and scored for SLP-76 microcluster localization (C). Mean scores±s.e.m. are shown ($n$=3). (D,E) J14.ST β2-KD were transfected with the indicated vectors and prepared and scored as in C. (D) Representative images and (E) mean scores±s.e.m. are shown ($n$=3). (F–H) Parental and β2-KD J14.SY-CRL cells were prepared and scored as in C. (F) Cells representing the indicated myosin phenotypes are shown. White arrowheads indicate centrally located pools of MLC-9 and SLP-76; red arrowheads highlight peripheral features. (G) Representative images and (H) mean scores±s.e.m. are shown ($n$=3). Replicates include ≥10 cells per condition, differences from the parental line are shown. *$P$<0.05, **$P$<0.01, ***$P$<0.001, ****$P$<0.0001 [post-hoc Bonferroni corrected tests versus J14.SY cells (C), J14.ST β2-KD cells (E), or wild-type J14.SY-CRL cells (H) are shown where one-way ANOVA tests confirm significant differences between groups].

Journal of Cell Science (2021) 134, jcs258602. doi:10.1242/jcs.258602

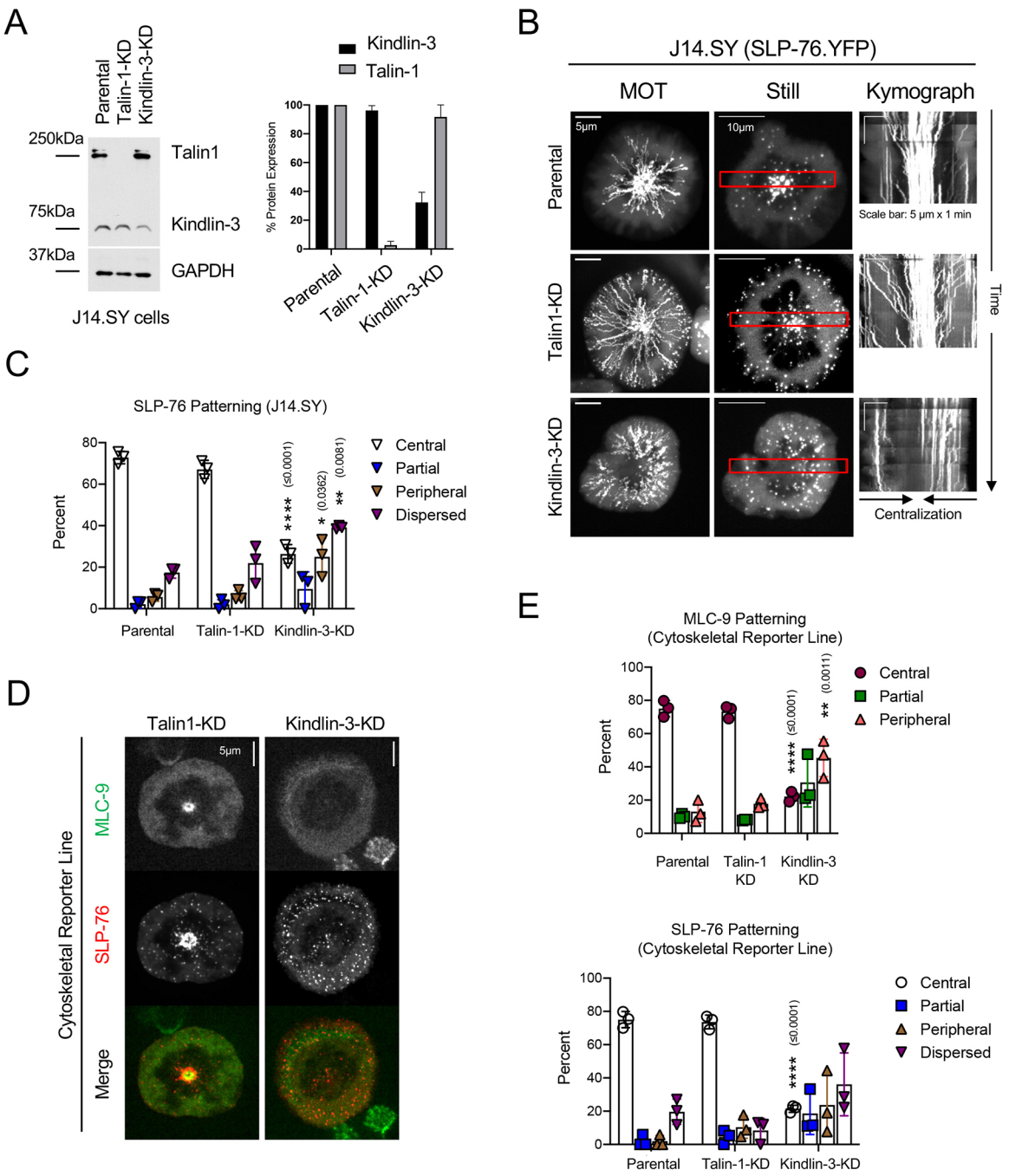


**Fig. 5. Kindlin-3, but not talin-1, regulates the centralization of TCR-induced SLP-76 microclusters and myosin filaments.** (A–C) Talin-1 and kindlin-3 were stably knocked down in three independent batches of J14.SY cells. (A) Quantification of knockdown efficiency. The western blot is representative and densitometry shows the mean±s.e.m. over three derivations. (B) Cells were stimulated, imaged and displayed as in Fig. 4A. (C) Cell lines were stimulated as in B, fixed after 7 min, imaged, and scored for location of SLP-76 microclusters as in Fig. 4. The mean±s.e.m. is shown ($n$=3). (D,E) Talin-1 and kindlin-3 were stably knocked down in J14.SY-CRL cells as in A. Cells were stimulated, fixed, imaged, and scored as in Fig. 4. (D) Representative images and (E) mean scores±s.e.m. are shown ($n$=3). Replicates include ≥10 cells per condition, differences from the parental line are shown. *$P$<0.05, **$P$<0.01, ****$P$<0.0001 [post-hoc Bonferroni corrected tests versus parental J14.SY cells (C) or J14.SY-CRL cells (E) are shown where one-way ANOVA tests confirm significant differences between groups].

2010; Roybal et al., 2015). The levels of SLP-76 that support sustained centripetal movements can be as low as 2.3-fold above those in the parental Jurkat E6.1 cell line. Comparable and greater increases in SLP-76 expression accompany the reactivation of human memory T cells and the activation of primary murine T cells by antigen (Clements et al., 1998; Hussain et al., 2002). Thus, physiological increases in SLP-76 expression could contribute to the centralization of microclusters and contractile actomyosin filaments in primary T cells. TCR-transgenic $CD8^+$ T cell blasts activated via high-quality ligands generate actomyosin arcs that are displaced towards the center of the immune synapse, partially separate from the distal actin cytoskeleton, and ultimately define the central domain in which TCR microclusters accumulate (Hong et al., 2017). Human T cell blasts stimulated on high-density TCR ligands develop ‘purse string’ like myosin structures that are also capable of separating from distal myosin filaments (Fig. S2A).



Journal of Cell Science

Journal of Cell Science (2021) 134, jcs258602. doi:10.1242/jcs.258602

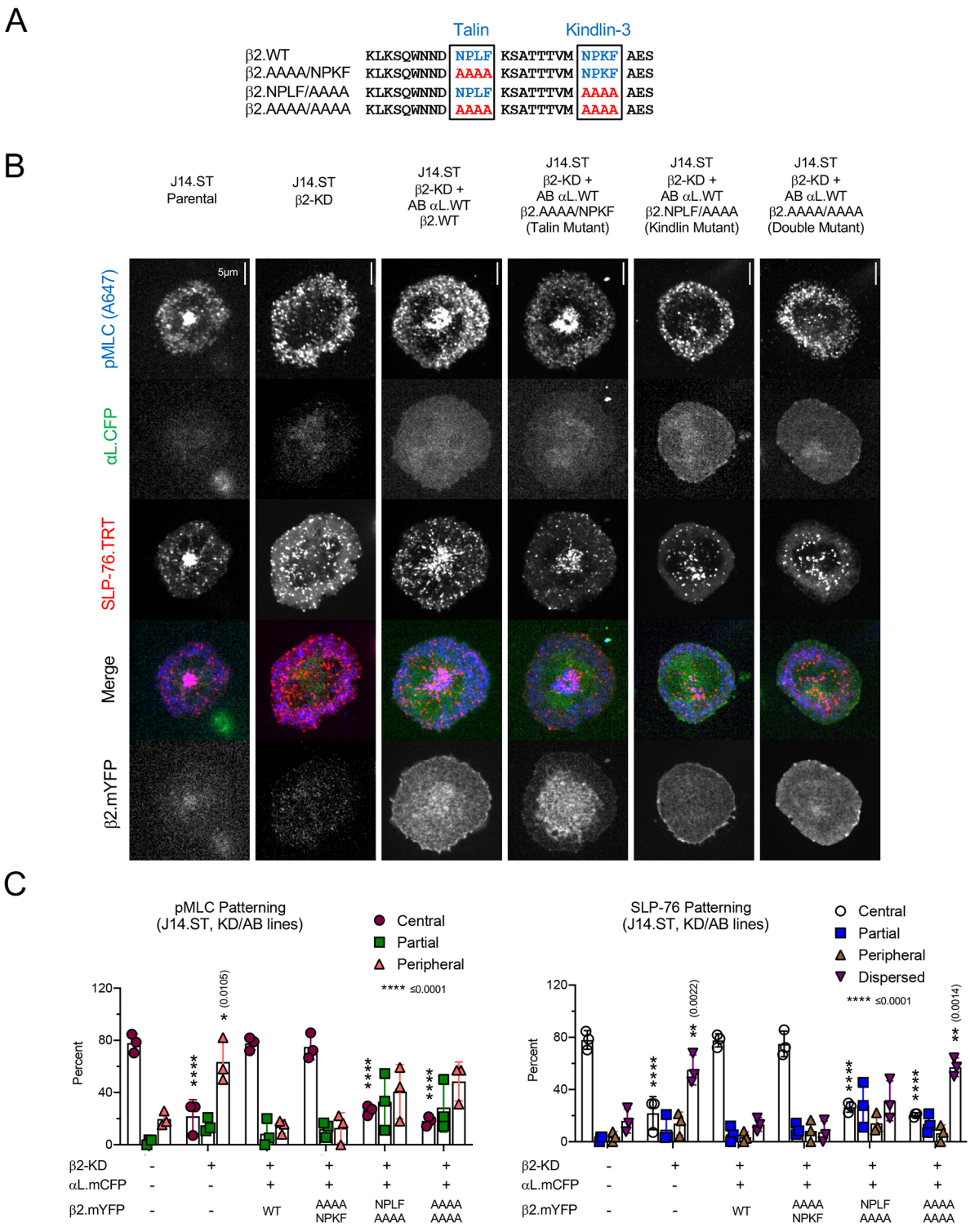


**Fig. 6. The distal NPKF binding motif in the β2 integrin cytoplasmic tail controls SLP-76 centralization and central myosin organization.** (A) Mutated binding motifs in the β2 integrin tail. (B,C) J14.ST β2-KD cells were transfected with wild-type αL.mCFP and mutant versions of β2.mYFP, stimulated on substrates coated with anti-CD3 (10 μg ml$^{-1}$), fixed after 7 min, and stained for pMLC. Cells were imaged and scored as in Fig. 4. (B) Representative images and (C) mean scores±s.e.m. are shown ($n$=3). Replicates include ≥10 cells per condition, differences from the parental line are shown. $^{**}P$<0.01, $^{****}P$<0.0001 (post-hoc Bonferroni corrected tests versus parental J14.ST cells are shown where one-way ANOVA tests confirm significant differences between groups).

These events closely parallel the formation of a central pool of SLP-76 microclusters bounded by a distinct inner ring of contractile myosin (Fig. 1B; Fig. S1D). The critical role of SLP-76 in these processes may be mediated via ADAP, as mutations that disrupt the interaction of ADAP with SLP-76 cause the immobilization and premature termination of SLP-76 microclusters and prevent the segregation of immune synapses into well-defined central and peripheral domains (Wang et al., 2004; Lewis et al., 2018). Thus,

Journal of Cell Science (2021) 134, jcs258602. doi:10.1242/jcs.258602

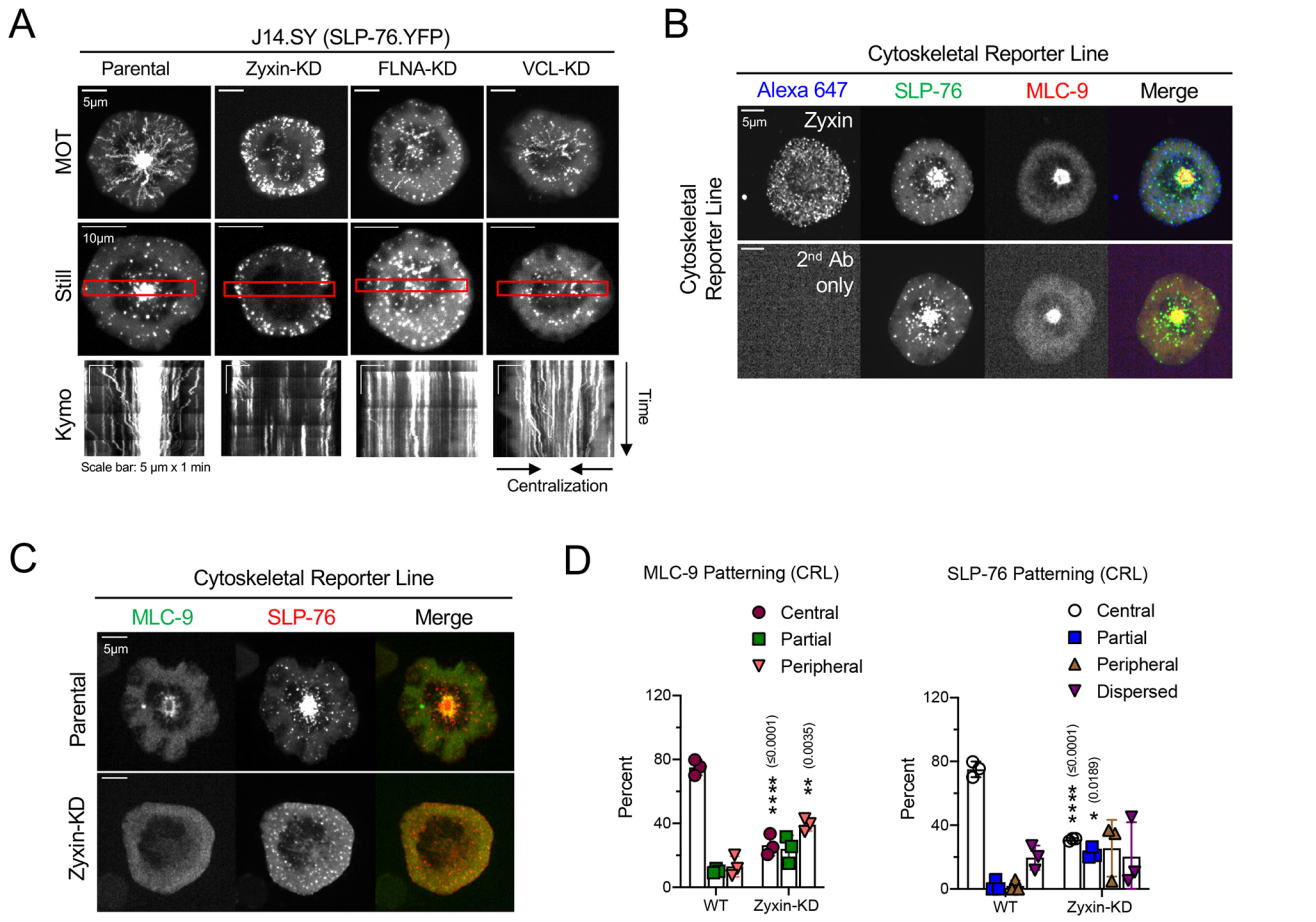


**Fig. 7. The actin associated protein zyxin is required for SLP-76 microcluster centralization and the central organization of myosin.** (A) Zyxin, Filamin-A (FLNA), and Vinculin (VCL) were stably knocked down in three independent batches of J14.SY cells. Cells were stimulated, imaged, and displayed as in Fig. 4A. (B) J14.SY-CRL cells were stimulated as in A, fixed after 7 min, and stained for zyxin. Representative images are shown. (C-D) J14.SY-CRL cells lacking zyxin were stimulated, fixed, and imaged as in B, and scored as in Fig. 4. (C) Representative images and (D) mean scores±s.e.m. are shown ($n$=3). Replicates include ≥10 cells per condition. *$P$<0.05, **$P$<0.01, ****$P$<0.0001 (post-hoc Bonferroni corrected tests versus parental J14.SY-CRL cells are shown where one-way ANOVA tests confirm significant differences between groups).

the formation of a well-defined cSMAC by agonist-stimulated effector T cells may require the compaction of contractile actomyosin structures by SLP-76- and ADAP-dependent processes (Grakoui et al., 1999; Schubert et al., 2012).

The spoke-like actomyosin filaments observed in SLP-76-expressing cells are oriented in a manner that could support the centripetal transport of SLP-76 microclusters via contraction along the long axis of these filaments. However, this would not explain the dependence of the central accumulation of TCR and SLP-76 microclusters on dynein motors and the microtubule cytoskeleton (Bunnell et al., 2002; Hashimoto-Tane et al., 2011). Based on our findings, we propose that SLP-76 centralization involves three distinct phases (Fig. S8A). In the first phase, SLP-76 microclusters are transported through the dSMAC via interactions with lamellipodial actin flows (Ditlev et al., 2019). In the second phase, SLP-76 microclusters engage dynein motors, but their movements through the pSMAC are constrained by interactions with slowly contracting actomyosin arcs (Murugesan et al., 2016). Finally, SLP-76 microclusters reach the inner boundary of the pSMAC and transition to a dynein-dependent mode that involves either their release from actomyosin arcs or the deformation of these arcs towards the center of the synapse. In the latter case, actomyosin spokes evolve from arcs experiencing centripetal forces applied by dynein motors. In this model, SLP-76 enhances the recruitment of dynein to the peripheral actomyosin system via the dynein-binding adapter ADAP, favoring arc deformation (Combs et al., 2006). The SLP-76-dependent coupling of dynein motors to lamellar actomyosin networks may also provide a platform for MTOC polarization and the maintenance of synaptic symmetry (Liu et al., 2013; Nath et al., 2016; Maskalenko et al., 2020). Thus, the movement of SLP-76 microclusters may provide insights into synapse stability, kinapse formation via symmetry breaking, and microtubule-dependent processes that support T cell signaling and cytolytic function. These systems might also be exploited to stabilize synapses and augment the effector functions of CAR T cells (Mayya et al., 2018, 2019).

VLA-4 and LFA-1 are specialized for distinct functions, such as rolling adhesion and synapse formation (Chigaev and Sklar, 2012). Here, we report that the suppression of β2 integrin mimics the suppression of myosin IIA and IIB and impairs the centripetal movement of microclusters and actomyosin filaments, even though the elimination of β1 integrin has no such effect. This unique role for LFA-1 may reflect its ability to stimulate the formation of lamellum-like ‘actin clouds’ via the adaptor ADAP (Suzuki et al., 2007). In addition, the loss of kindlin-3 impairs the adhesive function of LFA-1 to a greater extent than loss of VLA-4 (Manevich-

Journal of Cell Science (2021) 134, jcs258602. doi:10.1242/jcs.258602

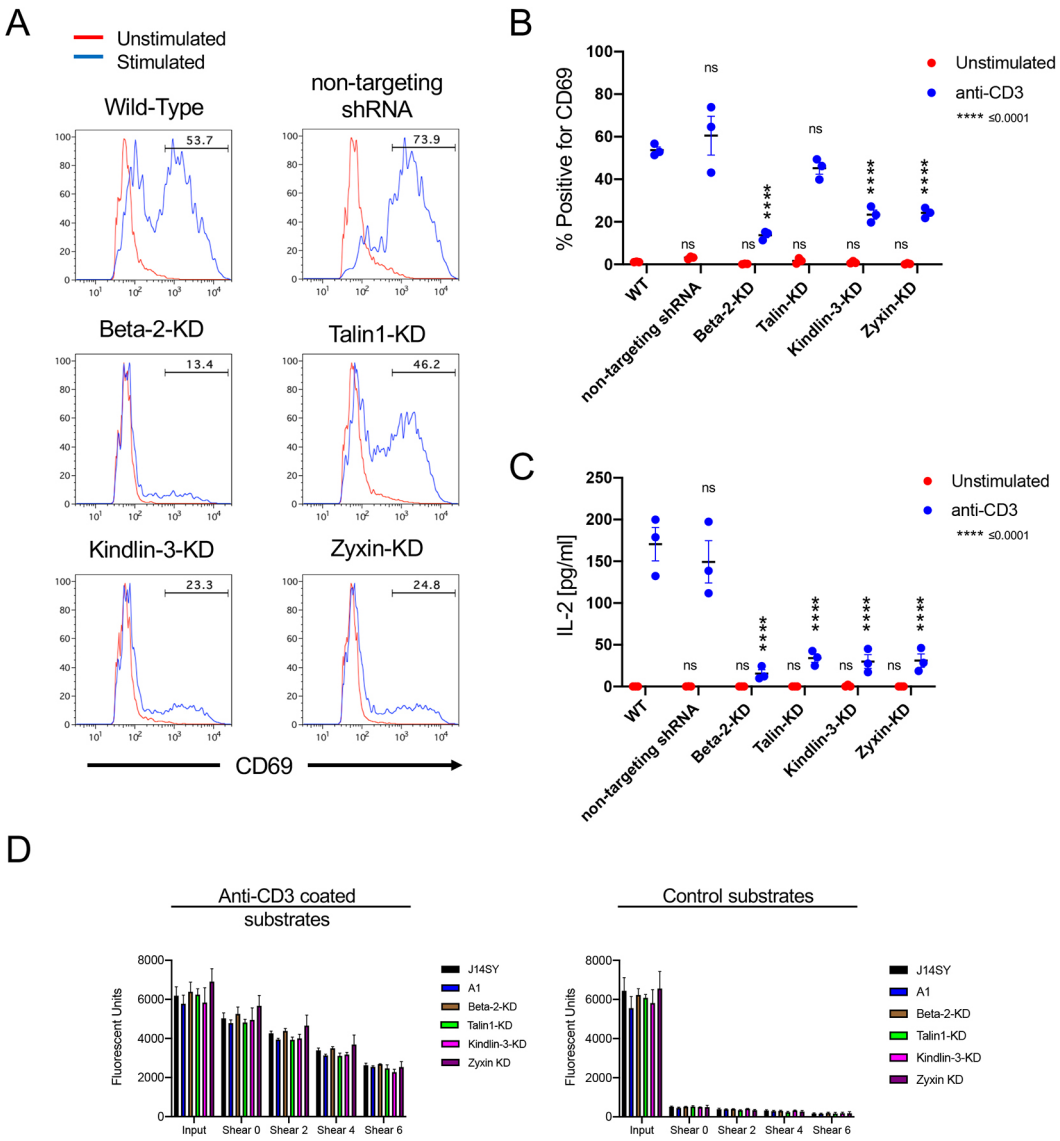


**Fig. 8. Proteins implicated in SLP-76 microcluster transport and myosin organization regulate TCR proximal signals.** (A–C) J14.SY cells and shRNA-expressing derivatives were stimulated as in Fig. 1A. Cells and supernatants were harvested after 24 h. (A) Representative histograms of CD69 expression (*x*-axis is CD69 intensity; *y*-axis is scaling is percent of maximum cell density). The bracketed region identifies cells staining positive for CD69. (B) CD69 expression and (C) IL-2 secretion are shown as the mean±s.e.m. (*n*=3, each in triplicate). Significant differences from the parental cell line are shown. ns, not significant; ****$P$<0.0001 (two-way ANOVA tests yielded significant differences by cell type and stimulation condition; post-hoc Bonferroni corrected comparisons with the parental J14.SY line are shown). (D) Fluorescently labeled J14.SY cells, A1 cells, and the indicated J14.SY derivatives were tested for retention on stimulatory and control substrates prepared as in A. Retained fluorescence was recorded after cycles of increasing shear force. The mean±s.e.m. is shown (*n*=3, each in triplicate). Two-way ANOVA tests were performed for shear and cell type using the Geisser–Greenhouse correction for matched samples; no differences were observed as a function of cell type.

Mendelson et al., 2009; Feigelson et al., 2011). Thus, the unique functions of LFA-1 might also reflect the preferential usage of specific effectors.

Although VLA-4 and LFA-1 both restrict the inward flow of actin when they encounter immobile ligands, VCAM-1 favors the immobilization of myosin filaments and SLP-76 microclusters in the extreme periphery of the contact, whereas ICAM-1 favors the retention of these structures in the pSMAC (Nguyen et al., 2008; Comrie et al., 2015b; Jankowska et al., 2018). The latter effect requires high doses of ICAM-1, most likely due to the limited expression of LFA-1 on Jurkat T cells (Jankowska et al., 2018). However, the distinct impacts of VLA-4 and LFA-1 on SLP-76 microclusters may reflect differences in their distributions, as high-affinity LFA-1 associates with actomyosin arcs, whereas the open form of VLA-4 is enriched in lamellipodia (Fig. S8B) (Mittelbrunn et al., 2004; Hyun et al., 2009; Yi et al., 2012; Murugesan et al., 2016).

In the absence of exogenously added integrin ligands, β2 integrin and kindlin-3 are required for the centripetal movement of SLP-76 microclusters and contractile myosin filaments, while β1 integrin and talin-1 are dispensable. This is consistent with the role of kindlin-3 in the centripetal movement of TCR microclusters and with the observation that the ‘tandem dimer’ (TD) variant of SKAP55 reconstitutes the centralization of contractile myosin filaments and SLP-76 microclusters, even though it can neither recruit talin-1 nor initiate integrin-dependent adhesion (Ophir et al.,

2013; Kondo et al., 2017). These findings are incompatible with conventional models of integrin activation, where integrins transition from a closed configuration ($E^{-}H^{-}$), to an extended, talin-dependent state ($E^{+}H^{-}$), and then to a kindlin-dependent extended, high-affinity configuration ($E^{+}H^{+}$). However, LFA-1 can progress to the $E^{+}H^{+}$ state via a kindlin-dependent high-affinity configuration that does not extend fully ($E^{-}H^{+}$) (Lefort et al., 2012; Fan et al., 2016, 2019; Wen et al., 2021). Since kindlin-3 might be directly recruited into SLP-76 microclusters via ADAP, this $E^{-}H^{+}$ state may be achievable even when SKAP55 is replaced with the talin-nonbinding TD chimera, described above (Kasirer-Friede et al., 2014). Subsequently, LFA-1 in the $E^{-}H^{+}$ state must couple SLP-76 microclusters to force-generating cytoskeletal systems, such as actomyosin arcs. Since dynein plays roles in both microcluster and actomyosin transport, and binds to ADAP, the $E^{-}H^{+}$ state might also influence synaptic architecture by facilitating the peripheral capture of microtubules or the loading of microcluster-bound dynein motors onto microtubules (Combs et al., 2006; Yi et al., 2013; Byron et al., 2015). Another important feature of this model is its ability to explain the preferential centralization of high-affinity ($mAb24^{+}$) LFA-1 relative to extended ($Kim127^{+}$) LFA-1 in T cell–B cell conjugates, as LFA-1 in the $E^{-}H^{+}$ state engages ICAM-1 in *cis* and would be expected to experience less resistance to lateral movement (Comrie et al., 2015a,b; Fan et al., 2016, 2019).

Although signaling via centralized signaling complexes is ultimately terminated, the mechanical forces generated during microcluster transport contribute to T cell activation (Udagawa and McIntyre, 1996; Lee et al., 2003; Mossman et al., 2005; Varma et al., 2006; Ilani et al., 2009; Vardhana et al., 2010; Judokusumo et al., 2012; Kumari et al., 2012; Murugesan et al., 2016; Hong et al., 2017; Jankowska et al., 2018). Here, we demonstrate that factors required for the deformation of the cortical actomyosin system and the centripetal transport of SLP-76 microclusters, namely, LFA-1, kindlin-3, and zyxin, are required to upregulate CD69. In contrast, talin-1, which plays no role in these transport processes, has no impact on CD69 expression. Our work provides useful insights into animal models, where a kindlin-3-binding site in β2 integrin is required for optimal CD69 expression, even though talin-1 is dispensable for this event (Wernimont et al., 2011; Morrison et al., 2015). Our findings also highlight the unique roles of LFA-1 and kindlin-3 in the dynein-dependent centripetal movements of actomyosin arcs and SLP-76 microclusters, and link these transport processes to subsequent TCR-proximal signaling events. The tensile forces exerted during these processes may drive changes in gene expression via mechano-sensitive pathways, including the phosphorylation of CasL and the nuclear translocation of MRTF-A (Yu et al., 2012; Hong et al., 2017; Guenther et al., 2019). The resolution of these issues will clarify the role of mechano-transduction in immune cell activation and will shed light on how myosin II inhibitors, which are being explored as therapies for multiple human diseases, are likely to impact immune cell function (Bond et al., 2013; Orgaz et al., 2020; Naydenov et al., 2021).

## MATERIALS AND METHODS

### Reagents

All antibodies were from commercial vendors and bound the expected targets when used at the indicated dilutions as verified using knockdowns, mutant cell lines and chimeric proteins. Antibodies used for immunofluorescence (IF), flow cytometry (FACS) and western blotting (WB) were against: myosin IIA (Poly19098, Biolegend #909801, San Diego, CA; IF 1:500, FACS 1:2500, WB 1:2000) and myosin IIB (Sigma #M7939, St Louis, MO; IF 1:200, FACS 1:2500, WB 1:1000). Goat-anti-rabbit-IgG conjugated to Alexa Fluor 647 (Invitrogen, #A21245, Carlsbad, CA) was used at 1:1000 for immunofluorescence and flow cytometry. Antibodies used for immunofluorescence were against: integrin α4 [Chemicon #CBL485Z (44H6), Burlington, MA; 1:100], phospho-myosin light chain 2 (Ser19) [Cell Signaling Technology (CST) #3675, Danvers, MA; 1:50], talin-1 [Sigma #T3287 (8D4); 1:500], zyxin (Thermo Fisher Scientific #PA5-78236, Waltham, MA; 1:500), and goat anti-rabbit-IgG conjugated to Alexa Fluor 568 (Invitrogen #A11036, Carlsbad, CA; 1:1000), goat anti-mouse-IgG conjugated to Alexa Fluor 647 (Invitrogen #A21240; 1:1000), and goat-anti-mouse-IgG1 conjugated to Alexa Fluor 647 (Invitrogen #A21240; 1:1000). Antibodies used for western blotting were against: integrin β2 [CST #73663S (D4N5Z); 1:1000], GADPH [CST #2118S (14C10); 1:1000], *Aequorea victoria* GFP [Clontech #632381 (JL-8); 1:2000], kindlin-3 [CST #13843S; 1:1000], talin-1 [CST #4021S (C45F1); 1:1000], zyxin (CST #3553S; 1:1000), SLP-76 (CST #4958S;1:1000), and goat anti-rabbit-IgG conjugated to HRP (Thermo Fisher Scientific PI31462; 1:10,000), goat anti-mouse-IgG conjugated to HRP (Thermo Fisher Scientific PI31432; 1:10,000), and goat anti-rabbit-IgG conjugated to DyLight800 (CST #5151P; 1:30,000). Antibodies used for flow cytometry include: CD69-A647 [Biolegend #310918 (FN50); 1:20], CD3-PE [BD Pharmingen, San Diego, CA, #555333 (UCHT1); 1:8), CD29-APC (BD Pharmingen #561794 (MAR4); 1:20] and CD18-APC [BD Pharmingen 551060 (6.7); 1:20]. T cells were stimulated using anti-CD3ε (OKT3) and anti-CD28 (9.3) from BioXCell (Lebanon, NH). Anti-CD43 (BD Pharmingen #555474 (1G10)] was used to promote adhesion without triggering T cell activation. Recombinant human VCAM-1 (862-VC-100) and ICAM-1 (720-IC-050) were from R&D Systems (Minneapolis, MN). Para-amino-blebbistatin (DR-AM-89) was from OptoPharma (Budapest, Hungary). Blebbistatin (BML-EI315), H1152 (ALX-270-423), and Y27632 (BML-EI299) were from Enzo Life Sciences (Farmingdale, NY). SMIFH2 (S4826), CK666 (SML0006), and EHNA (E114) were from Sigma. Colchicine (64-86-8) was from Cayman Chemical (Ann Arbor, MI). Linear polyethylenimine 25,000 (23966-2) was from Polysciences Inc. (Warrington, PA).

### Vectors and recombinant DNA

Lentiviral shRNA expression vectors targeting α-actinin-1 (TRCN0000055827), α-actinin-4 (TRCN0000055784), β2 integrin (TRCN0000236135), filamin-A (TRCN0000062528), kindlin-3 (TRCN0000431404), myosin IIB (TRCN0000123074), SKAP55 (TRCN0000006369), talin-1 (TRCN0000123104), vinculin (TRCN0000116755), and zyxin (TRCN0000286232) were purchased from Sigma. The lentiviral packaging vector psPAX2 (Addgene #12260) the VSV.G pseudotyping vector pMD2.G (Addgene #12259) were deposited by Didier Trono. The RFP-marked shRNA expression vector was created by subcloning mRFP1 (Roger Tsien, UCSD, USA) into the Clontech EGFP-n1 backbone, generating CMV-mRFP1-n1. The H1 promoter-driven shRNA expression cassette targeting human myosin IIA was assembled by annealing oligonucleotides NRS801 through NRS804 and subcloning the resulting insert into the BglII and HindIII sites of pFRT.H1p (Dan Billadeau, Mayo Clinic, USA). The entire H1-shRNA cassette was amplified by PCR using primers NRS753 and NRS754. The resulting PCR product was cut with AseI and NdeI and was installed into the AseI site upstream of the CMV promoter in mRFP1-n1, yielding the vector H1p-shMYH9/CMV-mRFP-n1. The lentiviral vector used to expresses SLP-76.YFP has been described previously; the lentiviral vector used to expresses SLP-76.TRT was developed from the former vector by replacing YFP with TagRFP-Turbo from TRT-n1 (Lewis et al., 2018). The lentiviral vector used to express F-Tractin.mRuby3 and mTurquoise.MLC-9 was developed by Tobias Meyer (Addgene #85146) (Hayer et al., 2016). The pEYFP-Tubulin vector encoding a tagged form human α-tubulin was obtained from Clontech (#6118-1). The vectors expressing EGFP-tagged forms of human myosin IIA and IIB were from Addgene (Addgene #11347 and #11348) deposited by by Robert Adelstein (Wei and Adelstein, 2000). Vectors expressing β2.mYFP and αL.mCFP were provided by Timothy Springer (Harvard Medical School, Boston, MA, USA) (Kim et al., 2003). An intermediate tailless form of β2.mYFP was prepared by excising the

Journal of Cell Science (2021) 134, jcs258602. doi:10.1242/jcs.258602

region between the EcoR I and Age I sites and installing a PCR product generated using primers KPE017 and KPE018. Constructs expressing β2.mYFP tail mutants were prepared by installing synthetic gBlocks from IDT (KPEG026-028) into the tailless vector using a silent Age I site and Gibson Assembly Master Mix from New England BioLabs (E2611S). Oligonucleotide sequences are provided in Table S1.

### Cell lines, cell culture, and transient transfection

Wild-type (E6.1) Jurkat leukemic T cells were obtained from the ATCC (TIB-152). SLP-76-deficient Jurkat J14 cells was a gift of Arthur Weiss (University of California San Francisco, CA, USA). β1-deficient Jurkat A1 cells were a gift of Yoji Shimizu (University of Minnesota Medical School, USA). The J14.SY, E6.1 ZAP-70.YFP, and E6.1 EGFP.β-actin cell lines have been described previously (Bunnell et al., 2001, 2002, 2006). E6.1 YFP.Tubulin was generated by transfecting E6.1 cells with linearized pEYFP-Tubulin and selecting in neomycin. Stable cell lines were generated via the lentiviral transduction of E6.1 cells with SLP-76.YFP, J14 cells with SLP-76.TRT (J14.ST), A1 cells with SLP-76.TRT (A1.ST) or SLP-76.YFP (A1.SY), and J14.SY cells with F-Tractin.mRuby3-P2A-mTurquoise.MLC-9 (J14.SY-CRL). Stable knockdown lines were generated via the transduction of J14.SY, J14.ST, or J14.SY-CRL cells with lentiviral particles targeting β2, SKAP55, talin-1, kindlin-3, zyxin, filamin-A, vinculin, α-actinin-1, or α-actinin-4. J14.SY cells lacking SKAP55 are referred to as JSKAP.SY cells. Knockdown lines were routinely re-derived to minimize adaptations to the loss of these proteins. Jurkat T cells and their derivatives were maintained in RPMI-1640 medium supplemented with 10% fetal bovine serum, 2 mM L-glutamine and 10 µg ml$^{-1}$ ciprofloxacin ('complete RPMI'). Transient transfections were performed using an ECM 830 electroporator (BTX), as described previously (Bunnell et al., 2006). HEK 293T cells were obtained from Lawrence Samelson (NIH) and maintained in DMEM supplemented with 10% fetal bovine serum (FBS), 2 mM L-glutamine, 100 units ml$^{-1}$ of penicillin and 100 µg ml$^{-1}$ of streptomycin, as described previously (Lewis et al., 2018). All cell lines retain, lack or express the expected proteins and chimeras, as assessed by western blotting, flow cytometry and imaging.

### Isolation and culturing of primary human T cells

Primary human T cells were isolated from human blood obtained commercially via New York Biologics. All samples were de-identified and acquired from consenting donors. Briefly, human primary CD4$^+$ and CD8$^+$ T cells were isolated from blood through an initial 30 min incubation with CD4$^+$ and CD8$^+$ human T cell Enrichment cocktails (Stem Cell Technologies, Cambridge, MA cat 15062 and 15063). Following this initial incubation, cells were diluted 1:1 in PBS and 2% FBS followed by Ficoll separation via centrifugation (1200 ***g*** for 20 min, no brake). Buffy coat layers were removed, diluted in PBS with 2% FBS, centrifuged (300 ***g*** for 10 min, low brake), and cultured in complete RPMI (see above) at a density of $10^6$ cells ml$^{-1}$ on tissue culture-treated Petri dishes coated with anti-CD3ε OKT3 (10 µg ml$^{-1}$) and anti-CD28 (2 µg ml$^{-1}$) for 3 days. Beginning on day 2, human recombinant IL-2 (Peprotech, 200-02; Rocky Hill, NJ) was added at a concentration of 200 units ml$^{-1}$. After day 3 of plate stimulation, CD4$^+$ and CD8$^+$ human primary T cells were removed from stimulatory coated petri dishes and cultured in T75 flasks in complete RPMI plus human recombinant IL-2 (200 units ml$^{-1}$).

### Production and use of lentiviral particles

Packaging reactions used HEK 293T cells at ∼70% confluency. For each 10 cm plate, a mix of 18 µl 1 mg ml$^{-1}$ linear polyethylenimine and 502 µl serum-free DMEM was incubated at room temperature for 5 min. In parallel, lentiviral transfer vectors (3 µg) were combined with psPAX2 (1.5 µg) and pMD2.G (0.5 µg) in 40 µl of serum-free DMEM. These cocktails were combined and incubated at room temperature for 30 min before adding dropwise to 293T cells. After 12–15 h, the transfection mixture was replaced with fresh DMEM. Lentiviral supernatants were harvested 36–48 h post transfection and any residual cells were removed using 0.45 µm filters (Thermo Fisher Scientific, SLHV033). To transduce Jurkat cells, equal parts of fresh RPMI, Jurkat cells, and lentiviral supernatants were combined. After 48 h, cells in the viral media were rinsed and immediately placed into selection medium containing either puromycin (1 µg ml$^{-1}$) or zeocin (200 µg ml$^{-1}$), as appropriate. After an additional 48 h, surviving cells were rinsed into fresh RPMI.

### Cell lysis and western blotting

Jurkat cells were lysed, as described previously, in ice-cold buffer containing 20 mM Tris-HCl (pH 8.0), 150 mM NaCl, 1 mM EDTA, 1% Triton X-100, 10 mM NaF, 1 mM $Na_3VO_4$ and Complete protease inhibitor cocktail (Roche) (Lewis et al., 2018). Proteins were resolved using Nu-PAGE 4–12% Bis-Tris gels from Invitrogen (NP0336), transferred to PVDF membranes (Immobilon-P or -F; Sigma, IPVH00010 or IPFL00010), and blotted using antibodies at the concentrations indicated above. All incubations and washes were in Tris-bufferred saline (TBS, 150 mM NaCl, 50 mM Tris-HCl, pH 7.4) with 0.1% Tween-20 (TBST) with the following exceptions: blocking was performed in TBS with 5% BSA, primary antibodies were diluted in TBST with 1% BSA and 0.02% sodium azide, and fluorescently stained gels were subjected to a final rinse in TBS. Detection was performed using SuperSignal West Pico (Invitrogen, 34580) and CL-Xposure film (Thermo, PI34091) or using a Odyssey CLx imager (LI-COR Biosciences, Lincoln, NE).

### T cell stimulation on glass substrates

Imaging and functional assays were performed in glass-bottomed 96-well plates (#4953) from Matrix Technologies (Indianapolis, IN). First, plates were incubated for 15 min in 1 M HCl in 70% ethanol and dried at 42°C for 30 min. Plates were then coated with 0.01% poly-L-lysine (Sigma P8920) for 20 min and dried at 42°C for 30 min. Subsequently, plates were sequentially coated with anti-CD3ε (OKT3), typically at 10 µg ml$^{-1}$ in PBS, and then, if required, with recombinant human (rh)VCAM-1 (1 µg ml$^{-1}$), rhICAM-1 (20 µg ml$^{-1}$) or anti-CD43 (10 µg ml$^{-1}$). Each binding was performed for 1 h at 37°C. Finally, plates were blocked with 1% BSA for 1 h at 37°C. Wells were rinsed with and stored in PBS. Plates were sealed and stored at 4°C for up to 48 h before use. Cells were stimulated on these glass substrates in complete RPMI (see above) supplemented with 25 mM Hepes (Cambrex Bio Science, East Rutherford, NJ).

### Dynamic and immunofluorescence imaging

For live-cell assays, imaging plates were maintained at 37°C, as described previously (Bunnell et al., 2003); Jurkat T cells were injected into the base of the well, allowed to initiate contacts, and then imaged at regular intervals for the indicated lengths of time. For fixed cell studies, Jurkat T cells were plated onto stimulatory substrates, allowed 7 min at 37°C to attach and spread, fixed in 1% PFA for 30 min at 37°C and rinsed with PBS. For immunofluorescence studies, all subsequent steps were performed in PBS supplemented with 0.1% saponin. Cells were then blocked in buffer containing 10% calf serum and 2% goat serum for 1 h at room temperature, followed by three 5 min washes. Primary antibodies were diluted into blocking buffer and allowed to bind for 1 h at room temperature, followed by three 5-min washes. Goat-derived secondary antibodies were diluted, allowed to bind and ultimately removed in the same manner. Confocal images were acquired with a Zeiss 200 M inverted microscope, 40× NA 1.3 Plan-Neofluar or 100× NA 1.45 Plan-fluar oil immersion objectives (Carl Zeiss AG, Jena, Germany), a CSU-10 confocal spinning-disk head (Yokogawa Electric, Tokyo, Japan). Image capture was performed with an Orca ER CCD camera, an ORCA Flash 4.0 v2 camera (Hamamatsu Photonics, Hamamatsu City, Japan) or an XR MEGA-10 intensified CCD camera (Stanford Photonics, Palo Alto, CA). Fluorescent proteins were resolved as previously described (Bunnell et al., 2006). Image acquisition was managed using Perkin-Elmer Ultraview or µManager software (Edelstein et al., 2010).

### Image processing

Image data was processed using custom AppleScripts (Apple Computer, Cupertino, CA) to manage tasks performed by the open source platforms ImageJ and Fiji (Schneider et al., 2012) or by iVision scripts (iVision, Atlanta, GA). All subsequent image processing and analysis was performed

using iVision. All normalizations are linear unless otherwise stated. Dim images were routinely despeckled to reduce the impact of 'hot' camera pixels. For Fig. 1D and Fig. S5C, cells were center aligned and averaged; relative intensities are provided as a function of radial distance from the cell center. Because of variations in cell diameter, image regions in Fig. S5A were edge aligned before averaging; relative intensities are presented as a function of distance from the cell edge. All channels in Fig. 1F,G and Fig. S2B were background corrected using a rolling ball filter with a radius of 346.2 nm; in Fig. S2C–E the same filter was applied to the myosin IIA and pMLC channels, but the SLP-76 channel was not modified. The filter employed in Fig. 3G is the iVision Sharpen Hat 5×5 filter. For Fig. S2C–E, myosin IIA images were converted into binary masks by scaling images to 50 nm pixel$^{-1}$, applying a rolling ball background correction filter, then a Sobel edge filter, and subtracting the edge-filtered image from the background-corrected image. This process was iterated with rolling ball sizes from 100 nm to 350 nm, in 50 nm steps, and the resulting subtracted images were averaged. Using this averaged image, a binary mask was generated by setting thresholds as low as possible without detecting objects outside of cells. The permissive region for void detection was defined as the peripheral region of the contact minus the myosin IIA-masked region. Voids within the permissive mask were detected by sequentially searching for all possible circles with diameters of 600, 500, and finally 400 nm; after each search, the detected objects were removed from the permissive mask. All voids with eccentricities <0.9 were accepted. The outer diameter of the myosin rings surrounding these voids was determined using the point at which the myosin IIA signal falls at 90% of the distance from the peak to the second minimum. For Figs S2D,E and S5B, SLP-76 microclusters were identified using local maxima. Detailed scripts are available from the corresponding author upon request.

### TCR-mediated adhesion assay

TCR-mediated adhesion assays were performed as previously described with the exception that the initial plate-binding time was reduced to 7 min (Nguyen et al., 2008; Ophir et al., 2013). Briefly, Jurkat T cells were loaded with 4 µM BCECF-AM dye from (Invitrogen, B-1170) in Hanks' balanced salt solution (HBSS) for 30 min at 37°C and then washed three times in HBSS. $5\times10^5$ cells were added per well, in triplicate, to control or anti-CD3-coated glass wells (10 µg ml$^{-1}$) substrates that were blocked with 5% BSA. Cells were allowed to bind for 7 min at 37°C and input BCECF fluorescence was read on a SpectraMax (Molecular Devices, San Jose, CA) plate reader (488 nm excitation, 530 nm emission, 515 nm cutoff). Unbound cells were removed by gentle pipetting and replaced with fresh medium following cycles of no or increasing shear, applied for 30 s using a Vortex-Genie2 plate shaker (Fisher Scientific) at the indicated speeds. Fluorescence readings was taken after each cycle of replacement.

### T cell activation assays

Jurkat T cells were stimulated in 24-well tissue culture plates maintained in a humidified tissue culture incubator with 5% $CO_2$. Each well received $5\times10^5$ cells in a final volume of 500 µl. Prior to the addition of cells, wells were left untreated or coated with anti-CD3 (10 µg ml$^{-1}$) in PBS for 1 h at 37°C. After 24 h, supernatants were harvested and the upregulation of CD69 was measured by flow cytometry. IL-2 secretion into the supernatant was measured using the Duo Set IL-2 ELISA kit (R&D Systems, DY202-05).

### Magnetic immuno-isolation and mass spectrometry of SLP-76 microclusters

Surface-activated magnetic beads 4.5 µm in diameter (M-450 tosylactivated dynabeads, #14013) were obtained from Invitrogen and functionalized with anti-CD3 (10 µg ml$^{-1}$), anti-CD43 (10 µg ml$^{-1}$), and/or recombinant human VCAM-1 (1 µg ml$^{-1}$). Beads were then blocked in 1% BSA and residual active sites were capped via the addition of 20 mM Tris-HCl (pH 7.4). Stimulations were initiated by mixing beads and cells at 2:1 ratio, with $5\times10^7$ cells ml$^{-1}$. After a 5 min co-incubation at 37°C, cells were fixed with 0.5 mM dithiobismaleimidoethane (DTME, Thermo Fisher Scientific #22335) for 15 min. Fixed cells were disrupted by sonication in detergent-free lysis buffer, beads were captured magnetically, and washed extensively. Magnetic isolates corresponding to $2\times10^7$ cell equivalents of J14.SY cells were analyzed by Coomassie staining and individual bands were excised for in gel reduction, alkylation and trypsinization. Liquid chromatography tandem mass spectrometry (LC/MS/MS) analyses were performed using a Thermo LTQ ion trap mass spectrometer. MS/MS spectra were searched against the NCBI non-redundant protein sequence database using the SEQUEST computer algorithm.

### Software and statistical analyses

Flow cytometry data was analyzed using FlowJo software. Statistical analyses were performed using Microsoft Excel and Prism. Based on previous studies, perturbations of SLP-76 microclusters typically yield normalized effect sizes ≥2. Under these conditions $n$=3 is sufficient to incorrectly reject the null hypothesis <5% of the time, with a power of 90%. Comparable effect sizes were observed here. All stable lines of lentiviral origin were derived at least twice. Cell scoring was conducted using iVision scripts that present de-identified images for analysis. For the analysis of clustering in each cell line, each category was analyzed by one-way ANOVA; post-hoc Bonferroni corrected comparisons versus the parental line are only shown if categories pass this initial test. CD69 and IL-2 assays were analyzed by two-way ANOVA; stimulation condition and cell-type yielded significant differences; post-hoc Bonferroni corrected comparisons within the stimulation group and versus the parental line are shown. Adhesion assays were analyzed by two-way ANOVA for shear and cell type using the Geisser–Greenhouse correction for matched samples; no differences were observed as a function of cell type. Two-tailed Student's $t$-tests for unpaired samples were used to compare the radial distributions of SLP-76 in the presence or absence of myosin IIA and/or IIB. Unless noted otherwise, *$P$<0.05, **$P$<0.01, ***$P$<0.001, ****$P$<0.0001.

#### Acknowledgements

We thank M. A. Fray for visualizing EGFP-tagged forms of myosin relative to SLP-76 and R. R. Brewka for her contributions to establishing the role of myosin II in microcluster movement. We recognize Jon DeGnorre and the Tufts University Core Facility for mass spectrometry and the W. M. Keck Foundation and the Eshe Fund for generous support of core facilities at Tufts.

#### Competing interests

The authors declare no competing or financial interests.

#### Author contributions

Conceptualization: K.P.E., S.C.B.; Methodology: K.P.E., N.R.S., M.-C.S., S.C.B.; Software: S.C.B.; Validation: K.P.E., A.L., N.R.S., F.A.S., H.I.M., M.J.O., K.N., M.-C.S., S.C.B.; Formal analysis: K.P.E., A.L., N.R.S., F.A.S., H.I.M., M.J.O., K.N., M.-C.S., S.C.B.; Investigation: K.P.E., A.L., N.R.S., F.A.S., H.I.M., M.J.O., K.N., M.-C.S., S.C.B.; Resources: K.P.E., M.-C.S., S.C.B.; Data curation: K.P.E., S.C.B.; Writing - original draft: K.P.E.; Writing - review & editing: K.P.E., S.C.B.; Visualization: K.P.E., A.L., N.R.S., F.A.S., M.J.O., S.C.B.; Supervision: K.P.E., M.-C.S., S.C.B.; Project administration: S.C.B.; Funding acquisition: S.C.B.

#### Funding

This work was supported by a Brain and Immuno-Imaging Award from the Dana Foundation, a Scientist Development Grant from the American Heart Association (0635546 T), and grants from the National Institutes of Health (NIH R01 AI076575-01 and R21-AG030931). Additional support was provided by NIH T32 AI007077 (K.P.E., N.R.S., M.J.O., and K.N.), P30 NS047243 (A.L.), and T32 GM008448 (F.A.S.). Deposited in PMC for release after 12 months.

#### References

**Babich, A., Li, S., O'connor, R. S., Milone, M. C., Freedman, B. D. and Burkhardt, J. K.** (2012). F-actin polymerization and retrograde flow drive sustained PLCγ1 signaling during T cell activation. *J. Cell Biol.* **197**, 775-787. doi:10.1083/jcb.201201018

**Baker, R. G., Hsu, C. J., Lee, D., Jordan, M. S., Maltzman, J. S., Hammer, D. A., Baumgart, T. and Koretzky, G. A.** (2009). The adapter protein SLP-76 mediates "outside-in" integrin signaling and function in T cells. *Mol. Cell Biol.* **29**, 5578-5589. doi:10.1128/MCB.00283-09

**Balagopalan, L., Barr, V. A., Sommers, C. L., Barda-Saad, M., Goyal, A., Isakowitz, M. S. and Samelson, L. E.** (2007). c-Cbl-mediated regulation of LAT-nucleated signaling complexes. *Mol. Cell. Biol.* **27**, 8622-8636. doi:10.1128/MCB.00467-07

**Barda-Saad, M., Braiman, A., Titerence, R., Bunnell, S. C., Barr, V. A. and Samelson, L. E.** (2005). Dynamic molecular interactions linking the T cell antigen receptor to the actin cytoskeleton. *Nat. Immunol.* **6**, 80-89. doi:10.1038/ni1143

**Barda-Saad, M., Shirasu, N., Pauker, M. H., Hassan, N., Perl, O., Balbo, A., Yamaguchi, H., Houtman, J. C. D., Appella, E., Schuck, P. et al.** (2010). Cooperative interactions at the SLP-76 complex are critical for actin polymerization. *EMBO J.* **29**, 2315-2328. doi:10.1038/emboj.2010.133

**Barr, V. A., Sherman, E., Yi, J., Akpan, I., Rouquette-Jazdanian, A. K. and Samelson, L. E.** (2016). Development of nanoscale structure in LAT-based signaling complexes. *J. Cell Sci.* **129**, 4548-4562. doi:10.1242/jcs.194886

**Beemiller, P., Jacobelli, J. and Krummel, M. F.** (2012). Integration of the movement of signaling microclusters with cellular motility in immunological synapses. *Nat. Immunol.* **13**, 787-795. doi:10.1038/ni.2364

**Bond, L. M., Tumbarello, D. A., Kendrick-Jones, J. and Buss, F.** (2013). Small-molecule inhibitors of myosin proteins. *Future Med. Chem.* **5**, 41-52. doi:10.4155/fmc.12.185

**Braiman, A., Barda-Saad, M., Sommers, C. L. and Samelson, L. E.** (2006). Recruitment and activation of PLCγ1 in T cells: a new insight into old domains. *EMBO J.* **25**, 774-784. doi:10.1038/sj.emboj.7600978

**Bunnell, S. C., Kapoor, V., Trible, R. P., Zhang, W. and Samelson, L. E.** (2001). Dynamic actin polymerization drives T cell receptor-induced spreading: a role for the signal transduction adaptor LAT. *Immunity* **14**, 315-329. doi:10.1016/S1074-7613(01)00112-1

**Bunnell, S. C., Hong, D. I., Kardon, J. R., Yamazaki, T., Mcglade, C. J., Barr, V. A. and Samelson, L. E.** (2002). T cell receptor ligation induces the formation of dynamically regulated signaling assemblies. *J. Cell Biol.* **158**, 1263-1275. doi:10.1083/jcb.200203043

**Bunnell, S. C., Barr, V. A., Fuller, C. L. and Samelson, L. E.** (2003). High-resolution multicolor imaging of dynamic signaling complexes in T cells stimulated by planar substrates. *Sci STKE* **2003**, Pl8. doi:10.1126/stke.2003.177.pl8

**Bunnell, S. C., Singer, A. L., Hong, D. I., Jacque, B. H., Jordan, M. S., Seminario, M.-C., Barr, V. A., Koretzky, G. A. and Samelson, L. E.** (2006). Persistence of cooperatively stabilized signaling clusters drives T-cell activation. *Mol. Cell. Biol.* **26**, 7155-7166. doi:10.1128/MCB.00507-06

**Byron, A., Askari, J. A., Humphries, J. D., Jacquemet, G., Koper, E. J., Warwood, S., Choi, C. K., Stroud, M. J., Chen, C. S., Knight, D. et al.** (2015). A proteomic approach reveals integrin activation state-dependent control of microtubule cortical targeting. *Nat. Commun.* **6**, 6135. doi:10.1038/ncomms7135

**Chigaev, A. and Sklar, L. A.** (2012). Aspects of VLA-4 and LFA-1 regulation that may contribute to rolling and firm adhesion. *Front. Immunol.* **3**, 242. doi:10.3389/fimmu.2012.00242

**Choudhuri, K., Wiseman, D., Brown, M. H., Gould, K. and Van Der Merwe, P. A.** (2005). T-cell receptor triggering is critically dependent on the dimensions of its peptide-MHC ligand. *Nature* **436**, 578-582. doi:10.1038/nature03843

**Choudhuri, K., Llodrá, J., Roth, E. W., Tsai, J., Gordo, S., Wucherpfennig, K. W., Kam, L. C., Stokes, D. L. and Dustin, M. L.** (2014). Polarized release of T-cell-receptor-enriched microvesicles at the immunological synapse. *Nature* **507**, 118-123. doi:10.1038/nature12951

**Clements, J. L., Ross-Barta, S. E., Tygrett, L. T., Waldschmidt, T. J. and Koretzky, G. A.** (1998). SLP-76 expression is restricted to hemopoietic cells of monocyte, granulocyte, and T lymphocyte lineage and is regulated during T cell maturation and activation. *J. Immunol.* **161**, 3880-3889.

**Combs, J., Kim, S. J., Tan, S., Ligon, L. A., Holzbaur, E. L. F., Kuhn, J. and Poenie, M.** (2006). Recruitment of dynein to the Jurkat immunological synapse. *Proc. Natl. Acad. Sci. USA* **103**, 14883-14888. doi:10.1073/pnas.0600914103

**Comrie, W. A., Babich, A. and Burkhardt, J. K.** (2015a). F-actin flow drives affinity maturation and spatial organization of LFA-1 at the immunological synapse. *J. Cell Biol.* **208**, 475-491. doi:10.1083/jcb.201406121

**Comrie, W. A., Li, S., Boyle, S. and Burkhardt, J. K.** (2015b). The dendritic cell cytoskeleton promotes T cell adhesion and activation by constraining ICAM-1 mobility. *J. Cell Biol.* **208**, 457-473. doi:10.1083/jcb.201406120

**Coussens, N. P., Hayashi, R., Brown, P. H., Balagopalan, L., Balbo, A., Akpan, I., Houtman, J. C. D., Barr, V. A., Schuck, P., Appella, E. et al.** (2013). Multipoint binding of the SLP-76 SH2 domain to ADAP is critical for oligomerization of SLP-76 signaling complexes in stimulated T cells. *Mol. Cell. Biol.* **33**, 4140-4151. doi:10.1128/MCB.00410-13

**Ditlev, J. A., Vega, A. R., Köster, D. V., Su, X., Tani, T., Lakoduk, A. M., Vale, R. D., Mayor, S., Jaqaman, K. and Rosen, M. K.** (2019). A composition-dependent molecular clutch between T cell signaling condensates and actin. *eLife* **8**, e42695. doi:10.7554/eLife.42695

**Dushek, O., Goyette, J. and Van Der Merwe, P. A.** (2012). Non-catalytic tyrosine-phosphorylated receptors. *Immunol. Rev.* **250**, 258-276. doi:10.1111/imr.12008

**Dustin, M. L.** (2008). Hunter to gatherer and back: immunological synapses and kinapses as variations on the theme of amoeboid locomotion. *Annu. Rev. Cell Dev. Biol.* **24**, 577-596. doi:10.1146/annurev.cellbio.24.110707.175226

**Edelstein, A., Amodaj, N., Hoover, K., Vale, R. and Stuurman, N.** (2010). Computer control of microscopes using μManager. *Curr. Protoc. Mol. Biol.* **92**, 14.20.1-14.20.17. doi:10.1002/0471142727.mb1420s92

**Fan, Z., Mcardle, S., Marki, A., Mikulski, Z., Gutierrez, E., Engelhardt, B., Deutsch, U., Ginsberg, M., Groisman, A. and Ley, K.** (2016). Neutrophil recruitment limited by high-affinity bent β2 integrin binding ligand in cis. *Nat. Commun.* **7**, 12658. doi:10.1038/ncomms12658

**Fan, Z., Kiosses, W. B., Sun, H., Orecchioni, M., Ghosheh, Y., Zajonc, D. M., Arnaout, M. A., Gutierrez, E., Groisman, A., Ginsberg, M. H. et al.** (2019). High-affinity bent β2-integrin molecules in arresting neutrophils face each other through binding to ICAMs in cis. *Cell Rep.* **26**, 119-130.e5. doi:10.1016/j.celrep.2018.12.038

**Feigelson, S. W., Grabovsky, V., Manevich-Mendelson, E., Pasvolsky, R., Shulman, Z., Shinder, V., Klein, E., Etzioni, A., Aker, M. and Alon, R.** (2011). Kindlin-3 is required for the stabilization of TCR-stimulated LFA-1:ICAM-1 bonds critical for lymphocyte arrest and spreading on dendritic cells. *Blood* **117**, 7042-7052. doi:10.1182/blood-2010-12-322859

**Freiberg, B. A., Kupfer, H., Maslanik, W., Delli, J., Kappler, J., Zaller, D. M. and Kupfer, A.** (2002). Staging and resetting T cell activation in SMACs. *Nat. Immunol.* **3**, 911-917. doi:10.1038/ni836

**Fritzsche, M., Fernandes, R. A., Chang, V. T., Colin-York, H., Clausen, M. P., Felce, J. H., Galiani, S., Erlenkämper, C., Santos, A. M., Heddleston, J. M. et al.** (2017). Cytoskeletal actin dynamics shape a ramifying actin network underpinning immunological synapse formation. *Sci. Adv.* **3**, e1603032. doi:10.1126/sciadv.1603032

**Grakoui, A., Bromley, S. K., Sumen, C., Davis, M. M., Shaw, A. S., Allen, P. M. and Dustin, M. L.** (1999). The immunological synapse: a molecular machine controlling T cell activation. *Science* **285**, 221-227. doi:10.1126/science.285.5425.221

**Griffiths, E. K., Krawczyk, C., Kong, Y.-Y., Raab, M., Hyduk, S. J., Bouchard, D., Chan, V. S., Kozieradzki, I., Oliveira-Dos-Santos, A. J., Wakeham, A. et al.** (2001). Positive regulation of T cell activation and integrin adhesion by the adapter Fyb/Slap. *Science* **293**, 2260-2263. doi:10.1126/science.1063397

**Guenther, C., Faisal, I., Uotila, L. M., Asens, M. L., Harjunpää, H., Savinko, T., Öhman, T., Yao, S., Moser, M., Morris, S. W. et al.** (2019). A β2-Integrin/MRTF-A/SRF pathway regulates dendritic cell gene expression, adhesion, and traction force generation. *Front. Immunol.* **10**, 1138. doi:10.3389/fimmu.2019.01138

**Hammer, J. A., III and Burkhardt, J. K.** (2013). Controversy and consensus regarding myosin II function at the immunological synapse. *Curr. Opin. Immunol.* **25**, 300-306. doi:10.1016/j.coi.2013.03.010

**Hammer, J. A., Wang, J. C., Saeed, M. and Pedrosa, A. T.** (2019). Origin, organization, dynamics, and function of actin and actomyosin networks at the T Cell immunological synapse. *Annu. Rev. Immunol.* **37**, 201-224. doi:10.1146/annurev-immunol-042718-041341

**Hashimoto-Tane, A., Yokosuka, T., Sakata-Sogawa, K., Sakuma, M., Ishihara, C., Tokunaga, M. and Saito, T.** (2011). Dynein-driven transport of T cell receptor microclusters regulates immune synapse formation and T cell activation. *Immunity* **34**, 919-931. doi:10.1016/j.immuni.2011.05.012

**Hashimoto-Tane, A., Sakuma, M., Ike, H., Yokosuka, T., Kimura, Y., Ohara, O. and Saito, T.** (2016). Micro-adhesion rings surrounding TCR microclusters are essential for T cell activation. *J. Exp. Med.* **213**, 1609-1625. doi:10.1084/jem.20151088

**Hayer, A., Shao, L., Chung, M., Joubert, L.-M., Yang, H. W., Tsai, F.-C., Bisaria, A., Betzig, E. and Meyer, T.** (2016). Engulfed cadherin fingers are polarized junctional structures between collectively migrating endothelial cells. *Nat. Cell Biol.* **18**, 1311-1323. doi:10.1038/ncb3438

**Hong, J., Murugesan, S., Betzig, E. and Hammer, J. A.** (2017). Contractile actomyosin arcs promote the activation of primary mouse T cells in a ligand-dependent manner. *PLoS ONE* **12**, e0183174. doi:10.1371/journal.pone.0183174

**Houtman, J. C. D., Yamaguchi, H., Barda-Saad, M., Braiman, A., Bowden, B., Appella, E., Schuck, P. and Samelson, L. E.** (2006). Oligomerization of signaling complexes by the multipoint binding of GRB2 to both LAT and SOS1. *Nat. Struct. Mol. Biol.* **13**, 798-805. doi:10.1038/nsmb1133

**Hunter, A. J., Ottoson, N., Boerth, N., Koretzky, G. A. and Shimizu, Y.** (2000). Cutting edge: a novel function for the SLAP-130/FYB adapter protein in $\beta_1$ integrin signaling and T lymphocyte migration. *J. Immunol.* **164**, 1143-1147. doi:10.4049/jimmunol.164.3.1143

**Hussain, S. F., Anderson, C. F. and Farber, D. L.** (2002). Differential SLP-76 expression and TCR-mediated signaling in effector and memory CD4 T cells. *J. Immunol.* **168**, 1557-1565. doi:10.4049/jimmunol.168.4.1557

**Hyun, Y.-M., Chung, H.-L., Mcgrath, J. L., Waugh, R. E. and Kim, M.** (2009). Activated integrin VLA-4 localizes to the lamellipodia and mediates T cell migration on VCAM-1. *J. Immunol.* **183**, 359-369. doi:10.4049/jimmunol.0803388

**Ilani, T., Vasiliver-Shamis, G., Vardhana, S., Bretscher, A. and Dustin, M. L.** (2009). T cell antigen receptor signaling and immunological synapse stability require myosin IIA. *Nat. Immunol.* **10**, 531-539. doi:10.1038/ni.1723

**Jacobelli, J., Chmura, S. A., Buxton, D. B., Davis, M. M. and Krummel, M. F.** (2004). A single class II myosin modulates T cell motility and stopping, but not synapse formation. *Nat. Immunol.* **5**, 531-538. doi:10.1038/ni1065

**Jankowska, K. I., Williamson, E. K., Roy, N. H., Blumenthal, D., Chandra, V., Baumgart, T. and Burkhardt, J. K.** (2018). Integrins modulate T cell receptor signaling by constraining actin flow at the immunological synapse. *Front. Immunol.* **9**, 25. doi:10.3389/fimmu.2018.00025

**Judokusumo, E., Tabdanov, E., Kumari, S., Dustin, M. L. and Kam, L. C.** (2012). Mechanosensing in T lymphocyte activation. *Biophys. J.* **102**, L5-L7. doi:10.1016/j.bpj.2011.12.011

**Kasirer-Friede, A., Kang, J., Kahner, B., Ye, F., Ginsberg, M. H. and Shattil, S. J.** (2014). ADAP interactions with talin and kindlin promote platelet integrin αIIbβ3 activation and stable fibrinogen binding. *Blood* **123**, 3156-3165. doi:10.1182/blood-2013-08-520627

**Kim, M., Carman, C. V. and Springer, T. A.** (2003). Bidirectional transmembrane signaling by cytoplasmic domain separation in integrins. *Science* **301**, 1720-1725. doi:10.1126/science.1084174

**Kliche, S., Breitling, D., Togni, M., Pusch, R., Heuer, K., Wang, X., Freund, C., Kasirer-Friede, A., Menasche, G., Koretzky, G. A. et al.** (2006). The ADAP/SKAP55 signaling module regulates T-cell receptor-mediated integrin activation through plasma membrane targeting of Rap1. *Mol. Cell. Biol.* **26**, 7130-7144. doi:10.1128/MCB.00331-06

**Kliche, S., Worbs, T., Wang, X., Degen, J., Patzak, I., Meineke, B., Togni, M., Moser, M., Reinhold, A., Kiefer, F. et al.** (2012). CCR7-mediated LFA-1 functions in T cells are regulated by 2 independent ADAP/SKAP55 modules. *Blood* **119**, 777-785. doi:10.1182/blood-2011-06-362269

**Kolega, J.** (2004). Phototoxicity and photoinactivation of blebbistatin in UV and visible light. *Biochem. Biophys. Res. Commun.* **320**, 1020-1025. doi:10.1016/j.bbrc.2004.06.045

**Kondo, N., Ueda, Y., Kita, T., Ozawa, M., Tomiyama, T., Yasuda, K., Lim, D.-S. and Kinashi, T.** (2017). NDR1-dependent regulation of Kindlin-3 controls high-affinity LFA-1 binding and immune synapse organization. *Mol. Cell. Biol.* **37**, e00424-e00416. doi:10.1128/MCB.00424-16

**Kumari, S., Vardhana, S., Cammer, M., Curado, S., Santos, L., Sheetz, M. P. and Dustin, M. L.** (2012). T lymphocyte myosin IIA is required for maturation of the immunological synapse. *Front. Immunol.* **3**, 230. doi:10.3389/fimmu.2012.00230

**Le Floc'h, A. and Huse, M.** (2015). Molecular mechanisms and functional implications of polarized actin remodeling at the T cell immunological synapse. *Cell. Mol. Life Sci.* **72**, 537-556. doi:10.1007/s00018-014-1760-7

**Lee, K.-H., Dinner, A. R., Tu, C., Campi, G., Raychaudhuri, S., Varma, R., Sims, T. N., Burack, W. R., Wu, H., Wang, J. et al.** (2003). The immunological synapse balances T cell receptor signaling and degradation. *Science* **302**, 1218-1222. doi:10.1126/science.1086507

**Lee, H.-S., Lim, C. J., Puzon-Mclaughlin, W., Shattil, S. J. and Ginsberg, M. H.** (2009). RIAM activates integrins by linking talin to ras GTPase membrane-targeting sequences. *J. Biol. Chem.* **284**, 5119-5127. doi:10.1074/jbc.M807117200

**Lefort, C. T., Rossaint, J., Moser, M., Petrich, B. G., Zarbock, A., Monkley, S. J., Critchley, D. R., Ginsberg, M. H., Fässler, R. and Ley, K.** (2012). Distinct roles for talin-1 and kindlin-3 in LFA-1 extension and affinity regulation. *Blood* **119**, 4275-4282. doi:10.1182/blood-2011-08-373118

**Lewis, J. B., Scangarello, F. A., Murphy, J. M., Eidell, K. P., Sodipo, M. O., Ophir, M. J., Sargeant, R., Seminario, M. C. and Bunnell, S. C.** (2018). ADAP is an upstream regulator that precedes SLP-76 at sites of TCR engagement and stabilizes signaling microclusters. *J. Cell Sci.* **131**, jcs215517. doi:10.1242/jcs.215517

**Liu, X., Kapoor, T. M., Chen, J. K. and Huse, M.** (2013). Diacylglycerol promotes centrosome polarization in T cells via reciprocal localization of dynein and myosin II. *Proc. Natl. Acad. Sci. USA* **110**, 11976-11981. doi:10.1073/pnas.1306180110

**Manevich-Mendelson, E., Feigelson, S. W., Pasvolsky, R., Aker, M., Grabovsky, V., Shulman, Z., Kilic, S. S., Rosenthal-Allieri, M. A., Ben-Dor, S., Mory, A. et al.** (2009). Loss of Kindlin-3 in LAD-III eliminates LFA-1 but not VLA-4 adhesiveness developed under shear flow conditions. *Blood* **114**, 2344-2353. doi:10.1182/blood-2009-04-218636

**Maskalenko, N., Nath, S., Ramakrishnan, A., Anikeeva, N., Sykulev, Y. and Poenie, M.** (2020). The DISC1-Girdin complex - a missing link in signaling to the T cell cytoskeleton. *J. Cell Sci.* **133**, jcs242875. doi:10.1242/jcs.242875

**Mayya, V., Judokusumo, E., Abu Shah, E., Peel, C. G., Neiswanger, W., Depoil, D., Blair, D. A., Wiggins, C. H., Kam, L. C. and Dustin, M. L.** (2018). Durable interactions of T cells with T cell receptor stimuli in the absence of a stable immunological synapse. *Cell Rep.* **22**, 340-349. doi:10.1016/j.celrep.2017.12.052

**Mayya, V., Judokusumo, E., Abu-Shah, E., Neiswanger, W., Sachar, C., Depoil, D., Kam, L. C. and Dustin, M. L.** (2019). Cutting edge: synapse propensity of human memory CD8 T cells confers competitive advantage over naive counterparts. *J. Immunol.* **203**, 601-606. doi:10.4049/jimmunol.1801687

**Ménasché, G., Kliche, S., Chen, E. J. H., Stradal, T. E. B., Schraven, B. and Koretzky, G.** (2007). RIAM links the ADAP/SKAP-55 signaling module to Rap1, facilitating T-cell-receptor-mediated integrin activation. *Mol. Cell. Biol.* **27**, 4070-4081. doi:10.1128/MCB.02011-06

**Mittelbrunn, M., Molina, A., Escribese, M. M., Yanez-Mo, M., Escudero, E., Ursa, A., Tejedor, R., Mampaso, F. and Sanchez-Madrid, F.** (2004). VLA-4 integrin concentrates at the peripheral supramolecular activation complex of the immune synapse and drives T helper 1 responses. *Proc. Natl. Acad. Sci. USA* **101**, 11058-11063. doi:10.1073/pnas.0307927101

**Monks, C. R. F., Kupfer, H., Tamir, I., Barlow, A. and Kupfer, A.** (1997). Selective modulation of protein kinase C-Θ during T-cell activation. *Nature* **385**, 83-86. doi:10.1038/385083a0

**Monks, C. R. F., Freiberg, B. A., Kupfer, H., Sciaky, N. and Kupfer, A.** (1998). Three-dimensional segregation of supramolecular activation clusters in T cells. *Nature* **395**, 82-86. doi:10.1038/25764

**Morrison, V. L., Uotila, L. M., Llort Asens, M., Savinko, T. and Fagerholm, S. C.** (2015). Optimal T cell activation and B cell antibody responses in vivo require the interaction between leukocyte function-associated antigen-1 and Kindlin-3. *J. Immunol.* **195**, 105-115. doi:10.4049/jimmunol.1402741

**Morse, E. M., Brahme, N. N. and Calderwood, D. A.** (2014). Integrin cytoplasmic tail interactions. *Biochemistry* **53**, 810-820. doi:10.1021/bi401596q

**Mossman, K. D., Campi, G., Groves, J. T. and Dustin, M. L.** (2005). Altered TCR signaling from geometrically repatterned immunological synapses. *Science* **310**, 1191-1193. doi:10.1126/science.1119238

**Murugesan, S., Hong, J., Yi, J., Li, D., Beach, J. R., Shao, L., Meinhardt, J., Madison, G., Wu, X., Betzig, E. et al.** (2016). Formin-generated actomyosin arcs propel T cell receptor microcluster movement at the immune synapse. *J. Cell Biol.* **215**, 383-399. doi:10.1083/jcb.201603080

**Nath, S., Christian, L., Tan, S. Y., Ki, S., Ehrlich, L. I. R. and Poenie, M.** (2016). Dynein separately partners with NDE1 and dynactin to orchestrate T cell focused secretion. *J. Immunol.* **197**, 2090-2101. doi:10.4049/jimmunol.1600180

**Naydenov, N. G., Lechuga, S., Huang, E. H. and Ivanov, A. I.** (2021). Myosin motors: novel regulators and therapeutic targets in colorectal cancer. *Cancers* **13**, 741. doi:10.3390/cancers13040741

**Nguyen, K., Sylvain, N. R. and Bunnell, S. C.** (2008). T cell costimulation via the integrin VLA-4 inhibits the actin-dependent centralization of signaling microclusters containing the adaptor SLP-76. *Immunity* **28**, 810-821. doi:10.1016/j.immuni.2008.04.019

**Ophir, M. J., Liu, B. C. and Bunnell, S. C.** (2013). The N terminus of SKAP55 enables T cell adhesion to TCR and integrin ligands via distinct mechanisms. *J. Cell Biol.* **203**, 1021-1041. doi:10.1083/jcb.201305088

**Orgaz, J. L., Crosas-Molist, E., Sadok, A., Perdrix-Rosell, A., Maiques, O., Rodriguez-Hernandez, I., Monger, J., Mele, S., Georgouli, M., Bridgeman, V. et al.** (2020). Myosin II reactivation and cytoskeletal remodeling as a hallmark and a vulnerability in melanoma therapy resistance. *Cancer Cell* **37**, 85-103.e9. doi:10.1016/j.ccell.2019.12.003

**Pauker, M. H., Reicher, B., Fried, S., Perl, O. and Barda-Saad, M.** (2011). Functional cooperation between the proteins Nck and ADAP is fundamental for actin reorganization. *Mol. Cell. Biol.* **31**, 2653-2666. doi:10.1128/MCB.01358-10

**Pauker, M. H., Hassan, N., Noy, E., Reicher, B. and Barda-Saad, M.** (2012). Studying the dynamics of SLP-76, Nck, and Vav1 multimolecular complex formation in live human cells with triple-color FRET. *Sci. Signal.* **5**, rs3. doi:10.1126/scisignal.2002423

**Peterson, E. J., Woods, M. L., Dmowski, S. A., Derimanov, G., Jordan, M. S., Wu, J. N., Myung, P. S., Liu, Q.-H., Pribila, J. T., Freedman, B. D. et al.** (2001). Coupling of the TCR to integrin activation by Slap-130/Fyb. *Science* **293**, 2263-2265. doi:10.1126/science.1063486

**Purbhoo, M. A., Liu, H., Oddos, S., Owen, D. M., Neil, M. A. A., Pageon, S. V., French, P. M. W., Rudd, C. E. and Davis, D. M.** (2010). Dynamics of subsynaptic vesicles and surface microclusters at the immunological synapse. *Sci. Signal.* **3**, ra36. doi:10.1126/scisignal.2000645

**Raab, M., Wang, H., Lu, Y., Smith, X., Wu, Z., Strebhardt, K., Ladbury, J. E. and Rudd, C. E.** (2010). T cell receptor "inside-out" pathway via signaling module SKAP1-RapL regulates T cell motility and interactions in lymph nodes. *Immunity* **32**, 541-556. doi:10.1016/j.immuni.2010.03.007

**Romzek, N. C., Harris, E. S., Dell, C. L., Skronek, J., Hasse, E., Reynolds, P. J., Hunt, S. W., III and Shimizu, Y.** (1998). Use of a β1 integrin-deficient human T cell to identify β1 integrin cytoplasmic domain sequences critical for integrin function. *Mol. Biol. Cell* **9**, 2715-2727. doi:10.1091/mbc.9.10.2715

**Roybal, K. T., Mace, E. M., Mantell, J. M., Verkade, P., Orange, J. S. and Wulfing, C.** (2015). Early signaling in primary T cells activated by antigen presenting cells is associated with a deep and transient lamellal actin network. *PLoS ONE* **10**, e0133299. doi:10.1371/journal.pone.0133299

**Saito, T., Yokosuka, T. and Hashimoto-Tane, A.** (2010). Dynamic regulation of T cell activation and co-stimulation through TCR-microclusters. *FEBS Lett.* **584**, 4865-4871. doi:10.1016/j.febslet.2010.11.036

**Schneider, C. A., Rasband, W. S. and Eliceiri, K. W.** (2012). NIH Image to Image J: 25 years of image analysis. *Nat. Methods*. **9**, 671-675. doi:10.1038/nmeth.2089

**Schubert, D. A., Gordo, S., Sabatino, J. J., Jr., Vardhana, S., Gagnon, E., Sethi, D. K., Seth, N. P., Choudhuri, K., Reijonen, H., Nepom, G. T. et al.** (2012). Self-reactive human CD4 T cell clones form unusual immunological synapses. *J. Exp. Med.* **209**, 335-352. doi:10.1084/jem.20111485

**Sherman, E., Barr, V., Manley, S., Patterson, G., Balagopalan, L., Akpan, I., Regan, C. K., Merrill, R. K., Sommers, C. L., Lippincott-Schwartz, J. et al.** (2011). Functional nanoscale organization of signaling molecules downstream of the T cell antigen receptor. *Immunity* **35**, 705-720. doi:10.1016/j.immuni.2011.10.004

**Sherman, E., Barr, V. A., Merrill, R. K., Regan, C. K., Sommers, C. L. and Samelson, L. E.** (2016). Hierarchical nanostructure and synergy of multimolecular signalling complexes. *Nat. Commun.* **7**, 12161. doi:10.1038/ncomms12161

**Sims, T. N., Soos, T. J., Xenias, H. S., Dubin-Thaler, B., Hofman, J. M., Waite, J. C., Cameron, T. O., Thomas, V. K., Varma, R., Wiggins, C. H. et al.** (2007). Opposing effects of PKCθ and WASp on symmetry breaking and relocation of the immunological synapse. *Cell* **129**, 773-785. doi:10.1016/j.cell.2007.03.037

**Stinchcombe, J. C. and Griffiths, G. M.** (2007). Secretory mechanisms in cell-mediated cytotoxicity. *Annu. Rev. Cell Dev. Biol.* **23**, 495-517. doi:10.1146/annurev.cellbio.23.090506.123521

**Suzuki, J.-i., Yamasaki, S., Wu, J., Koretzky, G. A. and Saito, T.** (2007). The actin cloud induced by LFA-1-mediated outside-in signals lowers the threshold for T-cell activation. *Blood* **109**, 168-175. doi:10.1182/blood-2005-12-020164

**Sylvain, N. R., Nguyen, K. and Bunnell, S. C.** (2011). Vav1-mediated scaffolding interactions stabilize SLP-76 microclusters and contribute to antigen-dependent T cell responses. *Sci. Signal.* **4**, ra14. doi:10.1126/scisignal.2001178

**Tojkander, S., Gateva, G. and Lappalainen, P.** (2012). Actin stress fibers–assembly, dynamics and biological roles. *J. Cell Sci.* **125**, 1855-1864. doi:10.1242/jcs.098087

**Udagawa, T. and Mcintyre, B. W.** (1996). ADP-ribosylation of the G protein Rho inhibits integrin regulation of tumor cell growth. *J. Biol. Chem.* **271**, 12542-12548. doi:10.1074/jbc.271.21.12542

**Valitutti, S., Dessing, M., Aktories, K., Gallati, H. and Lanzavecchia, A.** (1995). Sustained signaling leading to T cell activation results from prolonged T cell receptor occupancy. Role of T cell actin cytoskeleton. *J. Exp. Med.* **181**, 577-584. doi:10.1084/jem.181.2.577

**Vardhana, S., Choudhuri, K., Varma, R. and Dustin, M. L.** (2010). Essential role of ubiquitin and TSG101 protein in formation and function of the central supramolecular activation cluster. *Immunity* **32**, 531-540. doi:10.1016/j.immuni.2010.04.005

**Várkuti, B. H., Képiró, M., Horváth, I. A., Végner, L., Ráti, S., Zsigmond, A., Hegyi, G., Lenkei, Z., Varga, M. and Málnasi-Csizmadia, A.** (2016). A highly soluble, non-phototoxic, non-fluorescent blebbistatin derivative. *Sci. Rep.* **6**, 26141. doi:10.1038/srep26141

**Varma, R., Campi, G., Yokosuka, T., Saito, T. and Dustin, M. L.** (2006). T cell receptor-proximal signals are sustained in peripheral microclusters and terminated in the central supramolecular activation cluster. *Immunity* **25**, 117-127. doi:10.1016/j.immuni.2006.04.010

**Wang, H., Mccann, F. E., Gordan, J. D., Wu, X., Raab, M., Malik, T. H., Davis, D. M. and Rudd, C. E.** (2004). ADAP-SLP-76 binding differentially regulates supramolecular activation cluster (SMAC) formation relative to T cell-APC conjugation. *J. Exp. Med.* **200**, 1063-1074. doi:10.1084/jem.20040780

**Wei, Q. and Adelstein, R. S.** (2000). Conditional expression of a truncated fragment of nonmuscle myosin II-A alters cell shape but not cytokinesis in HeLa cells. *Mol. Biol. Cell* **11**, 3617-3627. doi:10.1091/mbc.11.10.3617

**Wen, L., Marki, A., Roy, P., Mcardle, S., Sun, H., Fan, Z., Gingras, A. R., Ginsberg, M. H. and Ley, K.** (2021). Kindlin-3 recruitment to the plasma membrane precedes high-affinity β2-integrin and neutrophil arrest from rolling. *Blood* **137**, 29-38. doi:10.1182/blood.2019003446

**Wernimont, S. A., Wiemer, A. J., Bennin, D. A., Monkley, S. J., Ludwig, T., Critchley, D. R. and Huttenlocher, A.** (2011). Contact-dependent T cell activation and T cell stopping require talin1. *J. Immunol.* **187**, 6256-6267. doi:10.4049/jimmunol.1102028

**Yi, J., Wu, X. S., Crites, T. and Hammer, J. A.III** (2012). Actin retrograde flow and actomyosin II arc contraction drive receptor cluster dynamics at the immunological synapse in Jurkat T cells. *Mol Biol Cell,* **23**, 834-852. doi:10.1091/mbc.e11-08-0731

**Yi, J., Wu, X., Chung, A. H., Chen, J. K., Kapoor, T. M. and Hammer, J. A.** (2013). Centrosome repositioning in T cells is biphasic and driven by microtubule end-on capture-shrinkage. *J. Cell Biol.* **202**, 779-792. doi:10.1083/jcb.201301004

**Yi, J., Balagopalan, L., Nguyen, T., Mcintire, K. M. and Samelson, L. E.** (2019). TCR microclusters form spatially segregated domains and sequentially assemble in calcium-dependent kinetic steps. *Nat. Commun.* **10**, 277. doi:10.1038/s41467-018-08064-2

**Yokosuka, T., Sakata-Sogawa, K., Kobayashi, W., Hiroshima, M., Hashimoto-Tane, A., Tokunaga, M., Dustin, M. L. and Saito, T.** (2005). Newly generated T cell receptor microclusters initiate and sustain T cell activation by recruitment of Zap70 and SLP-76. *Nat. Immunol.* **6**, 1253-1262. doi:10.1038/ni1272

**Yokosuka, T., Kobayashi, W., Sakata-Sogawa, K., Takamatsu, M., Hashimoto-Tane, A., Dustin, M. L., Tokunaga, M. and Saito, T.** (2008). Spatiotemporal regulation of T cell costimulation by TCR-CD28 microclusters and protein kinase C θ translocation. *Immunity* **29**, 589-601. doi:10.1016/j.immuni.2008.08.011

**Yu, Y., Fay, N. C., Smoligovets, A. A., Wu, H.-J. and Groves, J. T.** (2012). Myosin IIA modulates T cell receptor transport and CasL phosphorylation during early immunological synapse formation. *PLoS ONE* **7**, e30704. doi:10.1371/journal.pone.0030704

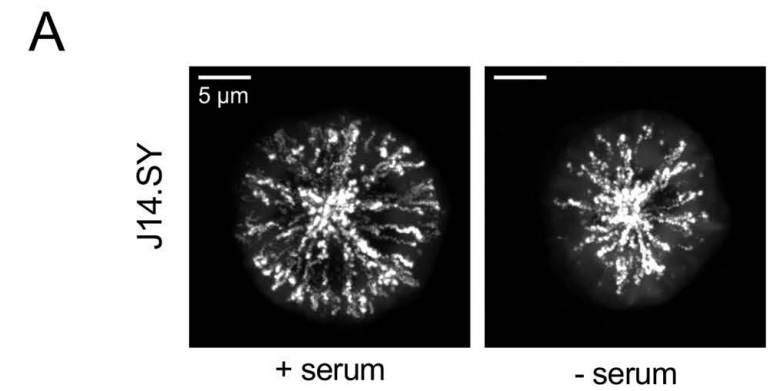


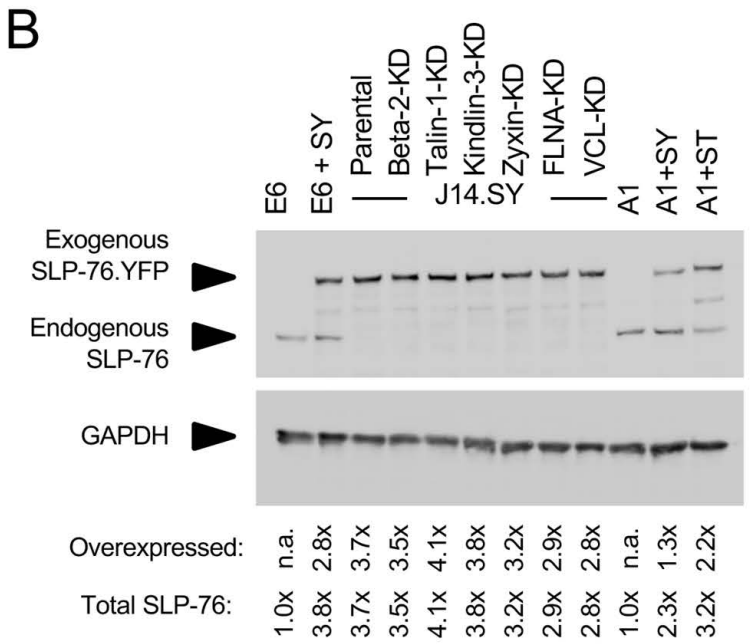


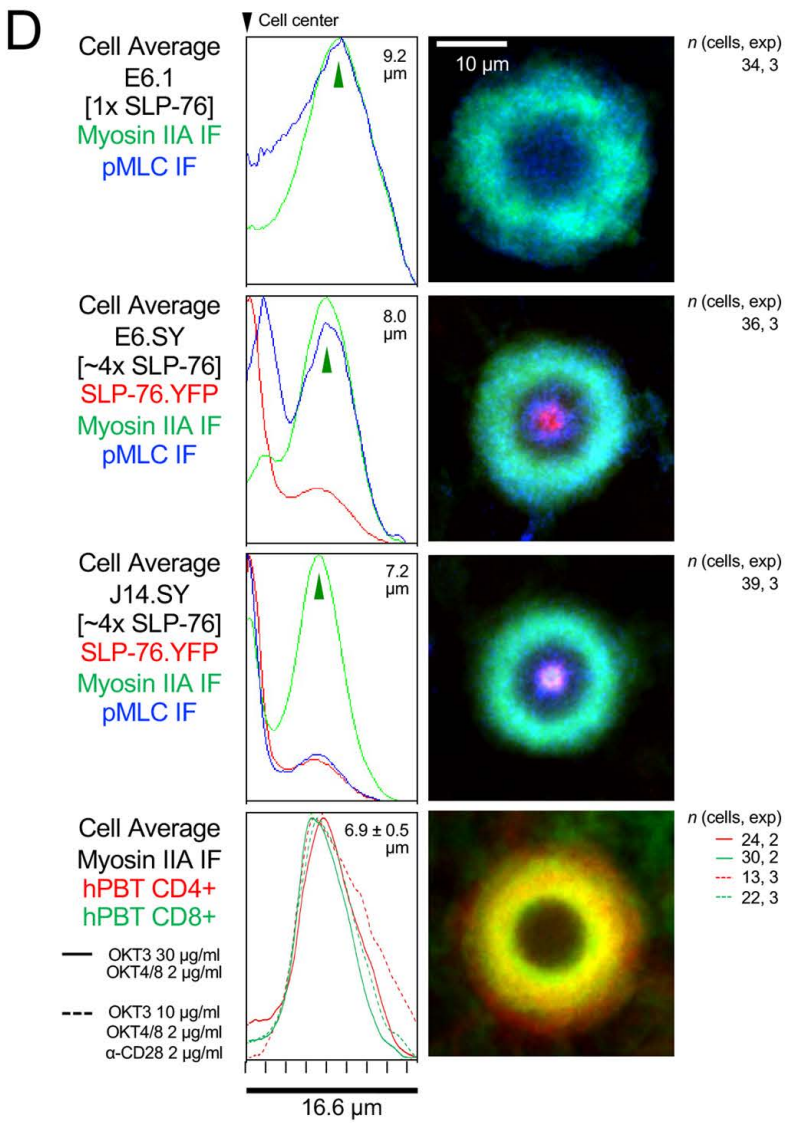


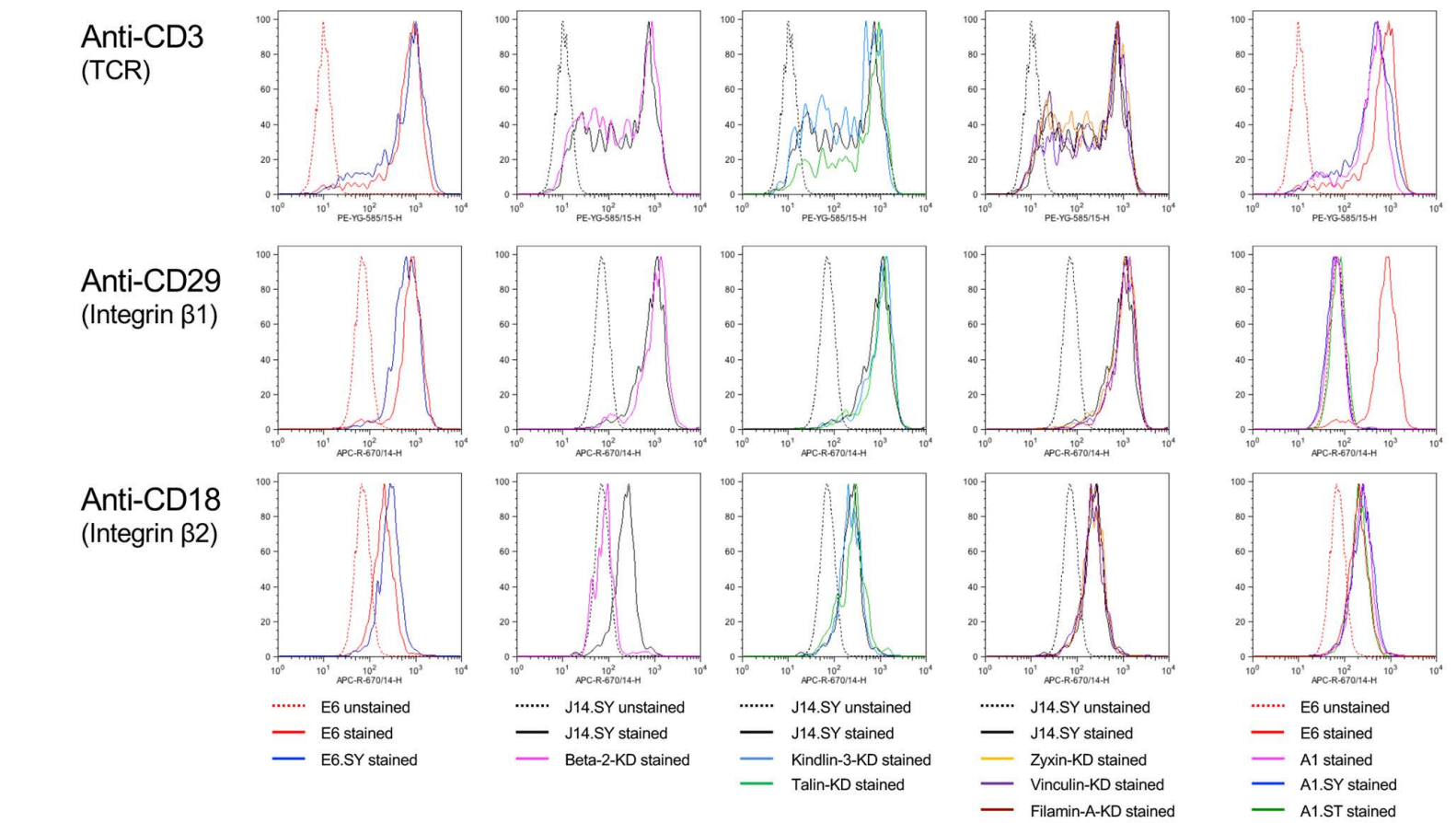

**Fig. S1. SLP-76 expression and protein knockdowns regulate the centripetal movement of myosin without affecting key surface markers.** (A) J14.SY cells were plated onto 10.0 µg ml-1 OKT3 coated glass wells in the presence or absence of serum and live cell imaged. Representative MOTs are shown. (B-C) Characterization of stable cells lines lacking Kindlin-3, Talin-1, Zyxin, Vinculin, or Filamin-A. (B) E6.1, A1, and J14.SY cells, compared with respective knockdown cell lines were immunoblotted for SLP-76. 'Overexpression' is for the exogenous band, relative to endogenous SLP-76 in the Jurkat E6.1 line; 'Total' includes endogenous SLP-76. (C) Cell lines from B were stained for CD3, CD29, and CD18. (D) Images of cells were center-aligned and averaged to generate composite images. Plots display the average intensities of the indicated proteins as a function of radial distance from the center of the cell. The radial positions of peak myosin IIA fluorescence are indicated. (D, upper panels) Cells acquired for Figure 1B were re-processed as described. (D, bottom panel) Primary human CD4+ and CD8+ T cell blasts were stimulated on substrates coated with antibodies targeting CD3ε, the appropriate co-receptor, and with or without antibodies targeting CD28. Fixed cells were stained for myosin IIA and processed as above. The average radial position (± s.d.) of peak myosin IIA fluorescence across the four conditions is indicated. Three independent experiments were performed in A-C; representative images are shown. The cumulative number of processed cells and the number of experiments from which they originate are displayed in D.

A

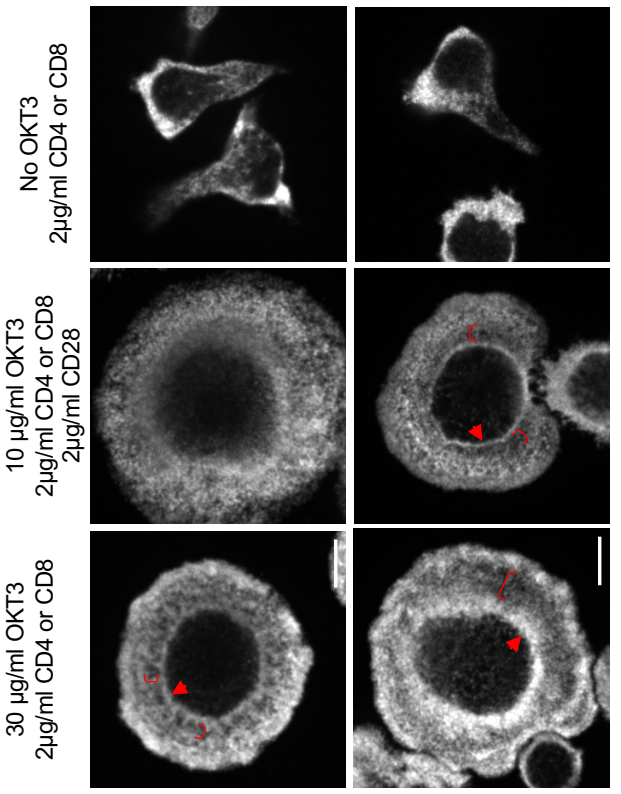


B

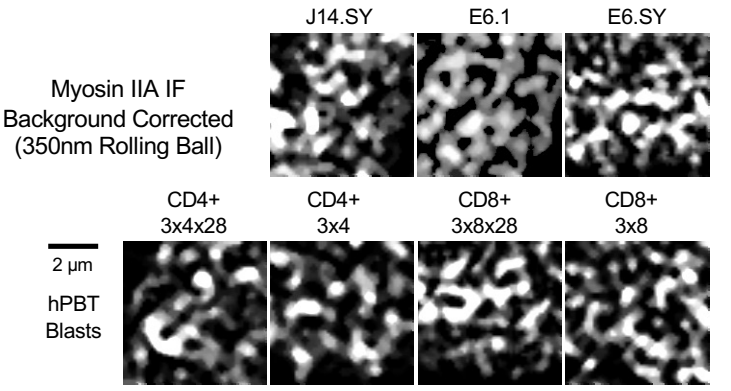


C

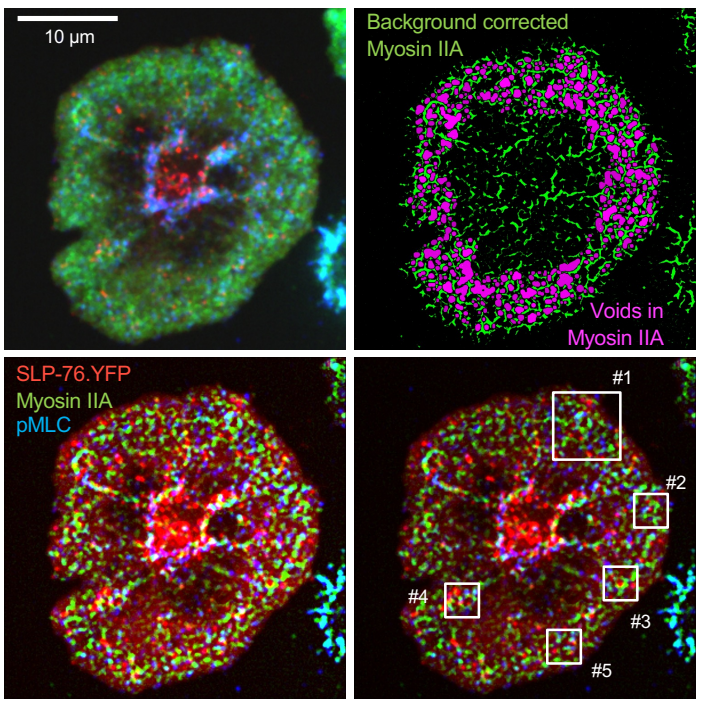


D

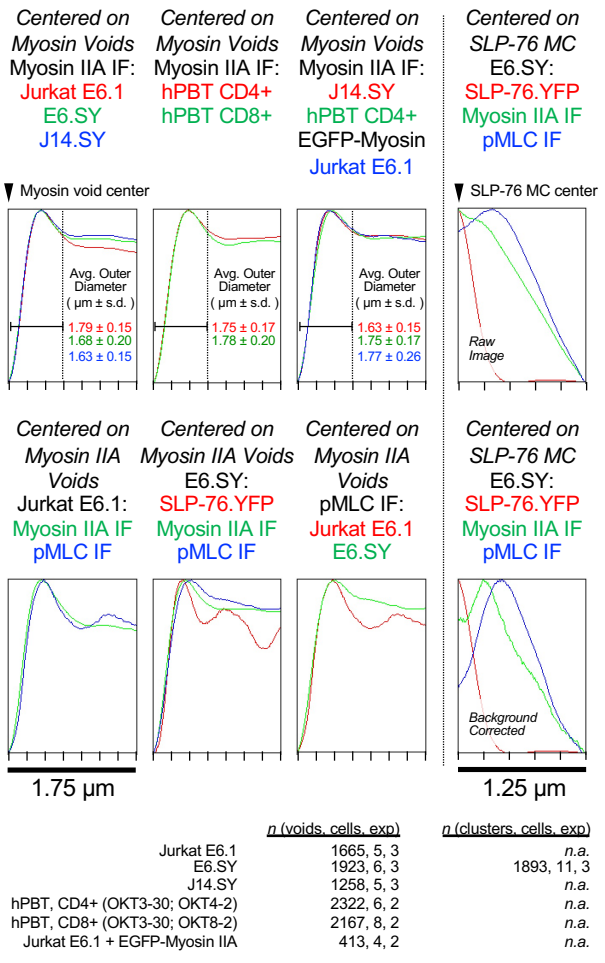


| | n (voids, cells, exp) | n (clusters, cells, exp) |
|---|---|---|
| Jurkat E6.1 | 1665, 5, 3 | *n.a.* |
| E6.SY | 1923, 6, 3 | 1893, 11, 3 |
| J14.SY | 1258, 5, 3 | *n.a.* |
| hPBT, CD4+ (OKT3-30; OKT4-2) | 2322, 6, 2 | *n.a.* |
| hPBT, CD8+ (OKT3-30; OKT8-2) | 2167, 8, 2 | *n.a.* |
| Jurkat E6.1 + EGFP-Myosin IIA | 413, 4, 2 | *n.a.* |

E

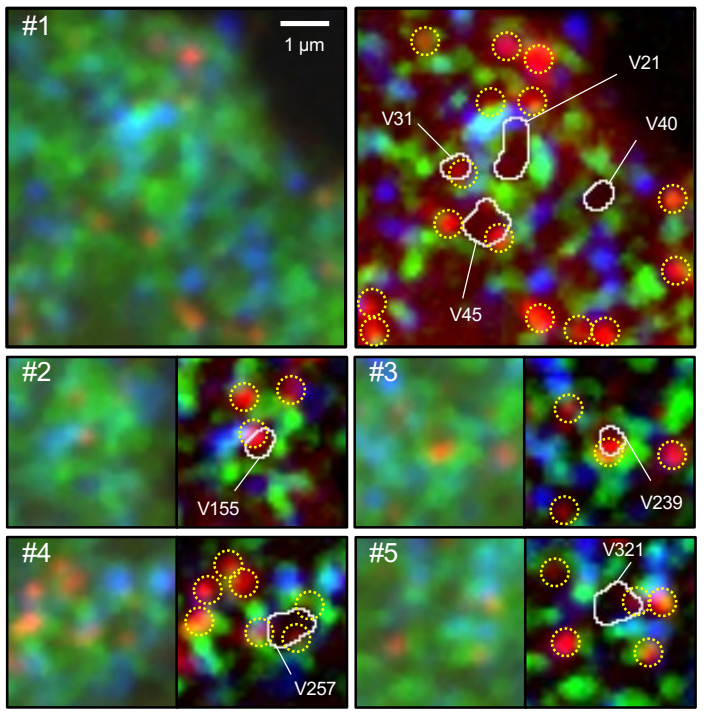

**Fig. S2. SLP-76 microclusters are enclosed within or attached to uniformly sized myosin IIA rings.** (A) Primary human CD4+ and CD8+ T cells were stimulated and imaged as described in Supplementary Figure 1D (bottom panel). Primary T cells were also stimulated on control substrates coated with co-receptor-specific antibodies (upper two panels). Representative images are shown. Three replicates were performed, except for the high-dose OKT3 condition, where *n*=2. (B) Enlarged, background corrected images were produced as in Figure 1F-G, using images acquired for Figure 1B and Supplementary Figure 2A. (C) Raw images of SLP-76.YFP, myosin IIA, and pMLC in Jurkat E6.1 cells and E6.SY cells were acquired for Figure 1B. Raw images of E6.1 cells expressing EGFP-tagged myosin IIA were acquired for Figure 2C. A representative E6.SY cell is shown (top left). Myosin IIA images were converted into binary masks (green) and 'voids' in the myosin IIA meshwork (magenta) were identified as described in the methods section. The central region of the synapse was excluded because it was not possible to reliably identify filamentous structures in this region (top right). For some subsequent analyses, the myosin IIA and pMLC channels were background corrected using a 350nm rolling ball filter (bottom left). Specific regions analyzed in E, below, are identified with white boxes (bottom right). (D, left) The average intensities of myosin IIA, pMLC, and SLP-76 were captured from raw images as a function of their radial distance from the centers of voids defined using images of myosin IIA. The plots display the average radial intensities of all cells within a group. The outer diameters displayed in the top row are the mean ± s.d. of values determined for myosin IIA in the cells of each group. (D, right) The average intensities of myosin IIA, pMLC, and SLP-76 were captured from raw images (upper) or background corrected images (lower) as a function of their radial distance from the centers of SLP-76 microclusters. The plots display the average radial intensities of all cells within a group. Replicates per condition are listed. (E) Representative raw and background corrected images derived from the cell in panel C, above, are provided to facilitate the interpretation of the data presented in panel D. A subset of the algorithmically identified voids are depicted using white outlines. All of the algorithmically identified SLP-76 microclusters present within these regions are highlighted using dotted yellow circles.

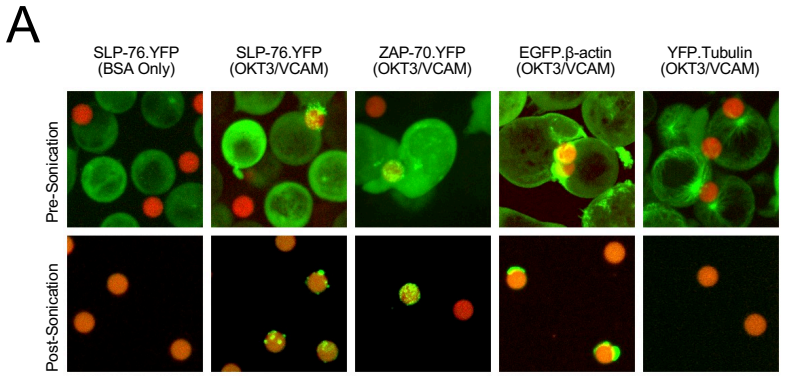


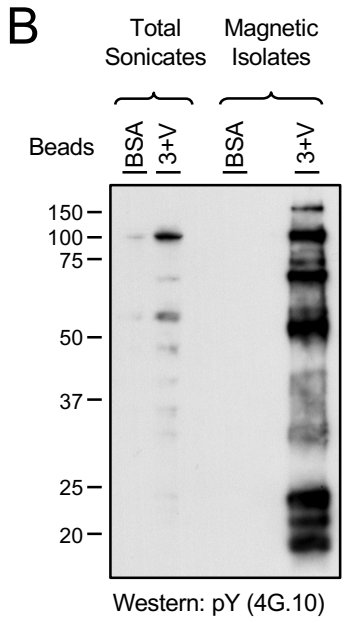


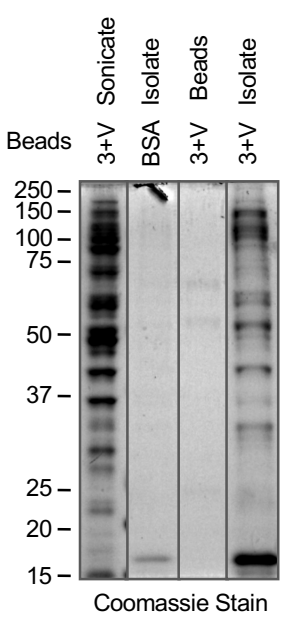


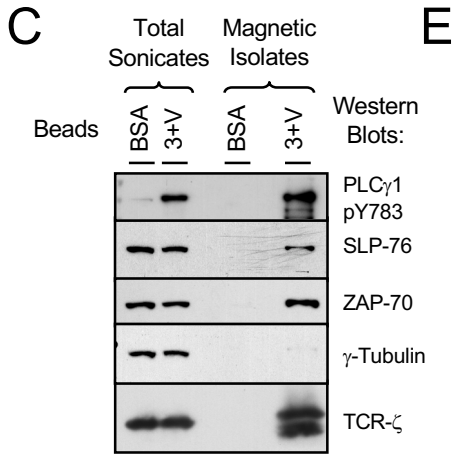


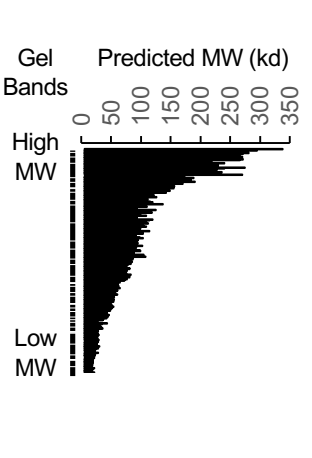


F

| Absolute IC | Band # | % Band TIC | Symbol | NCBI ID | Peptides | Description |
|---|---|---|---|---|---|---|
| 1.70E+06 | 30 | 7.38 | ACTB | 60 | 6x | Actin, Beta |
| 1.00E+06 | 26 | 6.55 | TUBB | 203068 | 1x | Tubulin, Beta |
| 5.00E+05 | 26 | 3.21 | TUBB4B | 10383 | 5x | Tubulin, Beta 2C |
| 4.70E+05 | 28 | 8.34 | PA2G4 | 5036 | 2x | Erb3BP1 |
| 2.60E+05 | 04 | 20.83 | MYH9 | 4627 | 18x | **Myosin IIA** |
| 1.80E+05 | 03 | 26.31 | TLN1 | 7094 | 52x | Talin 1 |
| 1.60E+05 | 26 | 1.04 | TUBA1A | 7846 | 2x | Tubulin, Alpha 10 |
| 8.10E+04 | 02 | 19.83 | FLNB | 2317 | 11x | Filamin-B |
| 5.80E+04 | 02 | 14.13 | FLNA | 2316 | 11x | Filamin-A |
| 4.80E+04 | 03 | 7.15 | SPTBN1 | 6711 | 10x | Spectrin, Beta |
| 4.40E+04 | 36 | 0.18 | CLTA | 1211 | 1x | Clathrin Light Chain A |
| 4.30E+04 | 04 | 3.36 | MYH10 | 4628 | 8x | **Myosin IIB** |
| 4.10E+04 | 12 | 4.84 | LCP2 | 3937 | 5x | **SLP-76 (YFP Fusion)** |
| 2.70E+04 | 26 | 0.17 | CORO1A | 11151 | 1x | Coronin 1A |
| 2.50E+04 | 06 | 8.28 | CLTC | 1213 | 9x | Clathrin Heavy Chain |
| 2.50E+04 | 30 | 0.11 | CAPG | 822 | 1x | Capping Protein, Gelsolin-Like |
| 2.40E+04 | 12 | 2.77 | ACTN4 | 81 | 1x | Actinin, Alpha 4 |
| 2.40E+04 | 30 | 0.11 | ACTR2 | 10097 | 1x | Arp2 (Arp2/3 Complex) |
| 2.00E+04 | 02 | 4.81 | SPTAN1 | 6709 | 8x | Spectrin, Alpha |
| 1.50E+04 | 19 | 0.90 | MSN | 4478 | 3x | Moesin |
| 1.30E+04 | 41 | 0.59 | RAB10 | 19325 | 1x | Rab10 |
| 9.20E+03 | 09 | 2.50 | CYFIP2 | 26999 | 2x | Pir121/Sra1 (WAVE Complex) |
| 9.20E+03 | 40 | 1.30 | SEC22B | 9554 | 1x | SEC22B |
| 8.30E+03 | 40 | 1.18 | RAB5C | 5878 | 2x | Rab5c |
| 7.80E+03 | 42 | 2.41 | CFL1 | 476022 | 2x | Cofilin 1 |
| 6.20E+03 | 40 | 0.87 | RAB11A | 8766 | 3x | Rab11a |
| 4.50E+03 | 45 | 0.66 | MYL6 | 281341 | 2x | **Myosin Light Chain 6** |
| 4.30E+03 | 05 | 1.84 | IQGAP1 | 8826 | 1x | IQGAP |
| 2.40E+03 | 42 | 0.74 | CD3E | 916 | 1x | **CD3ε (TCR)** |
| 1.80E+03 | 19 | 0.11 | SEPTIN9 | 10801 | 1x | Septin 9 |
| 1.50E+03 | 19 | 0.09 | KIFC1 | 3833 | 1x | Kinesin C1 |
| 1.20E+03 | 07 | 0.10 | KTN1 | 3895 | 1x | Kinectin 1b |
| 1.10E+03 | 44 | 0.16 | ARPC5 | 10092 | 1x | Arpc5 (Arp2/3 Complex) |
| 8.10E+02 | 41 | 0.21 | CD3D | 915 | 1x | **CD3δ (TCR)** |

G

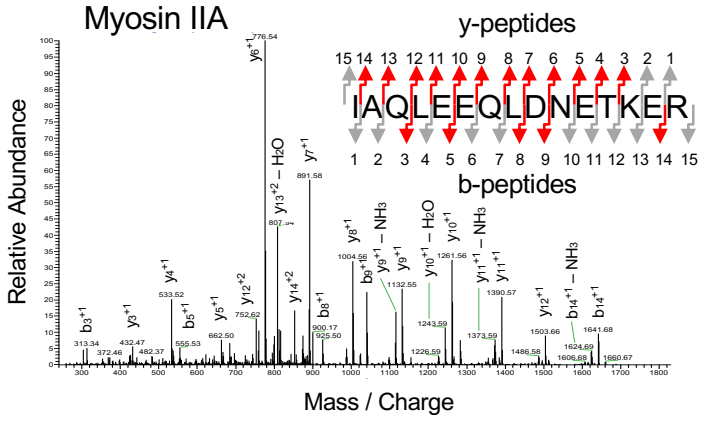


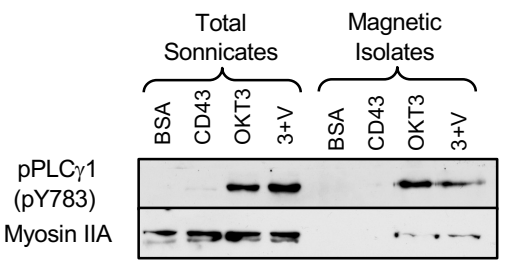


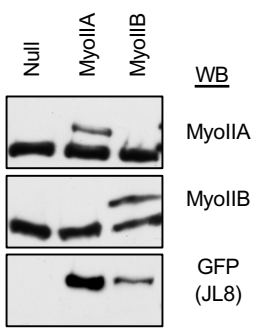


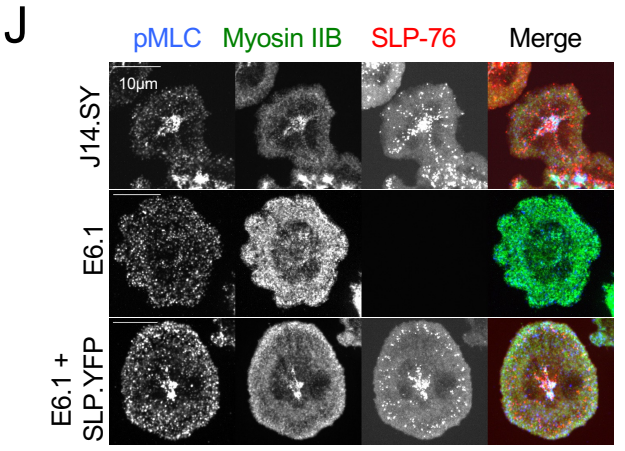

**Fig. S3. The magnetic immuno-isolation of integrin-immobilized SLP-76 microclusters and the identification of proteins retained within these structures.** (A) Stable T cell lines derived from Jurkat T cell lines were stimulated by co-incubation with 4.5 μm magnetic beads. These lines express stably express SLP-76.YFP (J14.SY), ZAP-70.YFP (E6.ZAP-YFP), EGFP. β-actin (E6.EGFP-Actin), or YFP.Tubulin (E6.YFP-Tubulin). Magnetic beads left untreated or coated with anti-CD3 (OKT3) and recombinant human VCAM-1 and then blocked with BSA. After a 5-minute co-incubation at 37°C, cells were fixed with DSP, a membrane-permeable, lysine-reactive, reversible crosslinking agent. After fixation, cells were disrupted by sonication, and bead-attached signaling complexes were purified from the total lysate by magnetic isolation. The bead-cell conjugates and bead-attached signaling complexes obtained pre- and post-sonication were visualized by confocal microscopy. Representative top-down projections of image stacks spanning 30 μm are shown. Fluorescent proteins are pseudocolored green; magnetic beads are pseudocolored red. (B-C) Total sonicates ($2x10^5$ cell equivalents) and magnetic isolates ($2x10^7$ cell equivalents) derived from J14.SY cells were examined by western blotting. (D) The same total sonicates, beads, and bead isolates were analyzed by Coomassie staining. (E-G) Slices cut from the rightmost lane of the gel in D were reduced, alkylated, and trypsinized in-gel. LC/MS/MS analysis was performed using a Thermo LTQ ion trap mass spectrometer. MS/MS spectra were searched against the NCBI non-redundant protein sequence database using the SEQUEST computer algorithm. (E) The predicted molecular weights of identified proteins accurately track their initial positions in the gel. (F) Table depicting the most abundant hits with roles in signal transduction, cytoskeletal function, and membrane transport. A complete list of hits is provided in Supplementary Table S2. Bands were numbered from top to bottom; thus, high molecular weight proteins have low band numbers. Absolute IC is cumulative ion current associated with all peptides contributing to a given hit. Percent band TIC is fraction of the total ion current associated with a given band that is contributed by a given hit. Peptides is the number of unique peptides that could be non-redundantly assigned to each hit. (G) A representative fragmentation spectrum for one of the peptides contributing to the identification of Myosin IIA in our magnetic immuno-isolates. (H) Total sonicates and magnetic isolates were independently derived from J14.SY cells and examined by western blotting. Samples were prepared using control BSA-coated beads (BSA) and beads coated with anti-CD3, either with (3+V) or without VCAM-1 (OKT3). A specificity control was provided by using beads coated with a non-stimulatory but pro-adhesive ligand, anti-CD43 (CD43). (I) Jurkat E6.1 cells were transiently transfected with EGFP-tagged myosin IIA (MyoIIA) or IIB (MyoIIB) and lysates blotted as indicated. (J) J14.SY cells, E6.1 cells, E6.1 cells stably transduced with SLP-76.YFP were stimulated as Fig. 1B, fixed after 7 minutes, and stained for myosin IIB and pMLC.

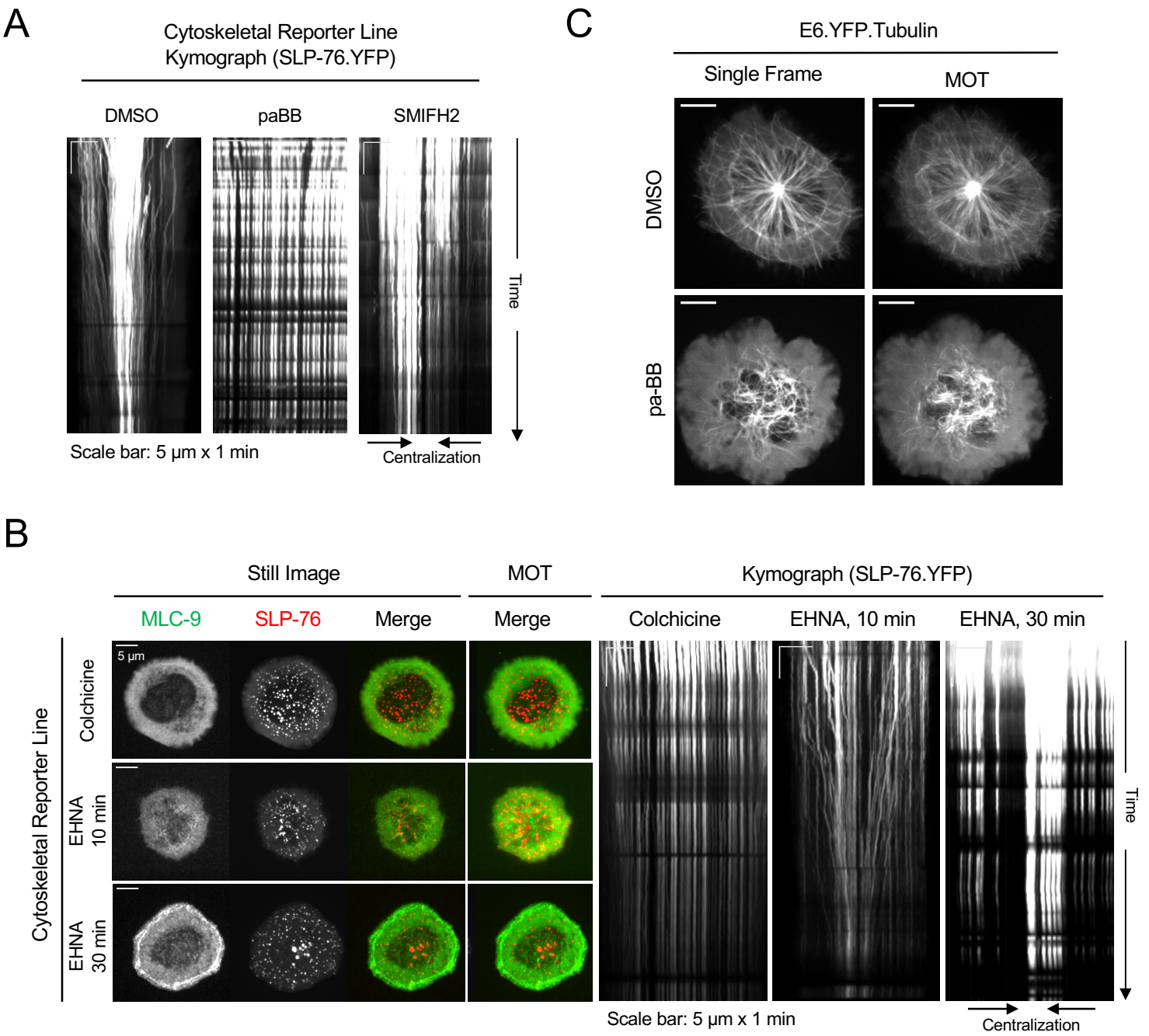


**Fig. S4. Myosin ATPase activity, formin function, intact microtubules and dynein ATPase activity are required for the co-accumulation of SLP-76 microclusters and contractile myosin filaments at the center of the contact.** (A) J14.SY-CRL cells were pretreated for 30 minutes with DMSO, or para-amino-blebbistatin (paBB, 50 µM), or for 10 minutes with SMIFH2 (25 µM) and then stimulated on substrates coated with anti-CD3 (10.0 µg $ml^{-1}$) and anti-CD43 (10.0 µg $ml^{-1}$). Each channel was imaged every 5.6 seconds for 150 frames (14 min). Kymographs track SLP-76 microcluster movement in the image stacks corresponding to Fig. 2I. (B) J14.SY-CRL cells were pretreated for 60 minutes with DMSO, or Colchicine (100 µM), or for 10 or 30 minutes with EHNA (1mM) and then stimulated on substrates coated with anti-CD3 (10.0 µg $ml^{-1}$) and anti-CD43 (10.0 µg $ml^{-1}$). Each channel was imaged every 5.6 seconds for 150 frames (14 min). (C) E6.YFP.Tubulin cells were pretreated with DMSO or with para-amino-blebbistatin (paBB, 50 µM) for 30 minutes and then plated onto OKT3 coated glass wells (10.0 µg $ml^{-1}$) and live cell imaged. YFP channel was collected every 2 seconds for 150 frames. Two replicates performed. Identical results were observed in three additional replicates using blebbistatin (50 µM)

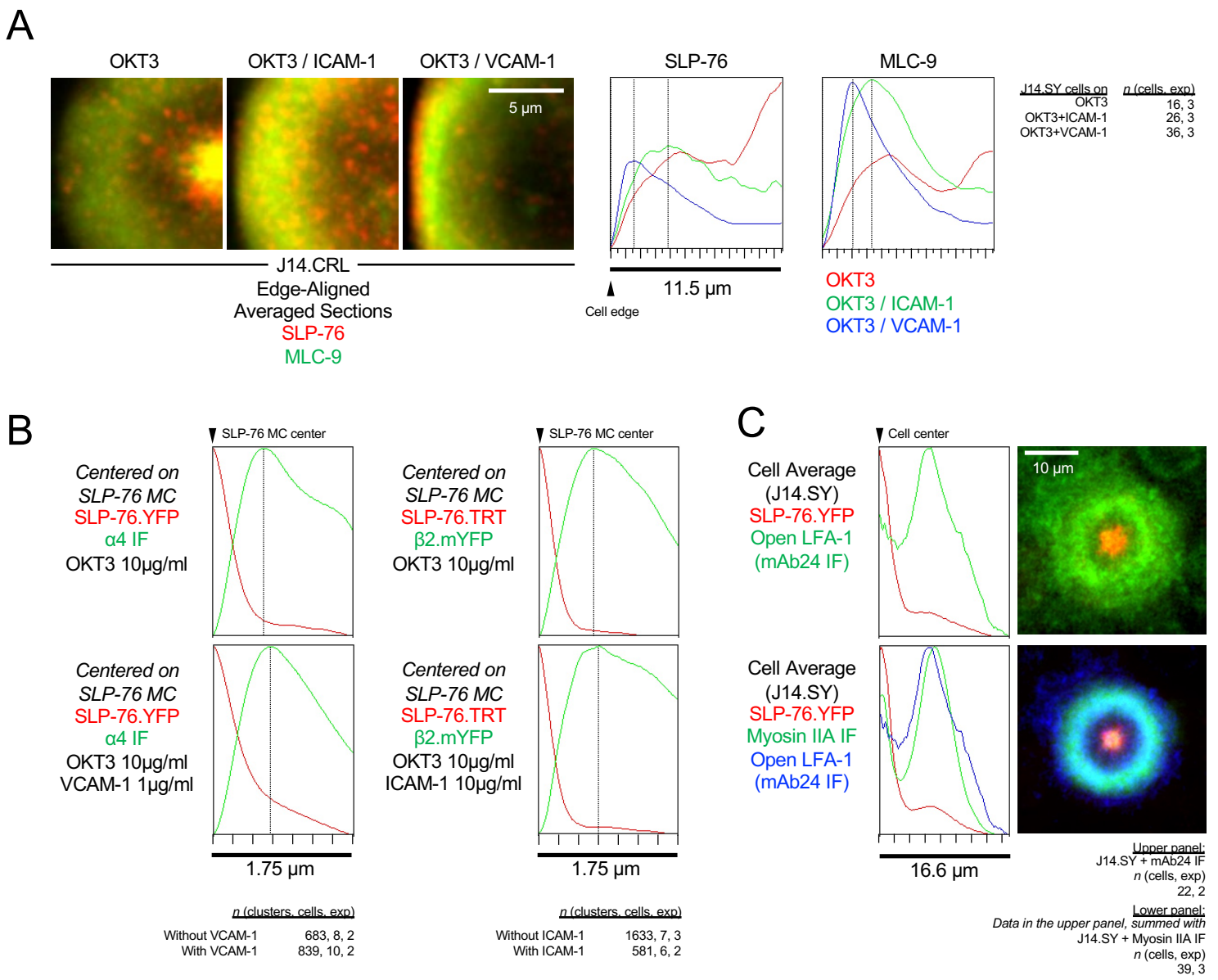


**Fig. S5. Integrins impact the movement of SLP-76 microclusters despite being excluded from SLP-76 microclusters.** (A) Regions acquired from the images obtained for Fig. 3B were aligned via the outer boundaries of cells and averaged (left panels). These images were then integrated vertically to generate fluorescence intensity profiles as a function of distance from the cell edge (right panels). (B) Radial intensity profiles relative to the centers of SLP-76 microclusters were generated from raw images. (B, left) A subset of the J14.SY cells analyzed in Fig. 3D were processed to generate radial intensity profiles. Cells were stimulated as indicated, fixed, and stained with α4. (B, right) J14.ST cells transiently transfected with β2.mYFP and α4.mCFP were stimulated as indicated, imaged with or without fixation, and processed to generate radial intensity profiles. (C) J14.SY cells stimulated on substrates coated with 10 µg $ml^{-1}$ OKT3 were stained with mAb24, fixed, and imaged. Because the staining with mAb24 was weak, images were center-aligned and averaged to generate composite images. The upper plot displays the average intensities of SLP-76.YFP and mAb24 as functions of radial distance from the center of the cell. For comparison, the lower panel sums this data with the J14.SY cells analyzed for myosin IIA in Fig. S1D. Replicate information is provided in all panels.

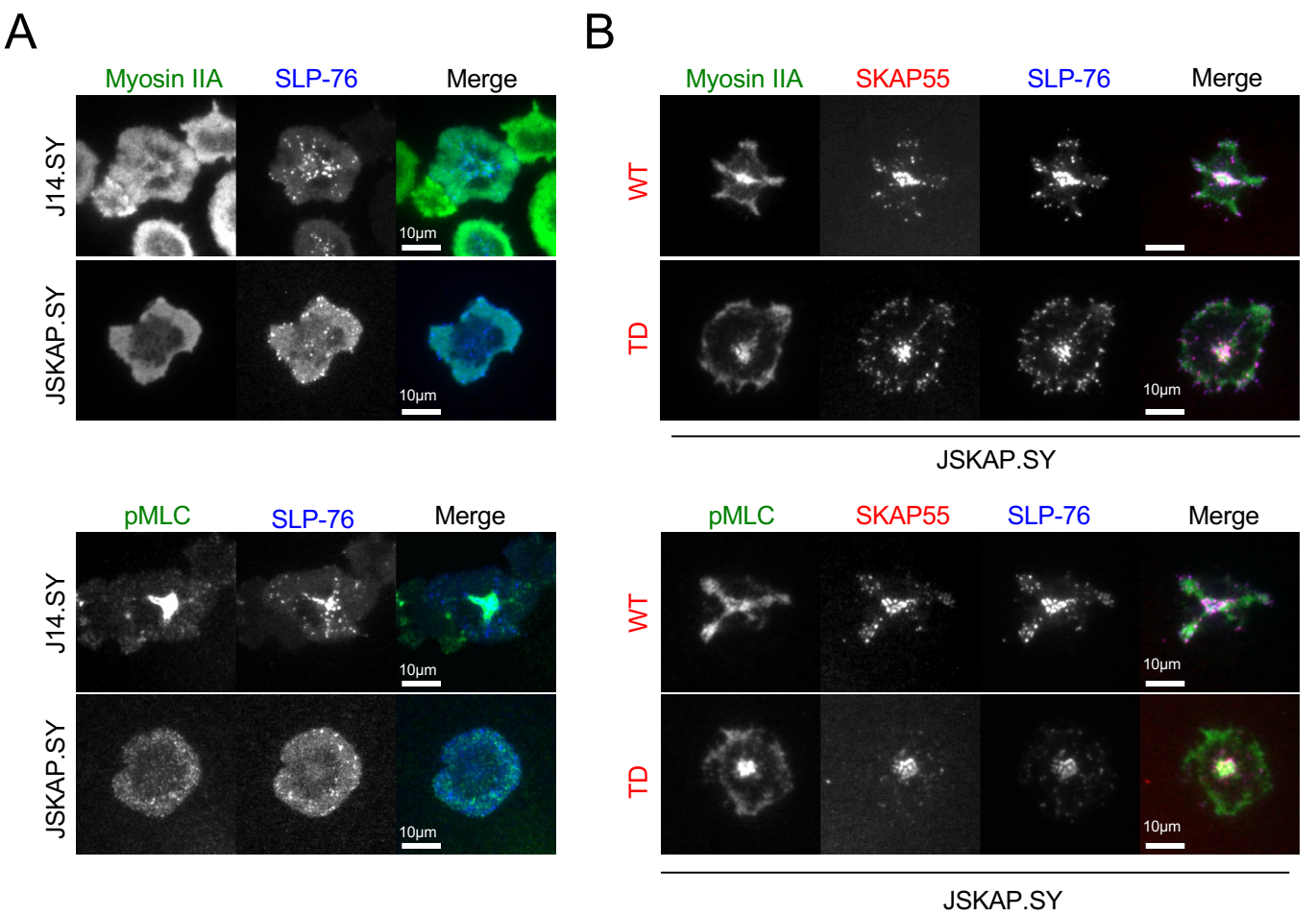


**Fig. S6. The N-terminus of SKAP55 is dispensable for SLP-76 microcluster centralization and the central accumulation of contractile myosin.** (A) The parental J14.SY cell line and its SKAP55-deficient derivative JSKAP.SY were stimulated on anti-CD3 coated glass substrates, fixed, and stained for either myosin IIA or phospho-MLC (pMLC). Representative images are shown, n=3. (B) JSKAP.SY cells were transiently transfected with either wild-type full length SKAP55 or with the tandem-dimer (TD) construct and stimulated, fixed, and stained as in A. Representative images are shown, Two replicates performed.

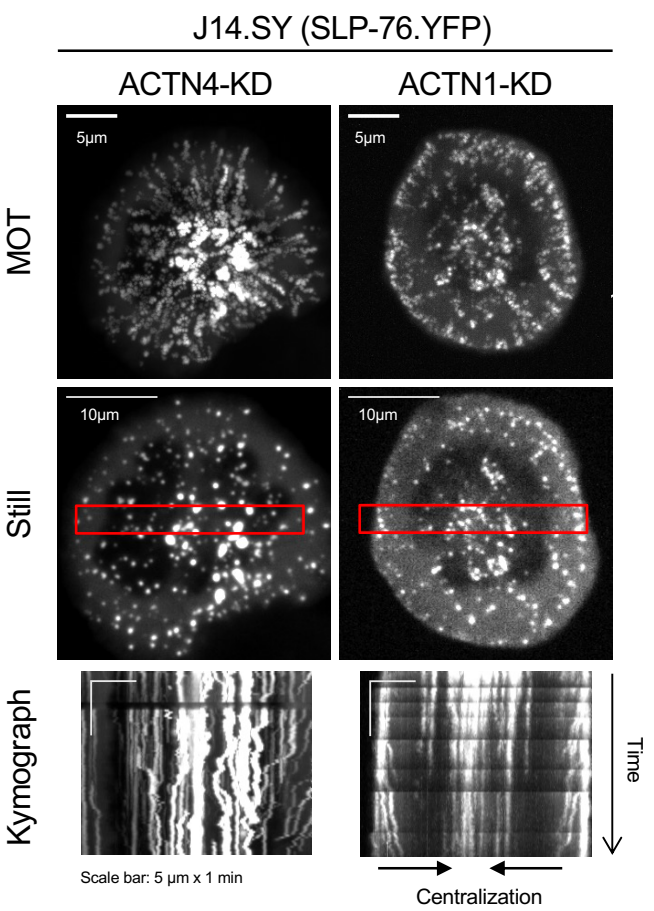


**Fig. S7. α- Actinin-1 and α- Actinin-4 play roles in SLP-76 microcluster centralization.** JJ14.SY cells were stably transduced with shRNAs targeting α-Actinin-4 (ACTN4) or α-Actinin-1 (ACTN1). These cells were stimulated on anti-CD3 coated glass substrates. SLP-76.YFP was imaged every 2 seconds for 150 frames (5 min). Representative still images and maximum-over-time (MOT) projections are shown; kymographs were derived from the indicated regions, n=2.

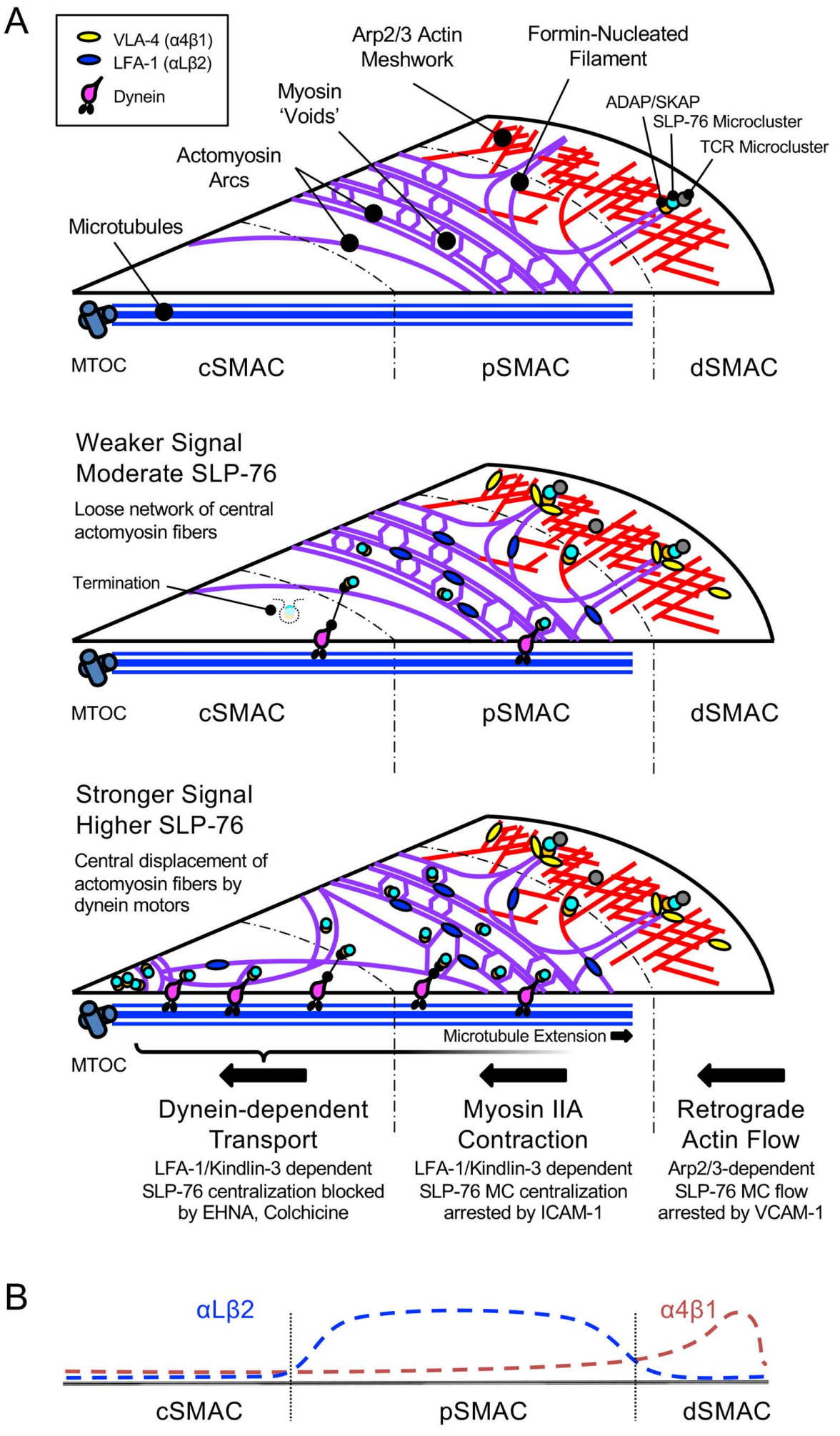

**Fig. S8. A model linking SLP-76 microclusters movement to cytoskeletal systems via LFA-1.** (A) Distal TCR engagement gives rise to TCR (grey circles) and SLP-76 (cyan circles) microclusters; SLP-76 microclusters recruit ADAP and SKAP55 (orange circles) which interact with F-actin and activate integrins. In the absence of integrin ligands, SLP-76 microclusters separate from TCR microclusters and are transported to the center of the synapse. In the absence of VCAM-1, SLP-76 microclusters are swept through the dSMAC by Arp2/3-dependent actin treadmilling. Subsequently, in the absence of ICAM-1, SLP-76 microclusters move through the pSMAC. During this process, SLP-76 microclusters interact with the margins of small (~1.75 μm) actomyosin rings, which are integrated into circumferential actomyosin arcs. LFA-1 (blue ovals) is directly incorporated into these arcs. Once SLP-76 microclusters exit the pSMAC, they can be internalized and terminated (upper panel) or can accumulate in the center of the contact (lower panel). In synapses induced by weak TCR ligands, the cSMAC is sparsely populated by actin filaments and SLP-76 microclusters do not reach the center of the contact. In contrast, when the TCR is potently stimulated and when SLP-76 is abundant, SLP-76 microclusters and contractile myosin filaments translocate towards the cSMAC. The latter process requires formins, myosin II, dynein, kindlin-3, and the kindlin-3-binding site in LFA-1, but does not require talin. We propose that persistent SLP-76 microclusters interact with dynein via ADAP, and thereby transmit dynein-dependent forces to formin-dependent actomyosin arcs within the pSMAC. If these forces exceed the tensile strength of these arcs, the arcs deform and rupture, allowing actomyosin filaments to accumulate in the center of the synapse. Conversely, the myosin-dependent rigidification of the lamellar actomyosin network may enable microcluster-associated dynein motors to polarize the MTOC and to drive microtubules into the periphery of the synapse. (B) A model describing the presumed locations of active integrins within the immune synapse.

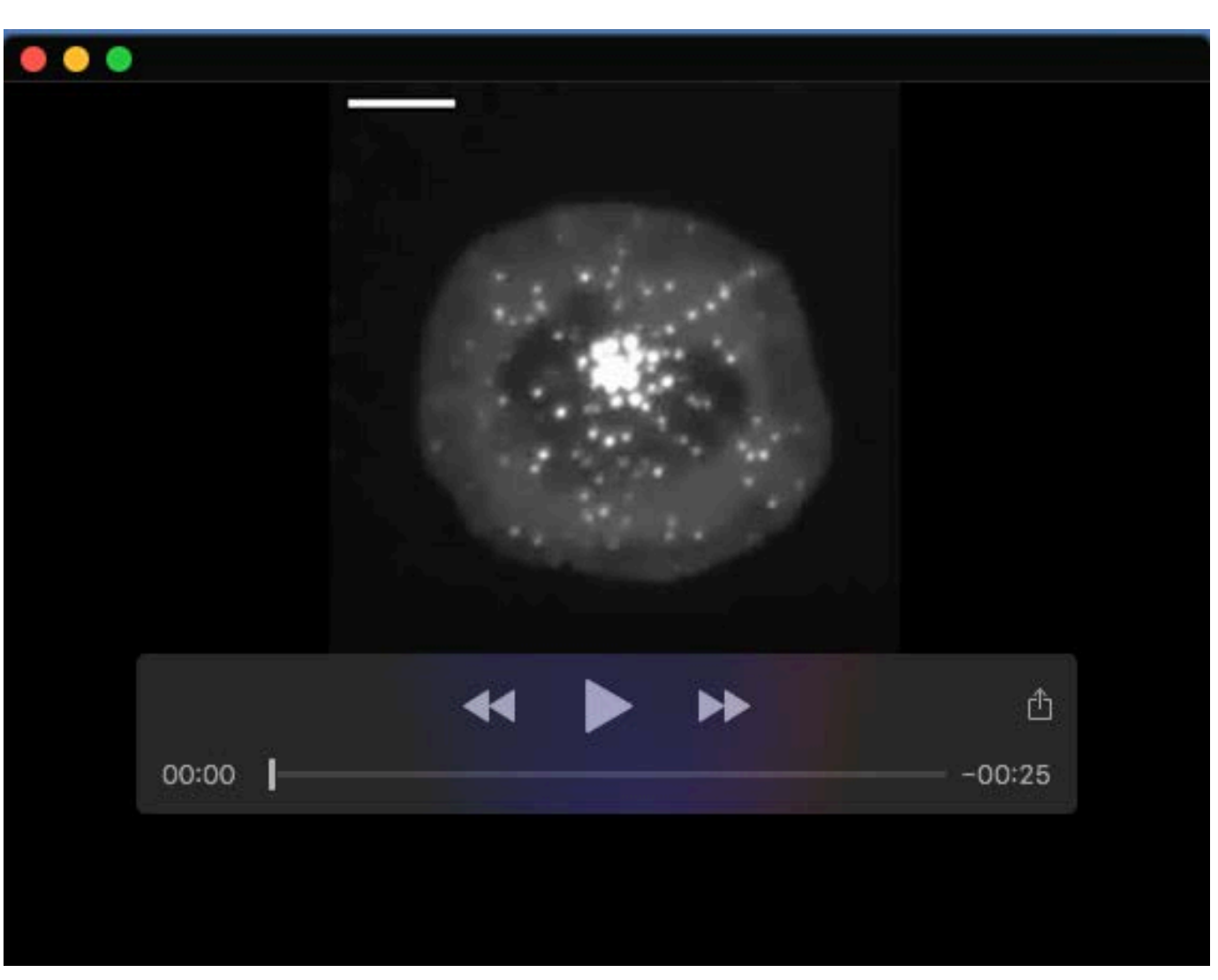


**Movie 1. Live cell imaging of J14.SY cells plated on anti-CD3 coated glass wells.** Wild-type J14.SY cells were stimulated on anti-CD3 coated glass substrates. SLP-76.YFP was imaged every 2 seconds for 150 frames (5 min). Movies play at 0.06 s frame$^{-1}$, yielding a 33.3x compression rate. Scale bar is 5 μm.

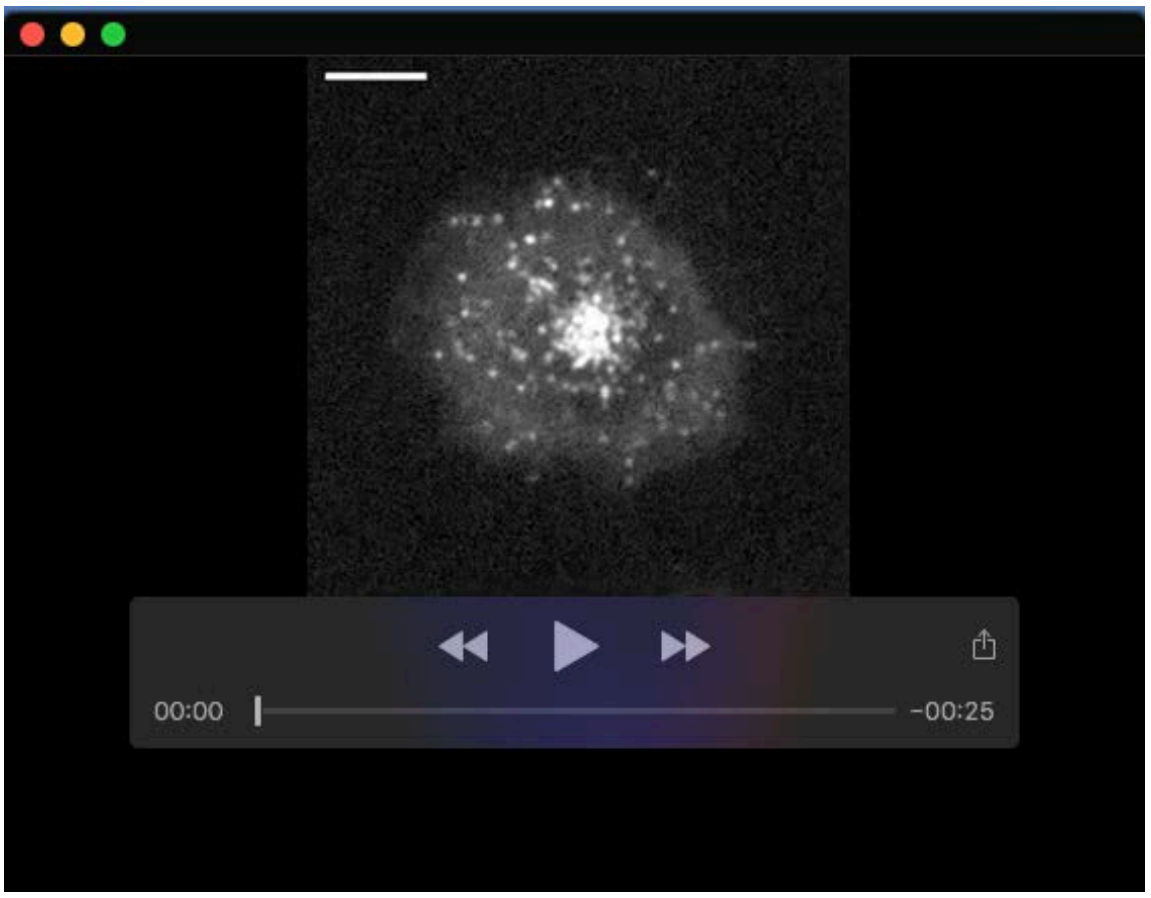


**Movie 2. Live cell imaging of A1.ST cells plated on anti-CD3 coated glass wells.** β1-deficient A1.ST cells were stimulated on anti-CD3 coated glass substrates. SLP-76.TRT was imaged every 2 seconds for 150 frames (5 min). Movies play at 0.06 s frame$^{-1}$, yielding a 33.3x compression rate. Scale bar is 5 µm.

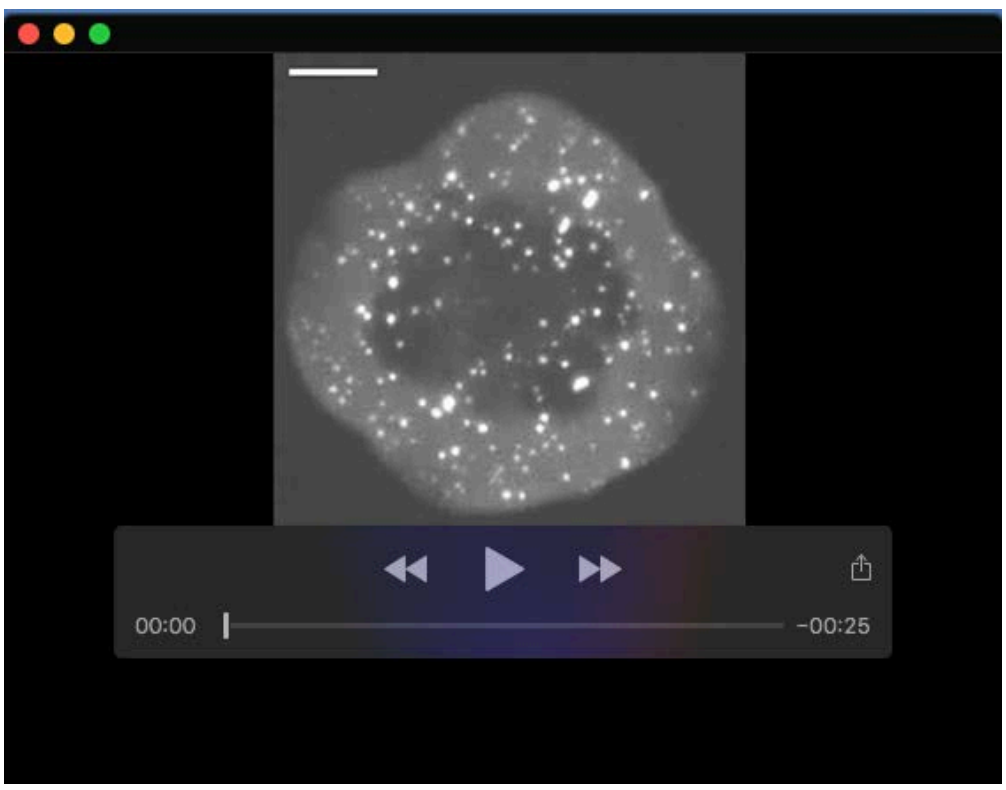


**Movie 3. Live cell imaging of β2 knockdown cells plated on anti-CD3 coated glass wells.** J14.SY cells were stably transduced with a shRNA targeting β2. Cells were stimulated on anti-CD3 coated glass substrates. SLP-76.YFP was imaged every 2 seconds for 150 frames (5 min). Movies play at 0.06 s frame$^{-1}$, yielding a 33.3x compression rate. Scale bar is 5 µm.

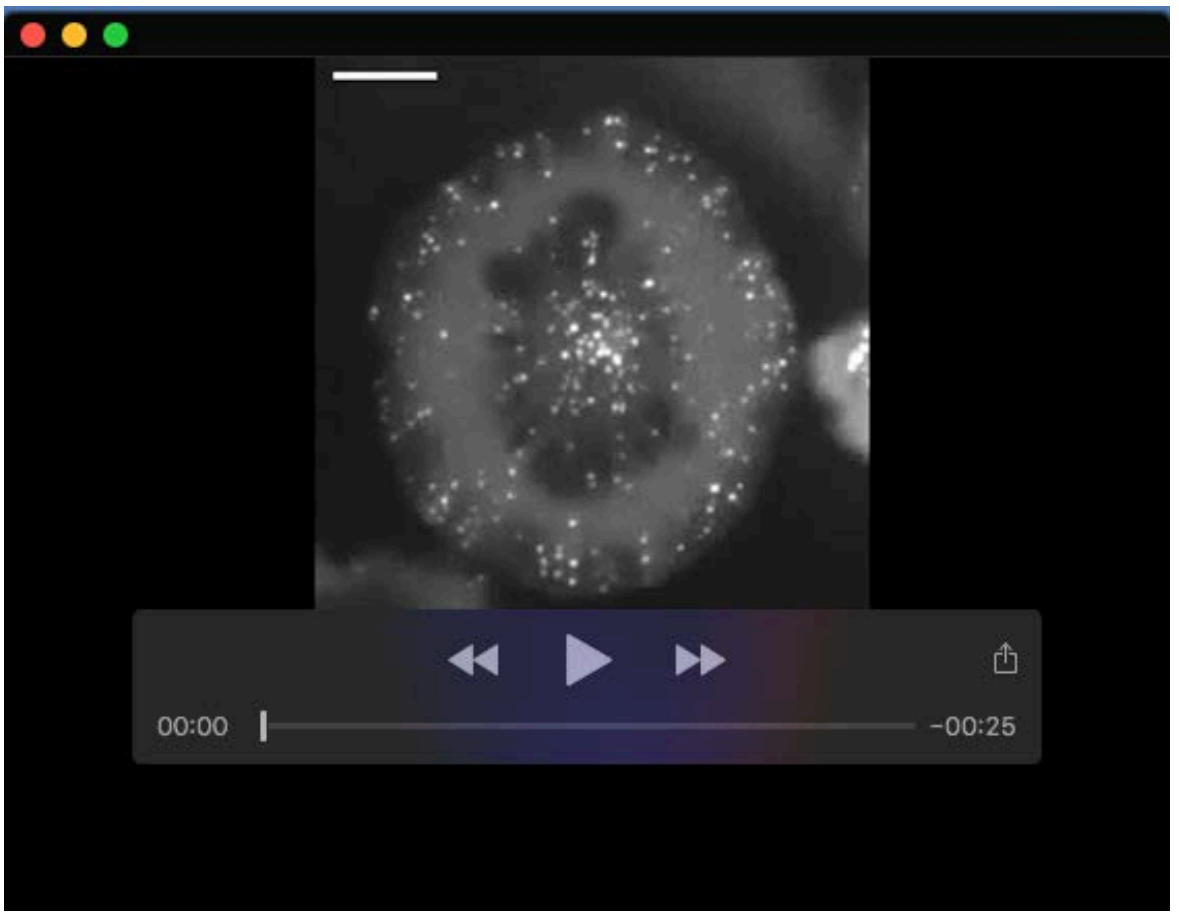


**Movie 4. Live cell imaging of Talin-1 knockdown cells plated on anti-CD3 coated glass wells.** J14.SY cells were stably transduced with a shRNA targeting Talin-1. Cells were stimulated on anti-CD3 coated glass substrates. SLP-76.YFP was imaged every 2 seconds for 150 frames (5 min). Movies play at 0.06 s frame$^{-1}$, yielding a 33.3x compression rate. Scale bar is 5 µm.

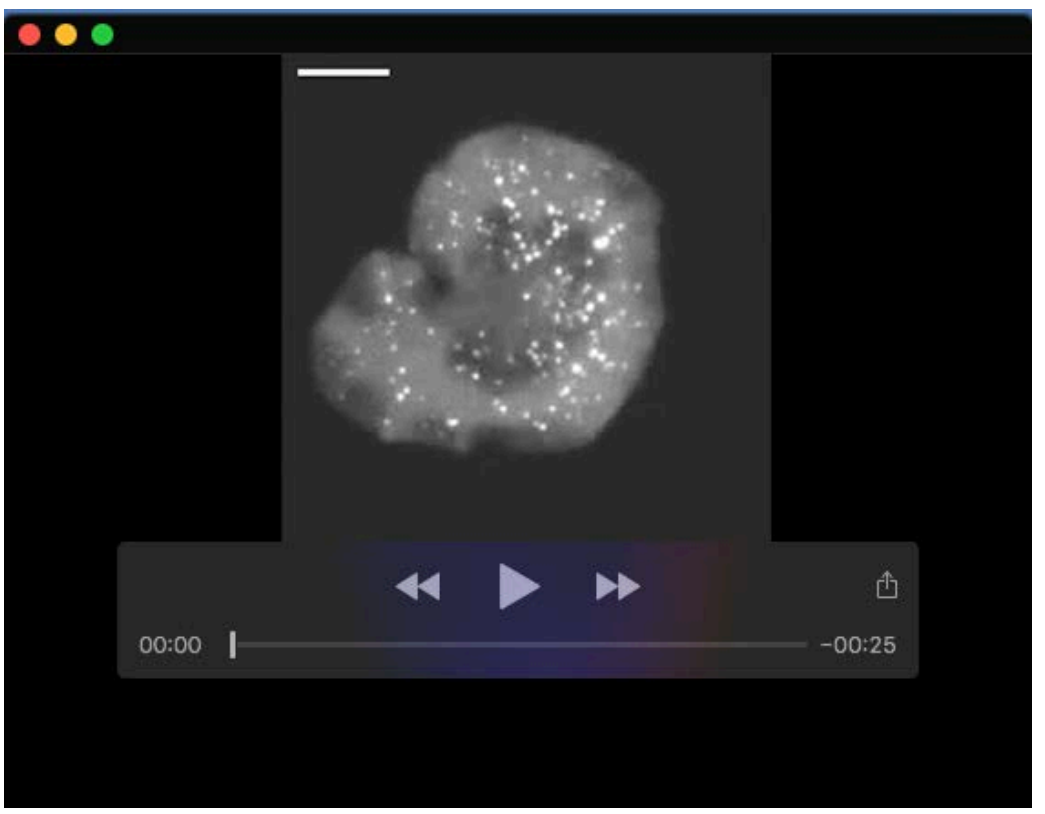


**Movie 5. Live cell imaging of Kindlin-3 knockdown cells plated on anti-CD3 coated glass wells.** J14.SY cells were stably transduced with a shRNA targeting Kindlin-3. Cells were stimulated on anti-CD3 coated glass substrates. SLP-76.YFP was imaged every 2 seconds for 150 frames (5 min). Movies play at 0.06 s frame$^{-1}$, yielding a 33.3x compression rate. Scale bar is 5 µm.

Journal of Cell Science • Supplementary information

**Table S1. Oligonucleotides used in vector construction**

| Oligo ID | Oligo Name | Sequence |
|---|---|---|
| **Oligos for MYH9 shRNA assembly** | | |
| NRS801 | MYH9.shRNA-1.f1 | GATCCGGCCAAACCTGCCGAATAAt t caagaga |
| NRS802 | MYH9.shRNA-1.r1 | ATAAt ct ct t gaaTTATTCGGCAGGTTTGGCCG |
| NRS803 | MYH9.shRNA-1.f2 | TTATTCGGCAGGTTTGGCCTTTTTGGA |
| NRS804 | MYH9.shRNA-1.r2 | AGCTTCCAAAAAGGCCAAACCTGCCGA |
| **Oligos for H1p-shRNA cassette amplification** | | |
| NRS753 | H1-shRNA.Rescue-5'-NdeI.f | gacagcCATATGCGAACGCTGACGTCATCAACC |
| NRS754 | H1-shRNA.Rescue-3'-AseI.r | ggcaaggcATTAATCGACGGt at cgAt AAGCTTCC |
| **Oligos for the production of tailless b2.mYFP** | | |
| KPE017 | Beta2.f1 | GACTGAATTCGACTACCCATCGGTGGGC |
| KPE018 | Beta2.r1 | CACATAGATGAGGTAcCGGTCCATCCCGT |
| **Gibson primers for Beta-2 tail mutants** | | |
| KPEG026 | b2-NPLF/AAAA | ACGCTGGAGCAGCAGGACGGGATGGACCGGt ACCTCATCTA TGTGGATGAGAGCCGAGAGTGTGTGGCAGGCCCCAACATCG CCGCCATCGTCGGGGGCACCGTGGCAGGCATCGTGCTGATC GGCATTCTCCTGCTGGTCATCTGGAAGGCTCTGATCCACCT GAGCGACCTCCGGGAGTACAGGCGCTTTGAGAAGGAGAAGC TCAAGTCCCAGTGGAACAATGATaat ccccttttcAAGAGC GCCACCACGACGGTCATGgct gct gccgcaGCTGAGAGTgg cggaCCGGTCGCCACCATGGTGAGCAAGGGCGAG |
| KPEG027 | b2-AAAA/NPKF | ACGCTGGAGCAGCAGGACGGGATGGACCGGt ACCTCATCTA TGTGGATGAGAGCCGAGAGTGTGTGGCAGGCCCCAACATCG CCGCCATCGTCGGGGGCACCGTGGCAGGCATCGTGCTGATC GGCATTCTCCTGCTGGTCATCTGGAAGGCTCTGATCCACCT GAGCGACCTCCGGGAGTACAGGCGCTTTGAGAAGGAGAAGC TCAAGTCCCAGTGGAACAATGATgcagcagct gccAAGAGC GCCACCACGACGGTCATGaaccccaagtttGCTGAGAGTgg cggaCCGGTCGCCACCATGGTGAGCAAGGGCGAG |
| KPEG028 | b2-AAAA/AAAA | ACGCTGGAGCAGCAGGACGGGATGGACCGGt ACCTCATCTA TGTGGATGAGAGCCGAGAGTGTGTGGCAGGCCCCAACATCG CCGCCATCGTCGGGGGCACCGTGGCAGGCATCGTGCTGATC GGCATTCTCCTGCTGGTCATCTGGAAGGCTCTGATCCACCT GAGCGACCTCCGGGAGTACAGGCGCTTTGAGAAGGAGAAGC TCAAGTCCCAGTGGAACAATGATgcagcagct gccAAGAGC GCCACCACGACGGTCATGgct gct gccgcaGCTGAGAGTgg cggaCCGGTCGCCACCATGGTGAGCAAGGGCGAG |

**Table S2. Proteomic characterization of signaling complexes induced via the co-ligation of the TCR and VLA-4.** The unique proteins and peptides identified in Fig. S3 are listed by source band. The molecular weights of the parent proteins are shown. Some peptides are present in more than one band. For each protein, the total number of unique peptides across all bands and the number of unique peptides in the relevant band are shown. The %TIC in Band is the fraction of the band-specific ion current that is derived from all of the peptides associated with a specific protein.

Click here to download Table S2